Synthèse, réactivité électrochimique et structure électronique de 1-R-métallatranes (M=Si,Sn)

Yu Wang

N° d'ordre :   **ANNÉE 2012**

THÈSE / UNIVERSITÉ DE RENNES 1
sous le sceau de l'Université Européenne de Bretagne

pour le grade de

DOCTEUR DE L'UNIVERSITÉ DE RENNES 1

Mention : Chimie

Ecole doctorale : Science de la Matière (sdlm)

présentée par

Yu WANG

Préparée à l'unité de recherche UMR CNRS 6226 ISCR
Chimie et Photonique Moléculaire
UFR Structure et Propriétés de la Matière

Synthesis, electrochemical reactivity and electronic structure of 1-R-metallatranes (M = Si, Sn)

**Thèse soutenue à Rennes
le 30 Novembre 2012**

devant le jury composé de :

Christa GROGGER
Professeur Université Technique de Graz,
Autriche/ *rapporteur*

Mohamed MELLAH
Maître de conférence-HDR
Université Paris sud / *rapporteur*

Floris CHEVALLIER
Maître de conférence-HDR
Université Rennes1 / *membre*

Viatcheslav JOUIKOV
Professeur Université Rennes1 /
directeur de thèse

Acknowledgement

During these three years, I received plenty of help from many people. I know I can't mention all of them here but I still would like to express my sincere gratitude to very persons who supported me at all times or through any condition throughout my thesis. First and foremost, I am extremely grateful to my thesis supervisor Pr. Viatcheslav Jouikov, who not only chose me for this thesis but also gave me a lot of valuable guidance and consistent encouragement, which I received throughout the research work.

Special thanks are due to Pr. Christa GROGGER and Dr. Mohamed MELLAH for accepting to be the reporters of my thesis and for the careful review and many suggestions that they provided on the original manuscript. I would like to thank Dr. Floris CHEVALLIER for being the member of my jury and providing many useful advices on my manuscript.

I would like to offer special thanks to laboratory "Chimie et Photonique Moléculaires" UMR 6226 for providing me very good working conditions and help at all time.

I would like to thank my boyfriend Mr. Jan Recho for being with me through all three years during my thesis and offering me encouragement and help anytime. I want to tell him 'without you I couldn't have achieved it'. Also very sincere thanks to my mum Mrs. Liu Ying who always supported my decision and accompanied me during the last three months of my thesis by taking very good care of my life. I am so lucky to have you as my family.

I am even luckier to have my friends by my side with no conditions. First I would like to thank one of my best friends Lena Driehaus for helping me, jogging with me every day, laughing or crying with me and preparing an extraordinary 'french-chinese pot' for me after my viva. I want to thank the couple Liu Ming and Bai Xiao for helping me to find all the solutions I needed to get used to the software LYX that I used for writing my thesis, as well as Yi Xiaohui for drawing the crystal figure for my thesis.

Grateful thanks to my colleagues in the laboratory Aline Vanryckeghem, Nada Marquise, Aude Sourdon, Nicolas Richy and Jonathan Daniel for helping the little foreigner from China to improve my poor French with 'nice' jokes and expressions. It is such a pleasure working with you as well as having coffee in the 'fume club'.

Summary

Metallatranes (M = Si, Ge, Sn) have been studied intensively during 50 years and have many applications in various domains namely physics, biology, medicine and so on. However their electrochemical properties were poorly studied up to date. In the present work, new metallatranes have been synthesized and characterized using different approaches and techniques (organic synthesis, cyclic voltammetry, preparative electrolysis, EPR, spectroelectrochemistry, cyclic voltammetry coupled with EPR, NMR, GC-MS). Several novel structures of metallatranes have been obtained and validated by XRD. Electrochemical measurements show that the electrooxidation of metallatranes occurs via electrochemically reversible one-electron transfer resulting in the corresponding cation radicals (CRs), detected by cyclic voltammetry, UV-vis spectroscopy and real-time EPR spectroscopy. The spin delocalization in these paramagnetic species has been characterized and supported by DFT calculations. We focused on the electronic properties of metallatranes and on various bonding systems between pentacoordinated silicon and N atom including the substituents. We also considered the issue of non-coordinating, non-nucleophilic supporting salts for electrochemistry as they provide good ionic conductivity in the solvents of low polarity and allow carrying out voltammetry and EPR experiments on unstable electrogenerated electrophilic and radical species.

Résumé

Les métallatranes (M=Si, Ge, Sn) ont fait l'objet d'un intérêt important de la communauté scientifique durant les 50 dernières années et ont des applications dans de nombreux domaines, de la physique à la biologie en passant par la médecine, etc... Cependant, leurs propriétés électrochimiques n'ont été étudiées que de façon très incomplète à ce jour. Dans le travail présenté ici, nous avons réalisé la synthèse de nouveaux métallatranes et les avons caractérisés, et ce par plusieurs approches et techniques différentes (synthèse organique, voltammétrie cyclique, électrolyse préparative, EPR, spectroélectrochimie, voltammétrie cyclique couplée à un EPR, RMN, GC-MS). Plusieurs nouveaux métallatranes ont été obtenus, et leurs structures validées par diffraction RX. Les mesures électrochimiques montrent que l'électrooxidation des métallatranes a lieu via des transferts électroniques réversibles, et les cations-radicaux (CRs) qui résultent de leur oxydation ont été détectés par voltammétrie cyclique, spectroscopie UV-visible, et spectroscopie EPR en temps réel. La délocalisation de spin dans ces espèces paramagnétiques a été caractérisée et soutenue par des calculs de DFT. Nous avons concentré nos efforts sur les propriétés électroniques des métallatranes et la nature des diverses liaisons entre l'atome de silicium penta-coordonné des silatranes d'une part, l'atome d'azote de la structure atrane, et les atomes de différents substituants d'autre part. Nous avons également étudié le problème posé par les sels du fond pour l'électrochimie, qui doivent être non-coordinants et non-nucléophiles, et doivent fournir une bonne conductivité ionique dans des solvants peu polaires. Ils permettent ainsi de mener des expériences de voltammétrie et de la RPE sur des espèces électrogénérées instables, notamment électrophiles ou des radicaux libres.

Key words

1. Silatranes	5. Cyclic voltammetry
2. Hypervalent silicon species	6. DFT calculations
3. Cation radicals	7. EPR spectroscopy
4. Electrochemistry	8. Non-cooridating electrolyte

Contents

1 Glossary

The abbreviations commonly used in the present manuscript:

3c-4e: 3 centers, 4 electrons bond (5c-6e: 5 centers 6 electrons bond, 6c-8e, etc...)

ACN: Acetonitrile

Bu: Butyl

C: concentration

CCDB: Cambridge Crystallographic DataBase

DDM: Dimethyl diazomalonate

DFT: Density functionnal theory

DMF: Dimethylformamide

E_p^a: Anodic peak potential

E_p^c: Cathodic peak potential

EPR: Electron paramagnetic resonance

F: Faraday's constant (96 485 C.mol^{-1})

Fc: Ferrocene

G: Gauss (unit of magnetic field strength)

GC: Glassy carbon

GC-MS: Gas Chromatography, coupled with Mass Spectrometry detector

HOMO: Highest occupied molecular orbital

i_p: Peak current

J: NMR coupling constant between 2 nuclei

K: equilibrium constant of a reaction

LAH: Lithium aluminum hydride

LUMO: Lowest unoccupied molecular orbital

NBO: Natural Bonding Orbital method

NMR: Nuclear magnetic resonance

ppm: Part per million

p-TsOH: *p*-toluenesulfonic acid

R-: Any functional group

R: Ideal gas constant (8,3145 J·mol^{-1}·K^{-1})

S: Entropy

SCE: Saturated calomel electrode

SN: Nucleophilic substitution

T_8: Octahedral silsesquioxanes

TBA: Tetrabutylammonium

TBAP: Tetrabutylammonium perchlorate

THF: Tetrahydrofurane

TMS: tetramethoxysilane

v : Scan rate, in cyclic voltammetry experiments

^{o}C: Degree centrigrade

α: Transfer coefficient of an electrode reaction

χ: electronegativity

δ: Chemical shift (NMR, ppm)

INTRODUCTION

2   Introduction

Since 1960, when a new class of organosilicon compounds, triptych-siloxazolidines, was firstly synthesized by Frye *et al.* [1], metallatranes, -the name that has been coined by Voronkov,- have been studied intensively over 50 years not only because of their unique transannular interactions between nitrogen of the atrane cage and the metal (Si, Ge and Sn) but also because of many applications in medicine and biology they found [2, 3, 4]. However the electrochemical properties of metallatranes did not catch enough attention and have been poorly studied [5] up to date.

Analysis of the literature on physical chemistry of metrallatranes prompts one to believe that they have big potential namely in the electrochemical aspect. First of all, in the cation radicals of this family, the hypervalent bond between N and the metal (Si, Ge and Sn) atom limits the spatial range of spin localization; protected by the three lateral branches of the atrane cage, the spin is trapped inside and is naturally isolated. Second, the atrane structure has axial symmetry and is in principle allowing the formation of long linear systems in this direction. Normal σ-conjugated polysilane chains are either chemically unstable or have poor electron conductivity because of poor overlap of silicon orbital. Bonding element of the extended metallatrane structures occupies the axial position and is intrinsically isolated. Now if an electron transfer can induce a positive charge to these linear systems, one might expect to obtain a new kind of conductive molecular wires (Figure 1) which are chemically stable, conformation-independent and allow electronic conjugation throughout their whole length. This would be a remarkable development compared to the normal σ-conjugated polysilane chains which are either not chemically stable or have poor electron conductivity because of poor overlap of silicon orbital. Thus we consider it is a completely different new concept for conducting chain molecules in which the electrons are able to be transferred along the chain.

In addition, the cation radicals of metallatranes, at least those already studied, show another remarkable feature: the distance between N and Si varies depending on the charge on N atom. Using this axial flexibility of the atrane system, we can modulate the chain length and realize different electrochemical functions, for instance an electrochemically addressable molecular muscle. For the above reasons, we decided to focus the present work on the electrochemical behavior of metallatrane-based systems.

To achieve this goal, the work presented in this manuscript was carried out starting from the synthesis of metallatranes and their structural characterization, to their electrochemical study and quantum chemical calculations. This manuscript is composed of four essential chapters. The first chapter provides bibliography and contains a historical overview of metallatranes, their structure and behavior as well as that of their cation radicals; some non-coordinating supporting electrolytes that have similar pentacoordinating structure of incorporated Si atoms were also considered.
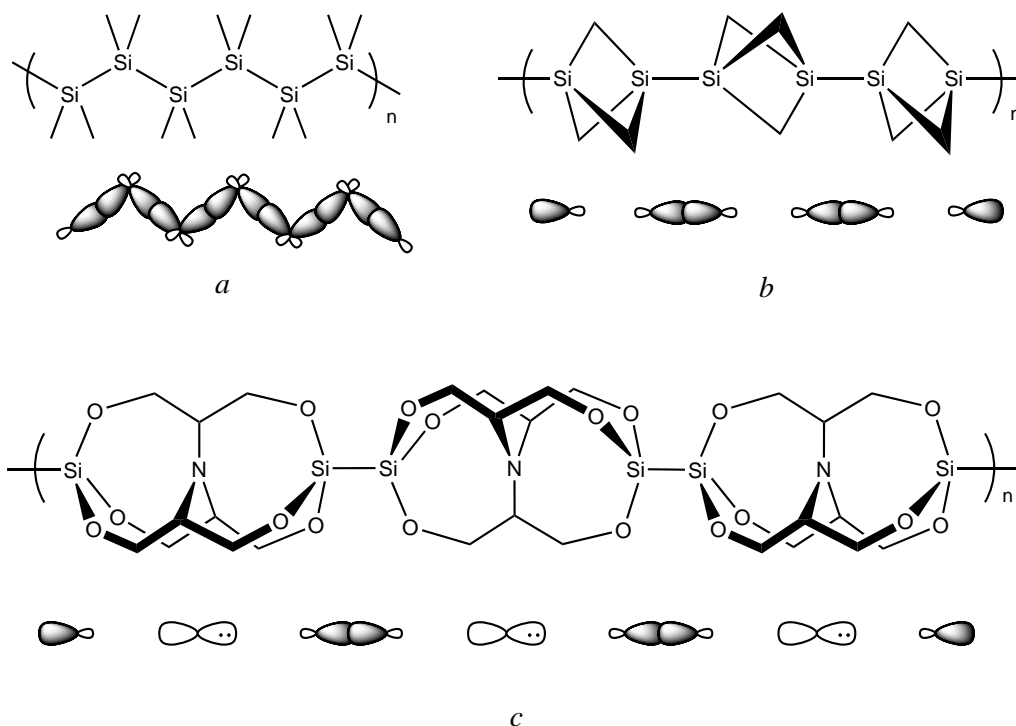
Figure 1: Different types of silicon chain molecules. *a.* σ-conjugated molecular chain with good electronic conductivity but poor chemical stability; *b.* Silicon chain molecule with good chemical stability but poor molecular orbital overlap; *c.* New molecular chain with atrane structure as elementary unit, which is supposed to provide efficient electron transfer and good chemical stability.

The second chapter concerns the experimental details, including chemical and electrochemical synthesis, physical and chemical characterization of the prepared compounds considered afterwards in other chapters of the manuscript. Two main chemical reactions as well as one electrochemical process were used for the synthesis of the metallatranes. NMR spectroscopy, GC-MS and XRD were used for the structural characterization. Cyclic voltammetry, chronoamperometry and EPR spectroscopy were used for analyzing electrochemical reactivity.

The following chapter includes the obtained results and discussions; it is divided into five subsections according to the metallatranes considered and finally one last section concerning new supporting electrolytes. The manuscript begins with simple 1-R-silatranes with substituents providing different electronic effects to the reaction center of the electron transfer. Then, bis-(silatranyl)alkanes and bi-silatranes are considered. These molecules with the atrane moiety doubled in different ways represent the first step of constructing a silylated chain allowing long-distance conjugative interactions. This discussion is followed by 1-R-stannatranes in which the metal of the atrane is changed from Si to Sn. Finally, we will present new non-coordinating silsesquioxane-based supporting electrolytes for the large use in electrochemistry

and organometallic chemistry.

The last chapter, based on the experiment, analysis and above discussion, gives a conclusion for the whole research on metallatranes.

References and appendix are given at the end of the manuscript.

BIBLIOGRAPHY

3   Bibliography

3.1   Silatranes, their structure and specific intramolecular bonding and their electrooxidation

To a great extent, it is due to their unique structure (see Figure 2) that silatranes are so attractive systems for researchers since they were first synthesized in 1960 by Frye *et al* [1]. Since then, silatranes have been very well studied in many aspects. Numerous silatranes were synthesized and characterized by different methods: molecular structure [6, 7, 8], dipole moments [9, 10, 11, 12], vibrational spectra [1, 9, 13, 14, 15], UV spectra [16, 17, 18], NMR spectra [9, 19, 20, 21], mass spectra [22, 23, 24, 25] and the results of other physical methods were reported. In addition, cleavage and retention of the silatrane ring were studied [26, 27] as well as other chemical reactions. A great deal of attention was paid to their biological activity.

First of all, the series of silatranes have common distinctive structure of the atrane fragment: three alkyl branches all connected with a nitrogen atom, on one end, and connected back together with a O_3SiR group on the other. Their cage can also be seen as three heterocyclic rings sharing two transannular atoms, silicon and nitrogen. The interaction between Si and N atoms is fascinating because the lone electron pair of the nitrogen acts as an electron-donor to silicon atom and is usually not available for the interactions with external Lewis acids, like BF_3. Thus silatrane could be considered as a compound bearing a pentacoordinate Si.
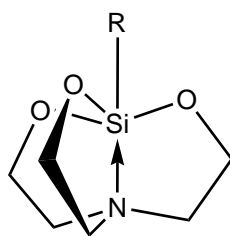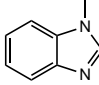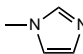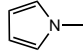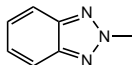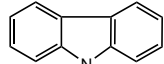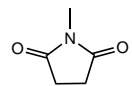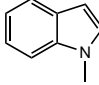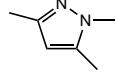
Figure 2: Silatrane structure

A large number of reports highlight the existence of the intermolecular N→Si bonding by means of single crystal diffraction analysis [28, 29]. Table 1 is a part of the large available crystallographic data, showing that the distance between Si and N ranges from 2.1Å to 2.7Å. This distinctly differs from either the usual Si-N bond length (1.7-1.8Å) or the sum of van der Waals radii of N and Si atoms (~ 3.5Å).

Table 1: Crystal data of selected silatranes [28, 29]

R	Si-N	Si-R	Si-O
Cl	2.02	2.15	1.65
CH_3	2.17	1.87	1.67
C_2H_5	2.21	1.88	1.66
$ClCH_2$	2.12	1.91	1.67
$Cl(CH_2)_3$	2.18	1.88	1.66
$3\text{-}O_2NC_6H_4$	2.12	1.91	1.66
CH_3O	2.22	1.67	1.66
	2.088	1.909	1.667
	2.088	1.898	1.664
	2.089	1.902	NR
	2.089	1.908	1.659
	2.097	1.897	NR
	2.102	1.910	NR
	2.110	1.910	NR
	2.118	1.663	1.913

Silatranes might exist in two main configurations of N atom: *exo* and *endo*. Without the valence molecular angles and bonds twisting, the interatomic N–Si distance of *endo* and *exo* structures is limited in a narrow range, 2.35-2.45 and 2.9-3.0 Å, respectively. According to the calculations, as the example of the 1-methylsilatrane molecule, the unstable *exo* form should transform naturely to the *endo* form which is relatively stable [7]. The *endo* form of silatranes is more stable due to whole set of factors related to configurational, dipole-dipole (electrostatic) and covalent interactions [29, 30]. For instance, from the molecular bonding orbital shown in Figure 3, it is obvious not only the atomic orbital of N and Si was necessarily involved but also the atomic orbital of oxygen participated into the formation of molecular bonding as well. According to the features of their frontier molecular orbital: highest occupied molecular orbital (HOMOs) in *endo* configuration is lower than *exo* configuration; and lowest unoccupied molecular orbital (LUMOs) is rather higher which also support the stability of *endo* configuration. Additionally, the energy gap between HOMO and LUMO decreases in

going from structure *endo* to *exo*. All the information indicates that *endo* structure of silatrane is more stable than *exo* form [31]. The quantum-chemical calculations also support that the electronic density "transfer" from the nitrogen atom is about 0.25 eV for the *endo* form of silatranes. Thus, the peculiar features of the silatrane structure are associated with the N→Si interaction [29].
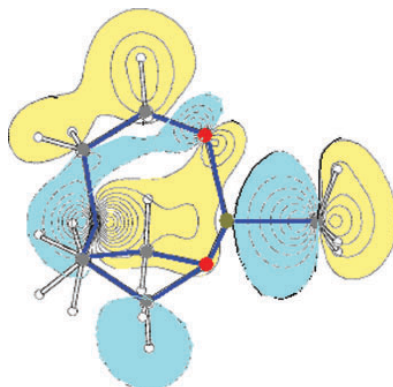
Figure 3: MO_{32} orbital of methylsilatrane showing contribution of N, Si and O atomic orbital [28].

3.1.1 Transannular bonds to Si

The interaction between metal and nitrogen atoms in metallatranes to this day cannot be perfectly explained by a single theory. Good results are obtained by the use of several theories, each theory modelising a different part of the molecule. The hybridization theory claims that silicon in silatranes is pentacoordinated, meaning valence orbital are hybridized as sp^3d. Like in other molecules with sp^3d hybridized silicon, the geometry of the Si in silatranes is a trigonal bipyramid with the silicon atom located in the center, and three oxygen atoms, one nitrogen atom and one atom from the substituent connected to Si located in the corners of each trigonal pyramid (Figure 4).

Three oxygen atoms and the substituent R form four σ bonds with Si whereas N and Si form a dative bond with the lone electron pair of the N atom as a donor element. Although this theory seems to explain the molecular geometry of silatrane well, it ignores the fact that the three heterocyclic rings in the silatrane structure will cause electron density to be different in the dative N-Si bond and in the covalent bond to the substituent on the other side of silicon atom.

Due to this change in electron density, the silicon atom is not on the plan of the three oxygen atoms so the geometry of silatrane is not a perfect trigonal bipyramid. The drawback of hybridization theory alone is that it presumes the involvement of d-orbital in the chemical bond. The 3d-orbital of the silicon atom contains comparatively high energy electrons, rather

11

unfit to hybridize. So, rather, 4s- and 4p-orbital of silicon atom must be considered to explain the electron configuration in the dative N$\rightarrow$Si bond. In this case, the orbital hybridization should not be sp^3d anymore but turns into a sp^3d4s hybridization (Figure 5).
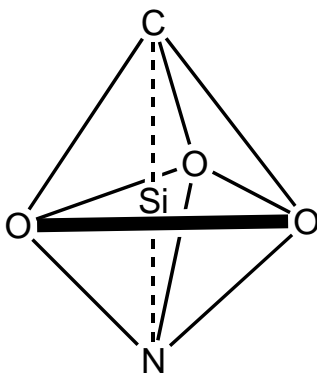

Figure 4: Structure of a silatrane Si atom as predicted by hybridization theory

To circumvent these issues, attempts to explain silatrane geometry using the molecular orbital theory (MO) were undertaken. In this theory the silatrane is considered as a hypervalent molecule. This is a theory first defined by Jeremy I. Musher in 1969 [32]. It involves a 3-centers-4-electrons (3c-4e) bond, which is described as a combination of three molecular orbital: a half filled p-orbital from the central silicon atom, one fully filled orbital from the lone electron pair of the nitrogen atom, and one half filled valence orbital from the substituent. The combination of these electrons results in a filled bonding orbital, a filled non-bonding orbital (HOMO) and an empty anti-bonding orbital (LUMO). In this theory, the 3s and the remaining 2p orbital of the silicon atom hybridize into sp^2 orbital and form three σ bonds with three oxygen atoms in the structure.

As follows from the electrochemical studies and DFT modelling of metallatranes [33, 34], the N-M-X 3-centers system behaves as a single orbital with electron availability from both sides, which thus remains open to further conjugative interactions. Now, extrapolating this 3c-4e bond (Figure 5), we expect to apply the same theory to imagine a 5c-6e bond with 2 metallatrane structures enabling a more extended conjugated electron system. In this 5c-6e bond, the central and terminal positions should be occupied by more electronegative elements, with less electronegative elements at the other two positions. Farnham *et al.* called the 5c-6e bond an extended hypervalent σ bond [35], because it is constructed by the combination of the two hypervalent $n_p \cdots \sigma^*$ 3c-4e metallatrane-like interactions through the central n_p orbital.

Such stabilized 5c-6e system can then be presented as $\sigma^* \cdots n_p \cdots \sigma^*$ extended hypervalent bonding. For instance, in bis(silyl)hydride niobocene complex $Cp_2Nb(SiClMe_2)_2H$ bearing an electron-withdrawing chloride substituent at silicon [36], direct interligand interaction causes the rehybridization at the silicon atom: the silicon orbital taking part in the five-center

six-electron $Cl\cdots Si\cdots H\cdots Si\cdots Cl$ bond develop more p character, and thus more s character is left for the bonding with other substituents, thus accounting for the shortening of the Nb-Si bond and the lengthening of the Si-Cl bond in $Cp_2Nb(SiClMe_2)_2H$. An approximate molecular orbital model which summarizes this 5c-6e idea developed by Nakanishi [37, 38] is shown in figure 6 below.
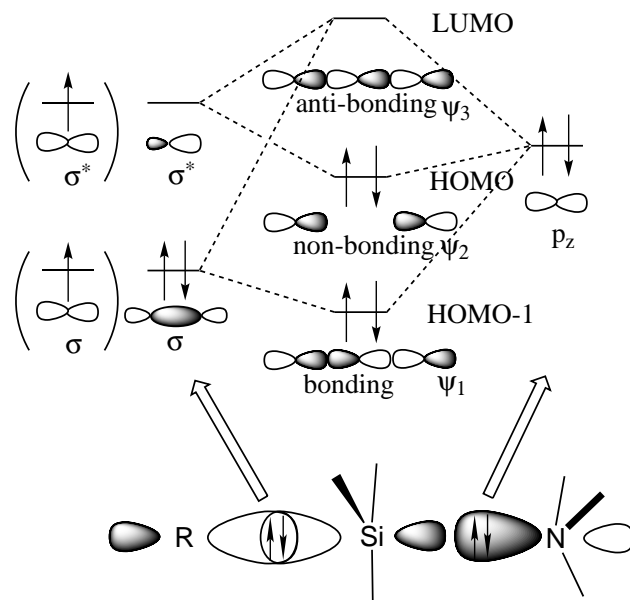
Figure 5: Molecular orbital diagram for 3c-4e bonding scheme
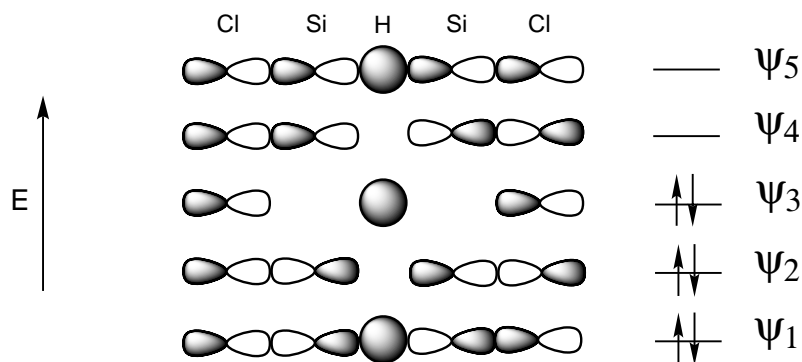
Figure 6: Approximate molecular orbital model of the 5c-6e bond

3.1.2 Electrooxidation of silatranes

To obtain a better understanding of the transannular dative bonding interaction between the silicon and the bridged nitrogen atom, the silatranyl radical cation is bound to attract attention. The silatranyl radical cation is expected to be formed when a silatrane loses one electron which would induce the electron density changes in this system and specifically at the level of transannular interaction between Si and N.
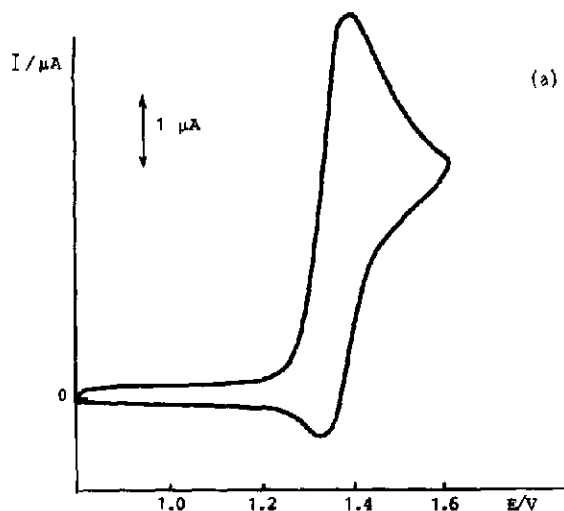
Figure 7: Cyclic voltammogram of 10^{-3} M solution of silatrane with R = C_2H_5 in ACN + TBAP on platinum electrode (scan rate 200 mV/s) at 20 °C [5].

The detection of the radical cation by cyclic voltammetry is very easy to achieve. In their 1993 paper, Broka *et al.* report [5] the electrochemical oxidation of silatranes using cyclic voltammetry and a rotating ring-disc electrode. A series of silatranes with different subsituents were studied by their method of cyclic voltammetry. The oxidation peak potentials are in the range 1.42-1.85 V (vs. SCE). The process is diffusion-controlled and proceeds by one-electron transfer. The results show that all silatranes exhibit irreversible electro-oxidation signals are at scan rates below 100 mV/s. When the scan rate increases, the process of oxidation for silatranes with R = CH_3, C_2H_5, CH_2=CH, C_6H_5 and *p*-Cl-C_6H_4 becomes partially reversible at the scan rate of 200 mV/s and room temperature (Figure 7). This suggests that cation radicals are created as the primary products of electro-oxidation and have relatively low stability. This process is coupled with chemical reactions with moderately low rate constants, which explains the irreversibility at low scan rates:
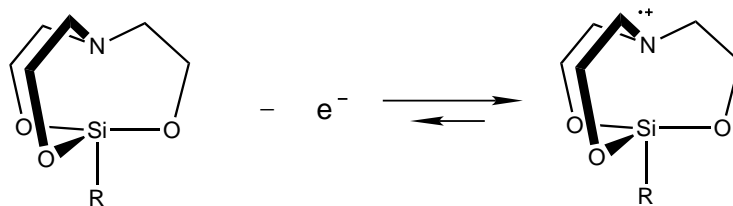
Scheme 1: Formation of radical cations of silatranes

The potentials of electro-oxidation are affected significantly by the electronic effects of the silane substituents (Table 2). Electron-donating substituents, by stabilizing the cation radical, facilitate electrooxidation, whereas electron-withdrawing subsituents shift the potentials of the

14

silatranes towards higher values.

Table 2: Electrochemical oxidation peak potentials[a] of silatranes [5]

Substituents of silatrane (R)	$E_p(V)$
H	1.70
CH_3	1.43
C_2H_5	1.42
CH_2Cl	1.85
OCH_3	1.53
OC_2H_5	1.53
Cl	not oxid
$CH_2{=}CH$	1.52
$HC{\equiv}C$	1.80
C_6H_5	1.55
p-C_6H_4Cl	1.60
2-furyl	1.45[b]
2-thienyl	1.60[b]
3-furyl	1.60[b]
3-thienyl	1.55[b]

[a] Experiments were carried out in ACN + 0.1 M TBAP. Working electrode was glassy carbon. All potentials vs. SCE.
[b] Voltammograms are ill-defined.
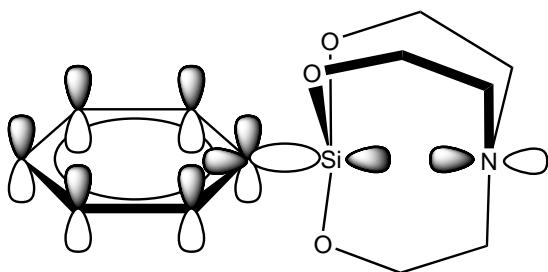
Figure 8: HOMO (atrane cage) and HOMO-1 (phenyl ring) orbital of silatranes (R = aryl)

Good correlations between the oxidation potentials and NMR data, as well as the pronounced effect of substituents (the value of $\rho_\pi^* = 0.4$ V shows that the reaction site might be close to the substituent), could be regarded as an argument that the nitrogen atom is the probable reaction site [5]. However, when considering the impact of the electronic effects of the substituent on the stability of cation radicals, it should be carefully taken into account that the p-orbital of aryl substitutents have no effect whatsoever on the 3c-4e silatrane bond. Indeed, p-orbital are oriented perpendicularly to the components of this dative bond, and therefore cannot have any interaction with them. In other words, mesomeric effects are not the actors

in such systems and can be ignored. In this context, an aryl substitutent would have a very similar effect as that of an alkyl substitutent (see Figure 8).

3.2 Electrooxidation of germatranes

Some previous work done in our laboratory must be mentioned as it set the direction of my work. Germanium derivatives are another large family of metallatranes. They were first synthesized in 1965 by Mehrotra and Chandra [39] and were widely studied in many aspects. Similarly to the parent silatranes, the intramolecular coordination between N and Ge atoms of the germatranes caught many attentions as the subject of studies, by structural characterization, NMR, mass-spectroscopy, UV, dipole moments measurements and other physico-chemical properties determinations as well as synthesis and chemical reactivity of germatranes.

1	R = H
2	R = *o*-Br
3	R = *m*-Br
4	R = *p*-Br
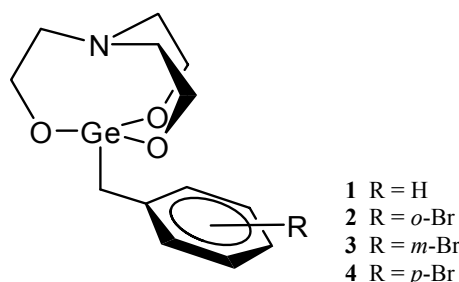
Figure 9: Germatranes **1-4**.

A great deal of the reported works confirm that the most important practical properties of germatranes are certainly those related to their versatile and high biological activity [2, 3, 4]. A series of ring-substituted bromobenzyl germatranes were studied in our laboratory. The electrooxidation of the germatranes (**1-4**) (Figure 9) and of the model compounds **6** and **7** (Figure 10) in CH_3CN and DMF solutions was studied [33]. All four germatranes studied show a distinct oxidation peak (Figure 11). Peak currents i_p for **1-4** are linear with the germatrane concentration and, for $v > 0.5-1$ V/s, with the square root of the scan rate ($i_p/v^{1/2} = \text{const.}$, Figure 12), thus suggesting diffusional control of the process. The electron stoichiometry for the first step of oxidation in all cases was determined either from direct comparison of the limiting currents of the germatrane and ferrocene, taking no account of the difference in their diffusion coefficients D, or combining voltammetry parameter $i_p/v^{1/2}$ with the Cottrell slope obtained from chronoamperometry at the same electrode and the same solution [40]. Beyond the lowest scan rates ($v \geqslant 0.2 - 0.5$ V/s) both methods provide the n values close to 1.
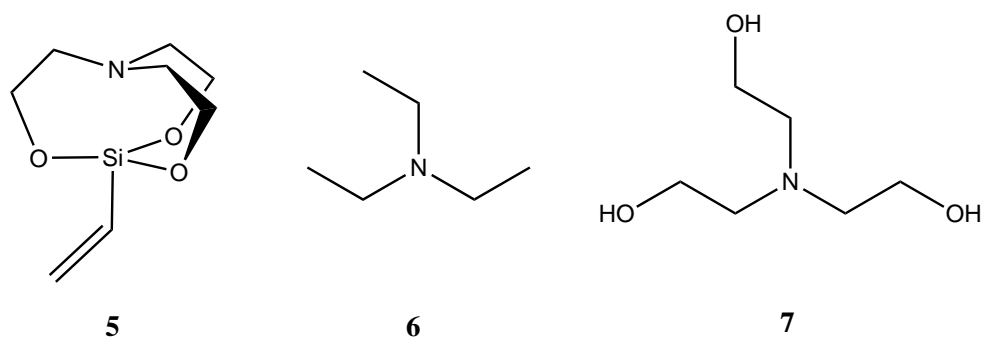
Figure 10: The model compounds **5**, **6** and **7**.

In the publication, the authors also pointed out [33] that a reverse peak appears on the voltammograms of the non-substituted **1** and, to a lesser extent, of *p*-Br benzylgermatrane (**4**) at higher scan rates (Figure 13). Because the oxidation peaks of both compounds are too large ($E_p^a - E_p^c = 118$ and 110 mV for **1** and **4**) to correspond to a perfectly reversible redox couple, the process can rather be characterized as a quasi-reversible one.
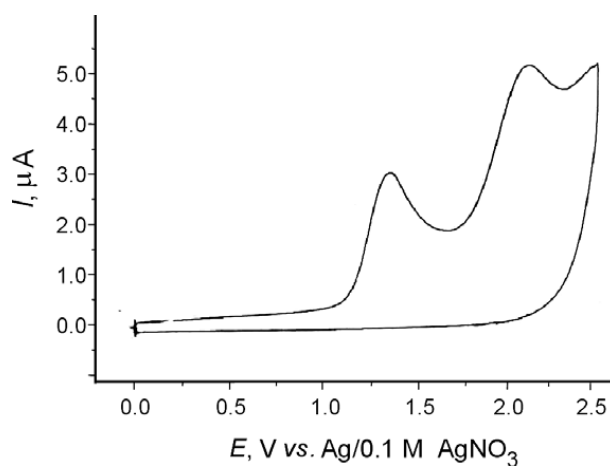
Figure 11: Cyclic voltammogram of **3** (C = 2 mmol/L) in $CH_3CN/0.1$ M Bu_4NPF_6 at a 0.7 mm glassy carbon electrode. v = 10 V/s; T = 22 ^{o}C.

17
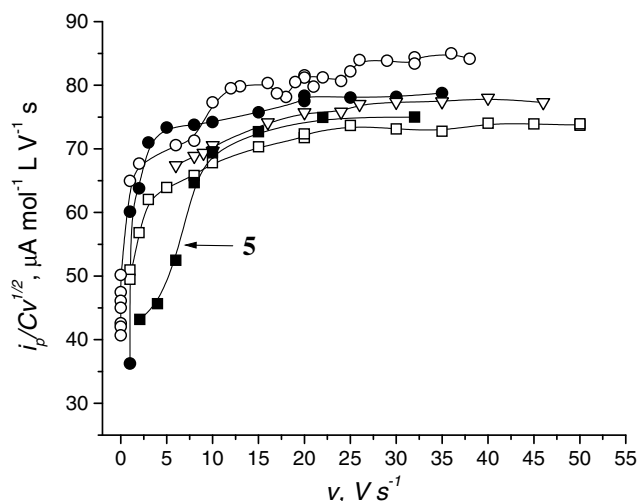
Figure 12: Normalized oxidation peak currents $i_p/\mathrm{C}v^{1/2}$ of: (○) -**1**; (●) -**2**; (▽) -**3**; (□) -**4**; (■) -**5**. Voltammetry at GC disc electrode, in $\mathrm{CH_3CN}/0.1$ M $\mathrm{Bu_4NPF_4}$.

Triethylamine (**6**) and triethanolamine (**7**) as comparisons also were studied by cyclic voltammograms and compared with four germatranes. In **6** and **7**, as is reflected by the trend in E_p (Table 3), the basicity of N is higher than in germatranes for the reason of N→Ge interaction in the latter, thus the protonation rate of **1-4** is slower. Also, slightly higher oxidation potentials of the germatranes versus E_p of silatranes [5] indicate larger involvement of the lone pair of N in N→Ge relative to N→Si dative interaction; consequently, this site is less available for oxidation and protonation.

yr
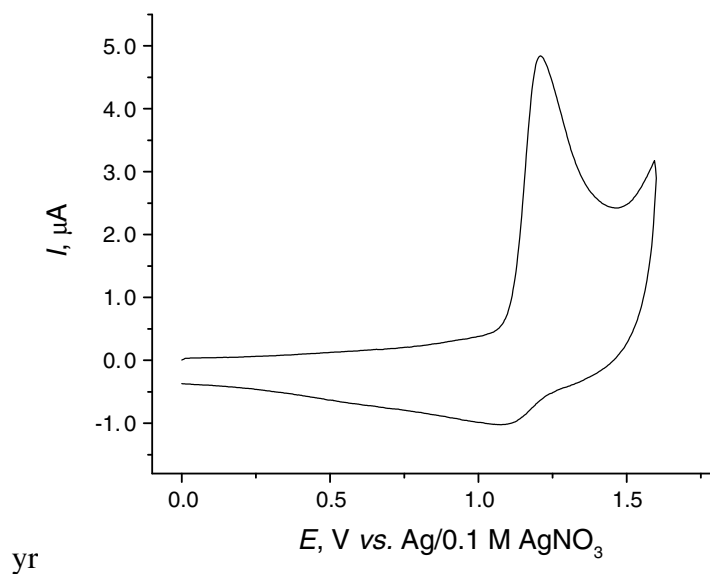
Figure 13: Cyclic voltammogram of **1** (C = 0.8 mmol/L) in $\mathrm{CH_3CN}/0.1$ M $\mathrm{Bu_4NPF_6}$ at a 0.7 mm glassy carbon electrode. v = 32 V/s; T = 22 ^{o}C.

The results of cyclic voltammetry combined with DFT B3LYP/6-311G calculations, have

shown that donor activity of the nitrogen atom is substantially reduced because of the dative N→Ge bond coordination compared to Et_3N and $(HOCH_2CH_2)_3N$.

Further, Soualmi *et al* [34] reported electrochemical oxidation of 1-substituted germatranes **1**, **4**, **8**, **9**, **10** and **11** (Figure 14) occurring via an electrochemically reversible electron transfer and resulting in germatrane cation radicals that were detected by cyclic voltammetry and studied by real time CW EPR - spectroelectrochemistry.

The involvement of $n(p_z)$ electrons of the atrane nitrogen into intramolecular N→Ge dative coordination substantially reduces the ease of electron withdrawal during the oxidation of germatranes (by about 500-600 mV) compared to parent tertiary amines and by about 70-100 mV compared to silatranes so far studied by cyclic voltammetry.

Table 3: Parameters of anodic oxidation of germatranes **1-4** and of the model compounds at a GC disc electrode

Cmpd	E_p (V)[a]		$E_p - E_{p/2}$ (V)		$\Delta E_p/\Delta lg(v)$ (mV)	
	CH_3CN	DMF	CH_3CN	DMF	CH_3CN	DMF
1	1.209		59		37	
2	1.285		101		45	
3	1.276		109		39	
4	1.236	1.364	83	74	33	34
5	0.774	0.795	169	124	36	41
6	0.582	0.888	193	145	64	
7	1.126		497		98	

n	E^o(V)	k_s^b	α^c	IP (eV)	σ^{*d}
1.1	1.149	11.1	0.80	6.016	1.526
1.0	1.237	4.1	0.57	6.238	1.994
1.0	1.225	2.0	0.60	6.225	1.703
0.9	1.202	4.4	0.74	6.105	1.660
1.0					
0.9					
0.9					

[a] Peak potential at v = 1 V/s vs. Ag/0.1 M $AgNO_3$ in CH_3CN.
[b] $k_s \times 10^2$ in cm/s.
[c] Transfer coefficient estimated as a mean of α from $\Delta E_p/\Delta lg(v) = 29.6/\alpha$ and $E_p - E_{p/2} = 1.85RT/\alpha F$ [41].
[d] Group inductive constants calculated according to $\sigma^* = 7.84\sum\{\Delta\chi_i(R_i/r_i)^2\}$ [42].
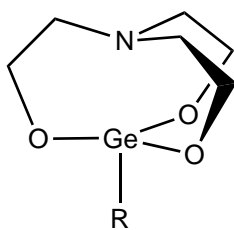
R = *o*-F-C$_6$H$_4$- (**8**), *o*-Br-C$_6$H$_4$- (**9**), *p*-Et$_2$N-C$_6$H$_4$- (**10**), *p*-Me$_2$N-C$_6$H$_4$- (**11**)

Figure 14: 1-Substituted germatranes **8-11**.

The values of nitrogen *hfc* constants in their EPR spectra are $a_N = 18 - 19$ G, this result shows a remarkable feature of aryl germatranes in the form of cation radicals that the nitrogen atom of atrane is practically planar. This is very typical for planar N-centered radicals. There is a difference of about 40 times of axial and equatorial α-methylene protons in the cation radicals in their response to the magnetic field. Neither is any contribution from Ge nor from the aromatic ring seen in the spin delocalization. While the N atom remains flat, the Ge atom in the cation radical of aryl germatranes is no more on but out of the $Ge(-O)_3$ plane.
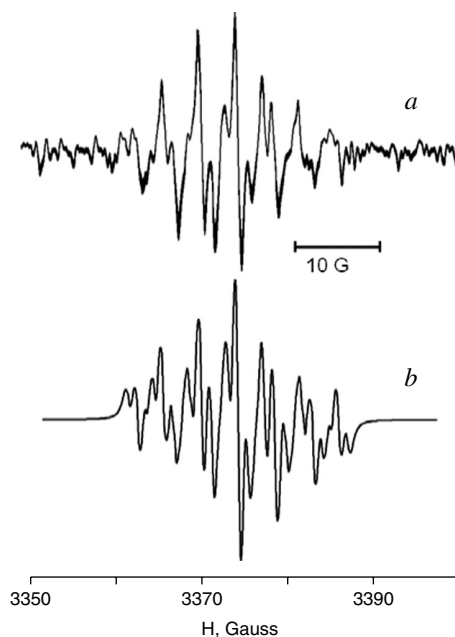
Figure 15: EPR spectrum of the cation radical of benzyl germatrane generated in CH_3CN–0.1 mol/L Bu_4NPF_6 at $E = 0.85$ V: (*a*) experimental and (*b*) simulated using the parameters in the text. Modulation amplitude $a = 0.4$ G; $T = 233$ K [34].

For the cation radicals of benzyl germatranes, we found quite a different spin distribution as shown followed: the aromatic system altogether with an "electron bridge" $\sigma(C–Ge)$ orbital accommodate the major part of the spin density while only a small part of it is residing on N

atom. Neither EPR spectroscopy (Figure 15) result nor DFT calculations congregate in that the atrane nitrogen in the cation radical adopts an *exo*-configuration. On the other hand, a remarkable molecular motion around Ge atom occurs which provides it much flatter and more similar to trigonal bipyramid. This is on the contrary to what was found for the cation radicals of aryl germatranes. For that we could summary that the main driving force determining the geometry of these species is that the 3c-4e bond $N–Ge–C_{sp2}$ upon oxidation and favored metal pentacoordination in the cation radicals of germatranes because of the importance of the interactions of Ge with its environment and with all three O atoms.

A distonic cation radical could be formed when nitrogen atom of atrane part 3c-4e bond (Ge–C fragment) has no possibility for lateral overlapping by its conjugative preferences and remains the unpaired electron. Because the conjugation is cut off by orthogonal orientation of the susceptible to conjugative interactions orbital of the substituent. If this N–(Ge–C) center is available for further conjugation, spin delocalization will find a new configuration which is more stable and spin density will shift to the aromatic system and only very small amount of it still seeing the atrane N atom. Thus the formation of distonic cation radicals observed for aryl germatranes might reflect a typical feature for the germatranes substituted with the groups "ending" electron transmission by the absence of further conjugation: aliphatic, vinyl and ethynyl substituents. If so, electrochemistry will provide a new insight into the electronic interactions in these compounds and open possibilities for designing molecular electronic devices with specific electronic, electromechanic and optical properties [34].

3.3 Stannatranes

In contrast to silatranes or germatranes, stannatranes have attracted much less attention than their lighter congeners in the family of metallatranes. Compared to Si or Ge atoms, Sn has evident strong metal properties and much larger atomic diameter. However, the presence of the transannular bond beween N and Sn in stannatranes was well established; moreover, the bond strength even slightly increases in the order Si < Ge < Sn [43].

$$Sn(O\text{-}t\text{-}Bu)_4 \quad + \quad N(CH_2CMe_2OH)_3 \xrightarrow[\text{-3 } t\text{-BuOH}]{\text{toluene}}$$
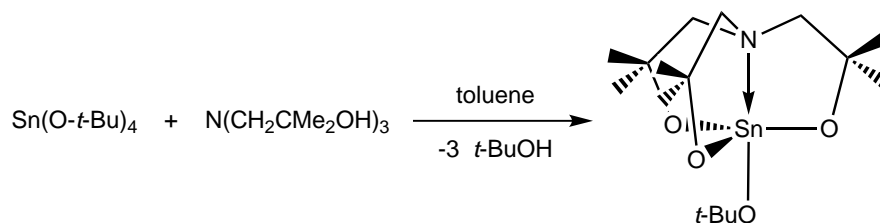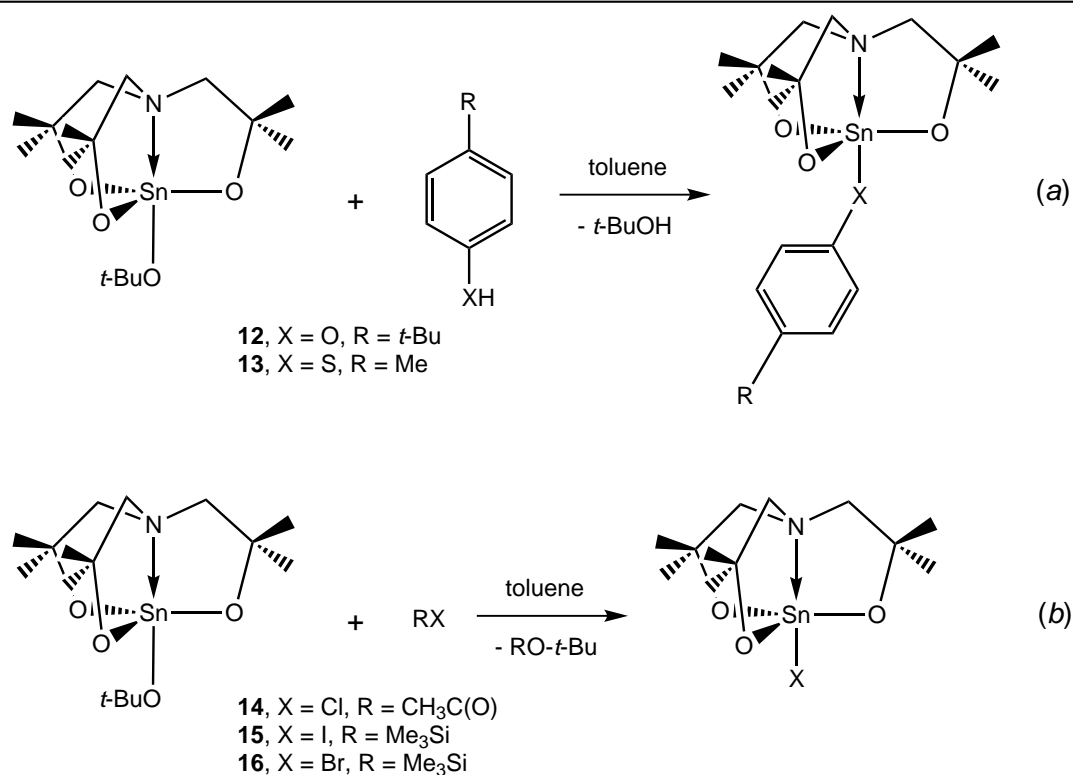
Scheme 2: Synthesis of *t*-butoxystannatrane

Whithin the cooperation with professor K. Jurkschat and his team at the department of inorganic chemistry in Technical University of Dortmund, a series of the stannatrane deriva-

tives of the type $N(CH_2CMe_2O)_3SnX$ have been synthesized and studied by XRD and cyclic voltammetry. Notably in this series of stannatranes, there is no tin-carbon bond as the atom connecting tin atom with the substituent is either 15 group element (O or S) or halogen. This feature is responsible for the nontoxicity of these compounds. Inorganic stannatranes of this type that lack any tin−carbon bond are scarce [44, 45, 46, 47] so it is interesting to investigate their structure and electrochemical properties.

The starting precursor of stannatrane was tin tetra-tertbutoxide, $Sn(O-tBu)_4$, which, reacting with tris(2-hydroxy-2-methyl-propyl)-amine, $N(CH_2CMe_2OH)_3$, gave the product t-butoxystannatrane as the starting material for the synthesis of a variety of inorganic stannatranes (Scheme 2).

12, X = O, R = t-Bu
13, X = S, R = Me

14, X = Cl, R = $CH_3C(O)$
15, X = I, R = Me_3Si
16, X = Br, R = Me_3Si

Scheme 3: Synthesis of stannatranes **12-16**.

The t-butoxystannatrane is highly sensitive to moisture, well soluble in dichloromethane, tetrahydrofurane, and diethylether and show moderate solubility in toluene and benzene. Thus, in an acid−base type reaction the treatment of the t-butoxystannatrane with p-tBu phenol, 4-methyl thiophenol gave the stannatranes **12** and **13**, respectively, in high yields (Scheme 3 (a)). The synthesis of the halogenido-substituted stannatranes **14-16** was achieved by the reaction of t-butoxystannatrane with acetyl chloride, $CH_3C(O)Cl$, and trimethylhalogenido silanes, Me_3SiX (X = Br, I), respectively (Scheme 3 (b)).

The five stannatranes are colorless or yellowish crystalline materials. Notably, on expo-

sure to air and light the color of the iodido-substituted stannatrane **15** changed to yellow. All compounds are soluble in benzene, toluene, dichloromethane and tetrahydrofurane, but at room temperature the chlorido and bromido derivatives **14** and **16** are only well soluble in dichloromethane or chloroform.

3.4 Radical cations of metallatranes (theoretical considerations)

Metallatranyl cations are of peculiar interest because they help to better understand the molecular structures and hypervalent bonding in the molecules of metallatranes. Belyakov *et al.* in 1999 [48] pointed out that the attractive interaction N-M(X) in atranes $XM(Y–CH_2–CH_2)_3N$ originates from the donation of the lone pair of the nitrogen atom into the antibonding $\sigma^*(M–X)$ orbital. This claim would imply that the N–M bond strength to depend on the electronegativity of the axial substituent X [30]. However, there is another approach, which states that the Coulomb interaction of the oppositely charged germanium and nitrogen atoms gives the major contribution to N–Ge bonding in germatranes [49]. Hence figuring out the structure of the corresponding cations would help to have a further knowledge about the interaction of M–X.
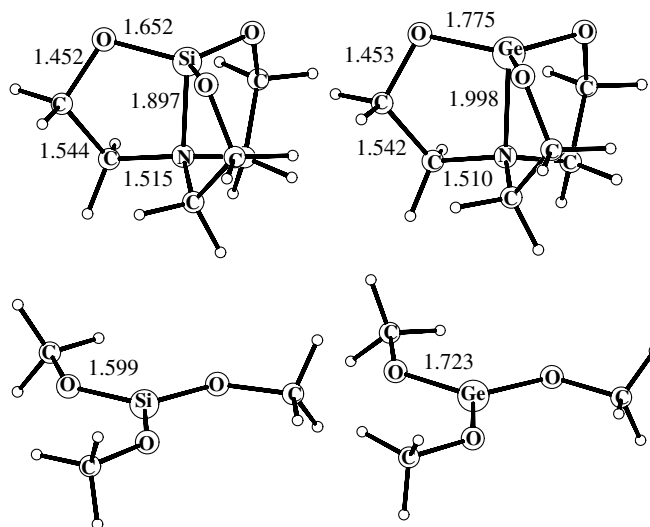
Figure 16: Equilibrium structures obtained by DFT calculations at the B3LYP/cc-p-VDZ level of theory of silatranyl and germatranyl cations and corresponding classical cations [50].

Sundius *et al.* in 2007 [50] carried out a series of calculations on the equilibrium structures of silatranyl and germatranyl cations as well as of corresponding fluoroatranes using DFT calculations at B3LYP/cc-p-VDZ level of theory, and analyzing ongoing changes in the bonding from germatranyl cation to a neutral molecule by using the NBO method. In the publication of this group, the electronic structure of the germatranyl cation is discussed. By comparing its structure with those of halogermatranes they try to analyze the changes in the transannular N–Ge bond induced by the evolution from neutral molecule to a cation [50]. From the

23

theoretical calculations, it is shown that loss of fluorine substituent shortens the interatomic distances of M–N and M–O (Figure 16). The cation M becomes tetracoordinated and the M–N bond formally becomes one of the sp^3 hybrid bonds. This inversion of the configuration at M demonstrates itself in the increase of the N–M–O bond angle which becomes larger than 90° [50].

By comparison with "classic" cations ($(CH_3O)_3Si^+$ and $(CH_3O)_3Ge^+$, for which bond lengths are shown in figure 16), M–O bonds in atrane cations are substantially lengthened (Figure 16). The shortening of M–O interatomic distances in "classic" cations may be explained by the charge transfer from oxygen lone pairs to the vacant p-orbital of M atom. On the other hand, the vacant p-orbital in the atrane cations is involved in N–Si bonding. This significantly decreases the stabilizing interaction between the oxygen lone pair and the vacant p-orbital of the metal [50].

Sundius *et al.* also considered the change of natural bond orbital and their interactions upon the transition from the germatranyl cation to the 1-fluorogermatrane which were revealed by the NBO analysis. The result showed that Ge–N bonding displays a larger covalent character in the cation and it may explain the identity of NBO as well as Mulliken positive charges on M in the germatranyl cation and in the 1-fluorogermatrane: the increase of positive charge on M upon the formation of a bond with fluorine is compensated by the increase of electron density in a M–N bond.

The study of orbital interactions in the germatrane cation radicals has been carried out in our laboratory previously using DFT B3LYP/ 6-311G calculations on a series of germatranes [34].
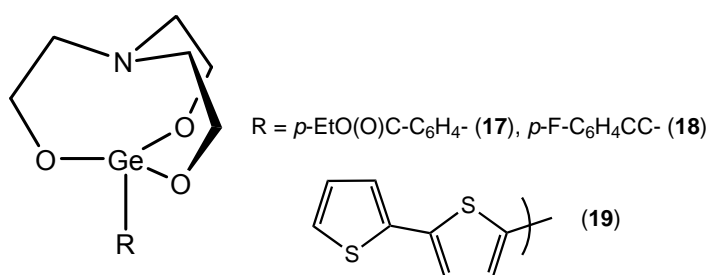
Figure 17: Germatranes **17-19**.

The analysis of the electrochemical reactivity, DFT calculations and the results of electrolysis show that the reaction center of the oxidation of the germatranes **1** and **17**, **8**, **9** and **18** is localized on the atrane N atom. Its n-electrons bring the main contribution to the HOMO of these compounds, though they are pointed towards Ge and hidden inside the atrane cage (Figure 18). The cation radicals of these germatranes exist in *endo*-configuration, the geometry around Ge atom being closer to trigonal bipyramid than in the neutral molecule. The

change of entropy ΔS, noticed using harmonic frequency analysis of **1** and **1**$^{+\bullet}$, has shown that the molecular geometry itself does not undergo substantial structural reorganization upon oxidation. Thus, the somewhat slow electron transfer kinetics of the oxidation of germatranes is mostly due to the solvent reorganization following remarkable charge redistribution in the cation radicals and not to a flip-flopping of N between *exo-* and *endo-* configurations.

Figure 18: HOMO of **1**, **10** and **19** according to B3LYP/6-311G

If a substituent with low own ionization energy ($Et_2NC_6H_4$, thienyl) is present in the germatrane molecule, the reaction center of oxidation is localized on this substituent and the atrane moiety only acts as a weak electron-donor substituent (Figure 18). When the atrane moiety itself undergoes the electron withdrawal, the germatranes follow an electrochemically reversible oxidation with a fas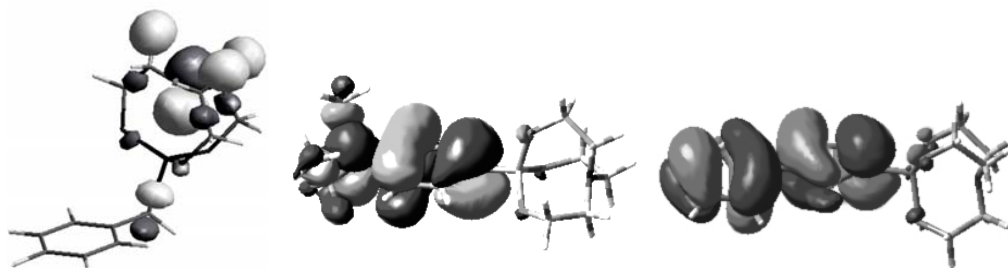t deprotonation of the cation radical, with the kinetics of this process being modulated by the electronic properties of the substituents at Ge. At higher scan rates, however, the electron transfer kinetics becomes the limiting factor impeding the observation of cation radicals. The deprotonation of the α-carbon atom of the atrane cage allows anodic substitution at this position, in particular with CN^- anion [33].

3.5 Supporting electrolytes

In our work, we considered a not so related to metallatrane chemistry, but very important for organometallic electrochemistry, issue of non-cooridinating, and non-nucleophilic supporting salts for electrochemistry. Here is a short exposition of this problem.

The importance of supporting electrolytes in electrochemistry is well recognized and needs not to be advocated [51]. Major requirements for these systems usually follow from their role in the electrochemical processes (but not limited to): to be not electroactive (within the range of potentials used), to provide an ionic dissociation and conductivity much larger than those due to the analyzed electroactive species added to the electrolyte and to have good solubility, chemical and electrochemical inertness, the ease of separation from the products of electrolyses and, in many cases, specific interactions with the electroactive substrates, electrogenerated intermediates or with the electrode (Li^+, Me_4N^+ and higher teraakylammonium salts, ionic liquids, Ph_4B^-, perfluorinated arylborates $(C_6F_5)_4B^-$ and $[(CF_3)_2C_6H_3]_4B^-$, $((CF_3)_3CO)_4Al^-$ etc)

[52, 53, 54, 55]. Stabilization and observation of electrophilic electrogenerated intermediates is often only possible using the supporting salt with an appropriate non-nucleophilic anion. In the case of weak interactions of the anions of supporting electrolyte with the analyte species of large size and delocalized charge, ion pairing occurs; this phenomenon was widely explored by cyclic voltammetry through the modification of ΔE ($E_2 - E_1$) potentials of successive electron transfers [56, 57, 58]. When electrophilic center is more localized, coordinating and even covalent interactions occur.

Silicon is less electronegative than carbon (Figure 19) and due to this virtue, organosilanes are almost always bearing a positive partial charge $+\delta$ centered on the silicon atom, which makes it very vulnerable to coordinating effects or nucleophilic substitution 2 (S_N2) and like other attacks from the nucleophilic species. This is even truer for siliconium cations and related species, often produced in anodic reactions of silicon organic compounds.

For this reason, even more than for most organic compounds, the electrochemistry of organosilanes requires the choice of a non-coordinating electrolyte; specifically, the choice of an appropriate non-nucleophilic counterion is often crucial [59].
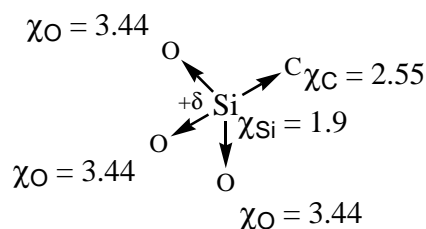
Figure 19: Electronegativity of Si center and other atoms in organosilanes (χ is the electronegativity using the Pauling scale) [60].

In particular, the sensitivity of alkoxysilanes to fluorides is well known. Fluoride containing anions like BF_4^-, PF_6^-, SbF_6^- actually exist in an equilibrium between said anion and free fluoride with the corresponding tri- or penta-coordinated neutral species, e.g. $PF_6^- \rightleftarrows PF_5 + F^-$. Given the very strong affinity of Si for fluoride anions, the use of such anions should therefore be avoided with organosilanes in most cases (except, naturally, when Si-F bond formation is the very effect the electrochemist wants to induce). We therefore looked for an alternative non-nucleophilic ionic system than might serve as supporting electrolyte under these conditions.

EXPERIMENTAL SECTION

4   Experimental Section

4.1   Solvents, supporting electrolytes

All the solvents that we used for either chemical syntheses or electrochemical tests were of analytical reagent grade purity (more than 99%). Acetonitrile (99.99%, Fisher Scientific), dichloromethane (> 99.95%, SDS), toluene (99.5%, VWR) and DMF (99.8%, VWR) dried by stirring them with calcium hydride followed by distillation under argon, and stored over molecular sieves 3Å, 8 to 12 mesh (ACROS); THF (99.9%, VWR) was distilled from sodium benzophenone ketyl.

$TBAPF_6$ (98%, ACROS) was used as the supporting electrolyte in cyclic voltammetry and chronoamperometry. It was dried by stirring the powder for 1h under high vacuum at 60 °C then stored under argon.

4.2   NMR spectroscopy

The ^{1}H and ^{13}C NMR spectra were recorded on Bruker ARX (300 MHz and 500 MHz) spectrometers. TMS (0.00 ppm) was used as internal standard for ^{1}H NMR chemical shifts in all solvents. The ^{119}Sn NMR spectra was recorded at the Regional Center of Physical Measurements of the West (CRMPO) on a Bruker AM 400 WB spectrometer. Me_4Sn was used as the internal standard reference (0.00 ppm). In ^{13}C NMR, chemical shifts were reported in ppm relative to the central line of the triplet of deuterated chloroform ($CDCl_3$, 77.16 ppm).

4.3   Gas chromatography (GC-MS)

The GC-MS spectra were recorded on a Hewlett-Packard 5890 Series II gas chromatograph, coupled to a Hewlett-Packard 5972 Series mass selective detector (70 KeV ionizing voltage).

4.4   X-ray crystallography (XRD)

X-ray crystallography was performed on Bruker SAINT [61]. The cell refinement was carried on Bruker SMART [61]; the structure was solved with the program(s) SIR97 [62] and was refined with the program(s) SHELXL97 [63] and the molecular graphics was processed with ORTEP-3 for Windows [64]. All the X-ray experiments were done by Thierry Roisnel and Vincent Dorcet (Institut des Sciences Chimiques de Rennes UMR 6226).

4.5   Electrochemical techniques

The electrochemical properties of the metalatranes were studied by cyclic voltammetry (CV), chronoamperometry, large-scale electrolysis and electron paramagnetic resonance (EPR) cou-

pled with cyclic voltammetry.

4.5.1 Cyclic voltammetry and chronoamperometry

Voltammetric and chronoamperometric experiments were performed using a PARSTAT 2273 potentiostat controlled by the PowerSuite sofware. A glassy carbon disc of 3 mm diameter or a 1 mm Pt disc was used as working electrodes. To assure the reproductivity and precision of the measurements, the working electrode was carefully polished and washed with acetone before each measurement. The counter electrode was platinum plate with 1 cm^2 surface area. The 0.1 M tetrabutylammonium hexafluorophosphate ($TBAPF_6$) solutions in acetonitrile CH_3CN, dichloromethane CH_2Cl_2 and DMF, were used as supporting electrolytes. The reference electrode was a stainless steel rod with a deposited layer of polypyrrole which was put into an electrolyte bridge filled with an inert electrolyte $TBAPF_6$ solution (0.1 M). The polypyrrole deposited reference electrode provides a stable and precise potential value [65]. IR-compensation facility of the potentiostat was always used to account for ohmic drops in the solution. To correct the experimental potentials, at the end of every experiment we added ferrocene and plotted its voltammogram. $E^0_{(Fc^+/Fc)} = 0.247$ V vs. SCE was used as the reference [66]. All the experiments were carried out under argon atmosphere at the room temperature of 20 °C.

4.5.2 Electrolyses

The electrolyses have been performed under argon atmosphere, at room temperature, in 50 ml cell equipped with a magnetic stirrer (Figure 20). The working electrode was made of glassy carbon fiber as it has the maximum working surface and a platinum wire electrode was used as reference. The counter electrode was put into small chamber with an electrolyte bridge at the bottom, which itself was placed in another bigger chamber with an electrolyte bridge as well. The glassy carbon fiber and platinum wire were fixed outside the bigger filter chamber and plunged into the 50 ml glass container mentioned above. The counter electrode was separated from the cathodic compartment by two electrolyte bridges in order to avoid migration of the product from the anodic reaction to the catholyte; the space between two chambers provided a static environment, mass transfer in which was effected only by slow natural diffusion.

4.5.3 Electron Paramagnetic Resonance (EPR) spectroscopy

EPR spectra were registered on a Bruker EMX (X-band) spectrometer with a Gunn diode operating at the working frequency 9.46 GHz, coupled with a standard rectangular cavity. The modulation frequency was 100 kHz, g-factors were corrected using DPPH as standard.
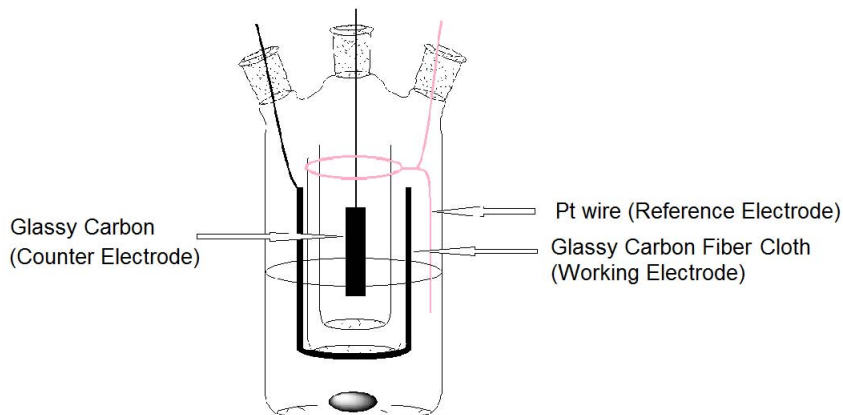
Figure 20: Electrolytic cell.

Microwave power was adjusted to 2-8 mW to maintain the EPR signal intensity below power saturation. EPR capillary spectroelectrochemical cell was a three-electrode version of the cell described in [67]. Post-processing and simulation of the EPR spectra were carried out using WINEPR System and WINEPR SimFonia software provided by Bruker [68][69].

4.6 Syntheses of silatranes and related products

4.6.1 Silatranes

To obtain the 1-R-substituded silatranes, we used a typical procedure reacting triethanolamine with the corresponding organotrichlorosilane. The Si–Cl bond is very easy to hydrolyze, hence this reaction goes very quickly even at room temperature. However, the main drawback of chlorosilanes as starting material is that they require extremely anhydrous conditions, since water, even in trace quantities, would be a much more potent nucleophile than alcohols. Triethanolamine was added to trichlorosilane under argon atmosphere and the reaction performed, leading to formation of our product and hydrochloric acid. For this reason, triethylamine was added as well, to neutralize said hydrochloric acid (Scheme 44.5.2). Using this method, tolyl, 1-naphthylmethyl, *t*-butyl and 2-cyanoethyl silatranes were synthesized using dichloromethane as a solvent.

   Tolylsilatrane. In a 50 ml Schlenk flask flushed with argon, *p*-tolyltrichlorosilane (2.26 g, 10 mmol) was dissolved in 30 ml of dry dichloromethane. In another Schlenk flask, triethanolamine (1.49 g, 10 mmol) and triethylamine (3.04 g, 30 mmol) were dissolved as

$$RSiCl_3 + N(CH_2CH_2OH)_3 \xrightarrow[3\ N(CH_2CH_3)_3]{OH^-} \text{(silatrane)} + 3\ N(CH_2CH_3)_3 \cdot HCl$$
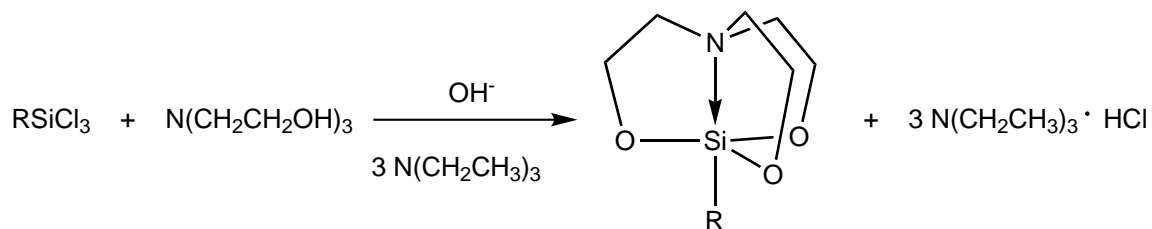
R = tolyl, 1-naphthylmethyl, *t*-butyl, 2-cyanoethyl

Scheme 4: Condensation of trichlorosilane and triethanolamine

well in 10 ml of dichloromethane under argon; the latter solution was then added slowly into the *p*-tolyltrichlorosilane solution under vigorous stirring. The reaction was exothermic, HCl was formed. The solution was stirred overnight (more than 12 h). A side product $N(CH_2CH_3)_3 \cdot HCl$ precipitated at the end of the reaction and filtered off on Celite; the solvent was then evaporated from the filtrate. The residue was purified by column chromatography (eluent: CH_3CN/CH_2Cl_2, 2 : 1 v/v) to give lightly colored tolylsilatrane in 70% yield. The product was recrystallized from acetonitrile to afford lightly colored, needle-shaped crystals.

^1H NMR (300 MHz, $CDCl_3$, 298K): δ_H: 7.596 (2H, d, J = 7.934 Hz, $2(CH_3CCH)$ **14,16**), 7.069 (2H, d, J = 7.422 Hz, $2(SiCCH)$ **13, 17**), 3.880 (6H, t, J = 5.873 Hz, $3(OCH_2)$ **3, 7, 10**), 2.904 (6H, t, J = 5.877 Hz, $3(NCH_2)$ **4, 6, 9**), 2.275 (3H, s, CH_3 **18**); ^{13}C NMR (75 MHz, $CDCl_3$, 298K): δ_C: 138.0, 137.2, 134.0, 128.1, 57.8, 51.2, 21.4;
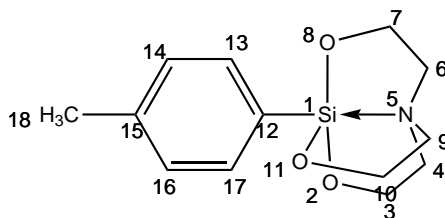
1-Naphthylmethylsilatrane. The procedure is the same as described for tolylsilatrane, with 1-napthylmethyltrichlorosilane (2.76 g, 10 mmol), triethanolamine (1.49 g, 10 mmol) and triethylamine (3.04 g, 30 mmol) as starting materials. Crystallization from CH_3CN and gave 2.14 g of 1-naphthylmethylsilatrane (68% yield) as colorless needle-shaped crystals.

^1H NMR (300 MHz, $CDCl_3$, 298K): δ_H: 8.296 (H, m, CH **22**), 7.760 (H, m, CH **19**), 7.526 (H, m, CH **16**), 7.371 (4H, m, 4(CH) **14, 15, 20, 21**), 3.712 (6H, t, J = 5.843 Hz, $3(OCH_2)$ **3, 7, 10**), 2.751 (6H, t, J = 5.841 Hz, $3(NCH_2)$ **4, 6, 9**), 2.46 (2H, s, CH_2Si **12**); ^{13}C NMR (75 MHz, $CDCl_3$, 298K): δ_C: 140, 133.7, 132.5, 128, 126.4, 126.2, 125.4, 124.6, 124.1, 123.8, 57.7, 51.2, 22.9;
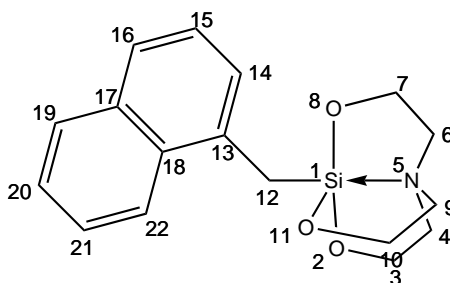
***t*-Butylsilatrane.** Same procedure as described for tolylsilatrane, with *t*-butyltrichlorosilane (0.29 g, 1.51 mmol), triethanolamine (1.10 g, 7.4 mmol) and triethylamine (2.24 g, 22.2 mmol) as starting materials. Crystallization from CH_3CN gave 0.23 g of *t*-butylsilatrane (65% yield).

^1H NMR (300 MHz, $CDCl_3$, 298K): δ_H: 3.707 (6H, t, J = 5.730 Hz, $3(OCH_2)$ **3, 7, 10**), 2.745 (6H, t, J = 5.720 Hz, $3(NCH_2)$ **4, 6, 9**), 0.895 (9H, s, $C(CH_3)_3$ **13, 14, 15**); ^{13}C NMR (75 MHz, $CDCl_3$, 298K): δ_C: 58.5, 51.8, 27.7, 19.4;
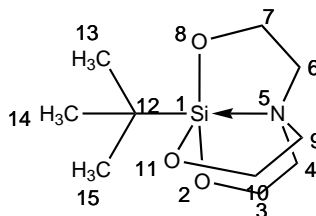
2-Cyanoethylsilatrane. The procedure is the same as described above, with starting materials 2-cyanoethyltrichlorosilane (0.61 g, 3.24 mmol), triethanolamine (0.48 g, 3.24 mmol) and triethylamine (0.98 g, 9.72 mmol). Crystallization from CH_3CN gave 0.47 g of the product 2-cyanoethylsilatrane (63.5% yield) as light yellow platy crystals.

^1H NMR (300MHz, $CDCl_3$, 298K): δ_H: 3.758 (6H, t, J = 5.875 Hz, OCH_2), 2.828 (6H, t, J = 5.873 Hz, NCH_2), 2.360 (2H, m, CH_2CN), 1.225 (2H, t, J = 7.109 Hz, $SiCH_2$); ^{13}C NMR (75 MHz, $CDCl_3$, 298K): δ_C: 123.2, 57.3, 51.0, 12.8, 8.4.
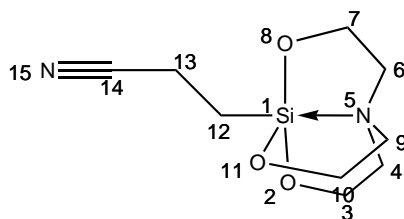
For some compounds, no trichlorosilyl derivatives were available commercially. To obtain these silatranes, we synthesized them by transesterification from trialkoxylsilane and triethanolamine. Silaphilic fluoride ions were added in catalytical quantities in the form of tetrabutylammonium fluoride because they are well-known reactants for the cleavage of organosilanes (typically for deprotection of alcohol groups); they were used here to trigger transesterification. The fluoride ion attacks the silicon atom, creating a penta-coordinated Si center. Thus activated silicon quickly undergoes transesterification with triethanolamine (Scheme 5).
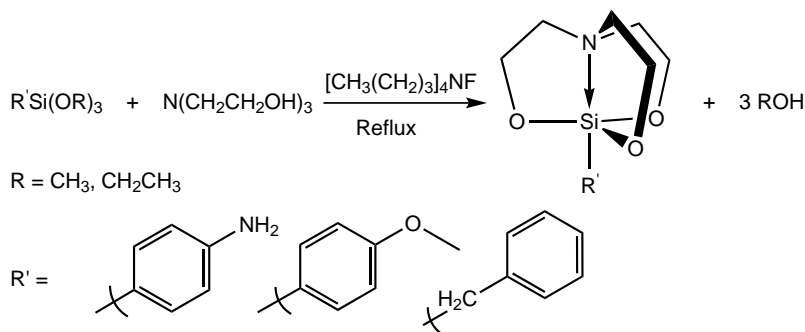
Scheme 5: Synthesis of silatranes by transesterification.

This method was applied to synthesize *p*-aminophenyl, *p*-methoxylphenyl and benzyl sila-trane using acetonitrile as solvent.

***p*-Aminophenylsilatrane.** In a 50 ml Schlenk flask flushed by argon atmosphere, *p*-aminophenyltrimethoxysilane (0.21 g, 1 mmol) was dissolved in 50 ml CH_3CN and 1% (0.3 ml) tetrabutylammonium fluoride (1 M in THF) was added to the solution above. The Schlenk flask was put into the oil-bath and heated to 90 °C. Triethanolamine (0.15 g, 1 mmol) was added into the solution above drop wise and the whole solution was refluxing overnight (more than 12 h). The solution was purified using silica column chromatography (eluent: CH_3CN/CH_2Cl_2, 2 : 1 v/v) and recrystallized from acetonitrile to afford 0.1 g light yellow *p*-aminophenylsilatrane crystals (yield 40%).

^1H NMR (300 MHz, $CDCl_3$, 298K): δ_H: 7.512 (2H, d, *J* = 8.392 Hz, 2(NH$_2$CC*H*) **14, 16**), 6.618 (2H, d, *J* = 8.392 Hz, 2(SiCC*H*) **13, 17**), 3.876 (6H, t, *J* = 5.833 Hz, 3(OCH$_2$) **3, 7, 10**), 3.577 (2H, s, NH$_2$ **19, 20**), 2.888 (6H, t, *J* = 5.837 Hz, 3(NCH$_2$) **4, 6, 9**); ^{13}C NMR (75 MHz, $CDCl_3$, 298K): δ_C: 154.8, 135.3, 126.0, 114.6, 57.9, 51.2;

***p*-Methoxylphenylsilatrane.** The procedure is the same as described above for *p*-amino-phenylsilatrane, with *p*-methoxylphenyltrimethoxysilane (0.23 g, 1 mmol) and triethanolamine (0.15 g, 1 mmol) as starting materials. Crystallization from CH_3CN gave 0.22 g of *p*-methoxy-phenylsilatrane (80% yield) as colorless platy crystals.

^1H NMR (300 MHz, $CDCl_3$, 298K): δ_H: 7.625 (2H, d, *J* = 8.658 Hz, 2(CH$_3$OCC*H*) **14, 16**), 6.795 (2H, d, *J* = 8.663 Hz, 2(SiCC*H*) **13, 17**), 3.870 (6H, t, *J* = 5.858 Hz, 3(OCH$_2$) **3, 7, 10**), 3.753 (3H, s, OCH$_3$ **19**), 2.885 (6H, t, *J* = 5.865 Hz, 3(NCH$_2$) **4, 6, 9**); ^{13}C NMR (75 MHz, $CDCl_3$, 298K): δ_C: 159.4, 135.4, 133.0, 112.9, 57.7, 54.9, 51;
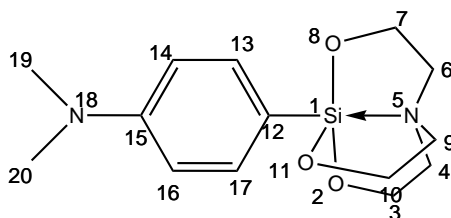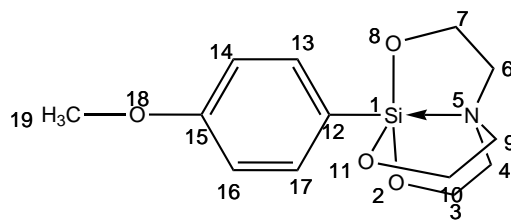
Benzylsilatrane. The procedure is the same as described, with benzyltriethoxysilane (0.38 g, 1.5 mmol) and triethanolamine (0.22 g, 1.5 mmol) as starting materials. Crystallization from CH_3CN gave 0.26 g of benzylsilatrane (65% yield) as colorless needle-shaped crystals.

^1H NMR (300 MHz, $CDCl_3$, 298K): δ_H: 7.197 (4H, m, Ph **2, 3, 5, 6**), 6.983 (1H, m, Ph **4**), 3.733 (6H, t, J = 5.833 Hz, 3(OCH$_2$) **3, 7, 10**), 2.772 (6H, t, J = 5.838 Hz, 3(NCH$_2$) **4, 6, 9**), 1.962 (2H, s, SiCH$_2$ **12**); ^{13}C NMR (75 MHz, $CDCl_3$, 298K): δ_C: 143.1, 129.0, 127.4, 123.0, 57.6, 51.1, 26.2.
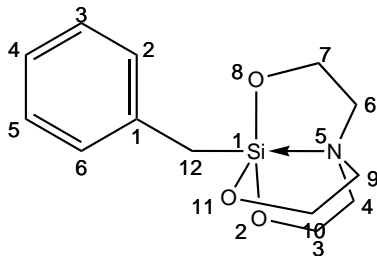
4.6.2 Bis-(silatranyl)alkanes

For the synthesis of bis-(silatranyl)alkanes, we had considered using the same method as the one previously used for silatrane synthesis. However, it didn't work very well. The product tended to polymerize when it was mixed with triethanolamine, and the resulting polymer was in mixture with the triethylammonium hydrochloride which could not be separated thereafter.

We therefore looked for another method in the hope that transesterification might work well in this case. So instead of using a chlorosilane, we first transformed the chlorosilane into corresponding acetylsilane, which was then reacted with triethanolamine to obtain the desired bis-silatrane (Scheme 6). The side product, acetic acid, would be removed easily by evaporation under vacuum [70].

Bis(silatranyl)methane. Bis(trichlorosilyl)methane (1.83 mL, 10 mmol), acetic anhydride (6.2 g, 60 mmol) and sodium acetate (200 mg) were placed in a two-necked flask fitted with a pressure equalising dropping funnel and a Vigreaux column with a distillation unit. The reaction mixture was heated to 60 °C while stirred for 4-5 h. After removal of acetylchloride formed during the reaction, the temperature was raised to 150 °C when unreacted acetic anhydride distilled over as well. The reaction mixture was cooled down to 0 °C then 20 mL
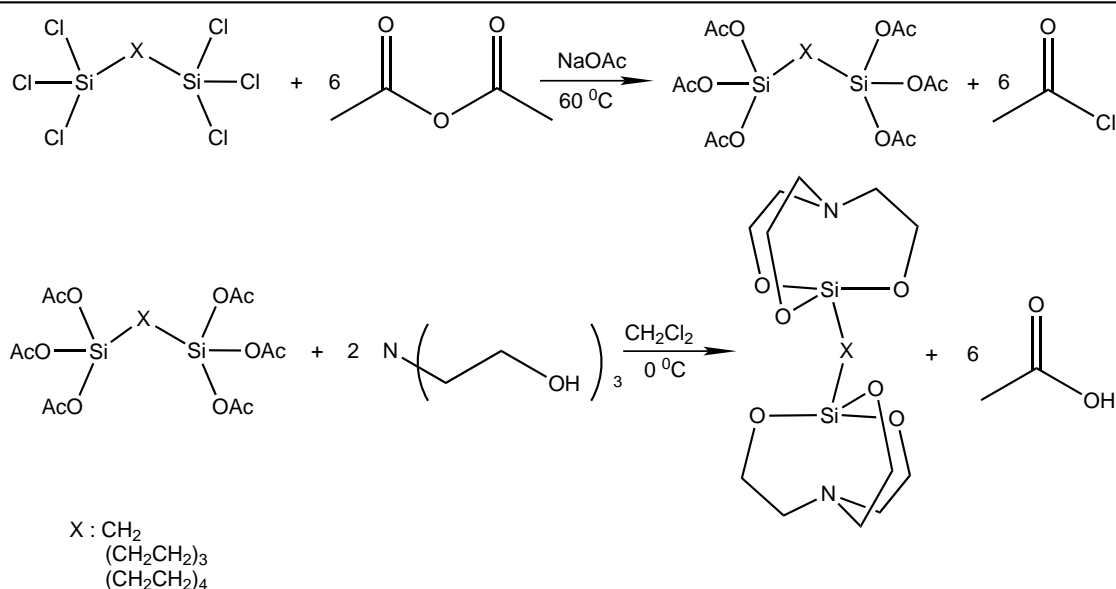
Scheme 6: Synthesis of bis-silatranes.

of dichloromethane was added into the mixture. Triethanolamine (2.65 g 20 mmol) dissolved in 10 mL of dichloromethane was drop wise added with vigorous stirring overnight (12 h). The white solid present in suspension was then removed by filtration and the filtrate was concentrated by rotary evaporator, affording a light colored solid bis(silatranyl)methane (2.5 g, 70%).

NMR (300 MHz, $CDCl_3$, 298K): δ_H: 3.798 (12H, d, J = 4.878 Hz, OCH$_2$ **3, 7, 9, 14, 18, 20**), 2.890 (12H, t, J = 4.897 Hz, NCH$_2$ **2, 8, 10, 15, 17, 22**), 1.253 (2H, s, SiCH$_2$Si **23**); ^{13}C NMR (75 MHz, $CDCl_3$, 298K): δ_C: 57.605, 53.744, 3.825;
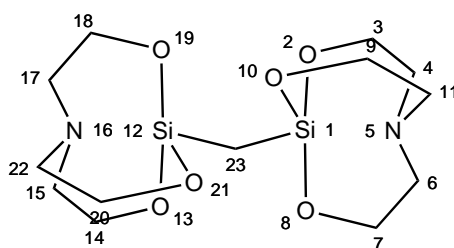
Bis(silatranyl)hexane. The procedure is the same as described for bis(silatranyl)methane, with bis(trichlorosilyl)hexane (2.65 mL, 10 mmol) and triethanolamine (2.65 mL, 20 mmol) as starting materials and obtained 2.25 g of bis(silatranyl)hexane (52% yield) as light yellow solid.

^1H NMR (300 MHz, $CDCl_3$, 298K): δ_H: 3.745 (12H, d, J = 5.787 Hz, OCH$_2$ **3, 7, 9, 14, 18, 20**), 2.772 (12H, t, J = 5.784 Hz, NCH$_2$ **2, 8, 10, 15, 17, 22**), 1.25 (8H, m, 2(CH$_2$CH$_2$) **24-27**), 0.419 (4H, m, 2(SiCH$_2$) **23, 28**); ^{13}C NMR (75 MHz, $CDCl_3$, 298K): δ_C: 58.005, 53.447, 30.996, 16.952, 12.095;
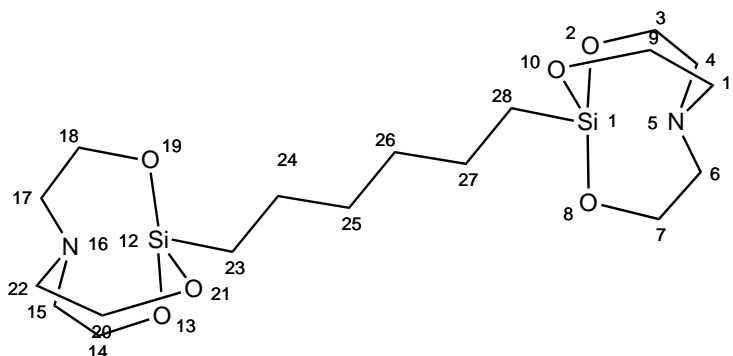
Bis(silatranyl)octane. The procedure is the same as described for bis(silatranyl)methane, with bis(trichlorosilyl)octane (2.97 mL, 10 mmol) and triethanolamine (2.65 mL, 20 mmol) as starting materials and obtained 3.18 g of bis(silatranyl)octane (69% yield) as light pink solid.

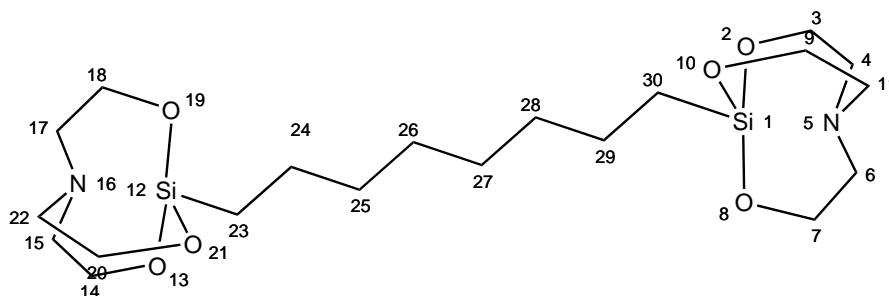^1H NMR (300 MHz, $CDCl_3$, 298K): δ_H: 3.751 (12H, d, J = 5.789 Hz, OCH$_2$ **3, 7, 9, 14, 18, 20**), 2.779 (12H, t, J = 5.783 Hz, NCH$_2$ **2, 8, 10, 15, 17, 22**), 1.245 (12H, m, $3(CH_2CH_2)$ **24-29**), 0.415 (4H, m, $2(SiCH_2)$ **23, 30**); ^{13}C NMR (75 MHz, $CDCl_3$, 298K): δ_C: 57.985, 51.200, 31.588, 22.655, 14.126.

4.6.3 Bi-silatranes

Tris(1,3-dihydroxy-2-propyl)amine   In order to prepare these compounds, we followed the synthesis reported in [71]. Based on this method, we adjusted some steps in the way more adapted to our later synthesis.

The 1,3-dihydroxyacetone dimer (starting product) can better be seen, as the name indicates, as the hemiacetal of two molecules of 1,3-dihydroxyacetone (*a* in Scheme 7). The addition of ammonia NH_4^+ on this ketone will form an imine (dehydratation rection *b* in Scheme 7). The addition of the hydride H^- from the borohydride BH_2CN allows to reduce the imine back to an amine (*c* in Scheme 7), which can then react with the C=O group of a second molecule of 1,3-dihydroxyacetone to form the branched imine (*d*, *e* in Scheme 7). After the first reaction, we obtained a white sticky liquid residue which was dissolved in water and has been passed through an ion-exchange column (Amberlite, IR-120, H^+).

35
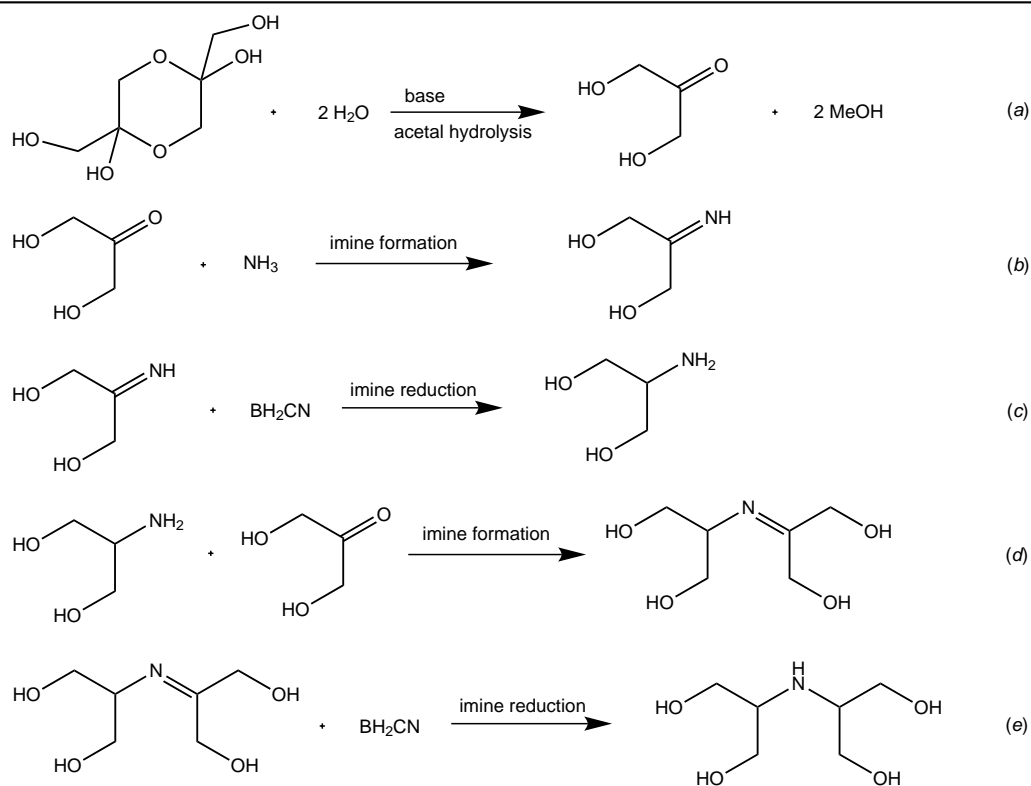
Scheme 7: Synthesis of intermediate tetrahydroxy diisopropylamine

Before usage, the Amberlite resin was twice soaked in 7% HCl solution for 24h, then packed in the column and washed with water until the exit flow turns neutral. We then injected our product (dissolved, in water) and eluted it with water until all impurities were flushed out, and the outlet flow turns neutral once more. Finally, we then passed a solution of aqueous ammonia (1.00 M) to wash out the pure product from the column.

This tetrahydroxy diisopropylamine was dissolved in methanolic HCl to form the corresponding ammonium chloride. Then the solvent was removed under vacuum, which is a very crucial point to the whole reaction. The H_2O must be absolutely removed from the product to let the reaction be able to start in an anhydrous environment. Under argon, the ammonium chloride was dissolved in anhydrous DMF, before 2,2-dimethoxypropane (DMP) and the catalyst p-toluenesulfonic acid monohydrate (p-TsOH) were added. The solution was stirred at least 12 h until the solution became very turbid. The solution was neutralized with triethylamine. The mixture was concentrated in vacuum, the residue redissolved with triethylamine and ethyl acetate. The ammonium salts were simply filtered off, and the solvent evaporated to afford an orange colored viscous liquid. Recrystalization in hexane followed: however, even with heating, the viscous liquid cannot be dissolved completely into hexane. The hot 2-phases solution was put to the refrigerator immediately. On cooling, white crystals formed right at the interface between hexane and the orange colored viscous liquid. This partial recrystalization

36

step was repeated several times to obtain 25% yield of bis(4,4-dimethyl-3,5-dioxanyl)amine (Scheme 8).
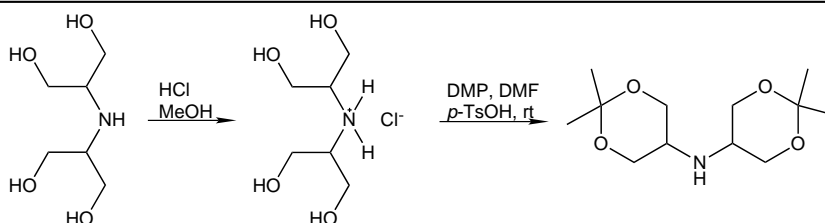
Scheme 8: Hydroxy group protection

The next step was to introduce the third branch to the tetrahydroxy diisopropylamine, and we did it by inserting an N–H bond to the secondary amine with a carbene or carbenoid generated from a diazocarbonyl compound, which is the key step in the synthesis of the target tertiary amine. Dimethyl diazomalonate (DDM) was chosen as the source of carbenoid. DDM was synthesized by a diazo transfer reaction (Scheme 9).
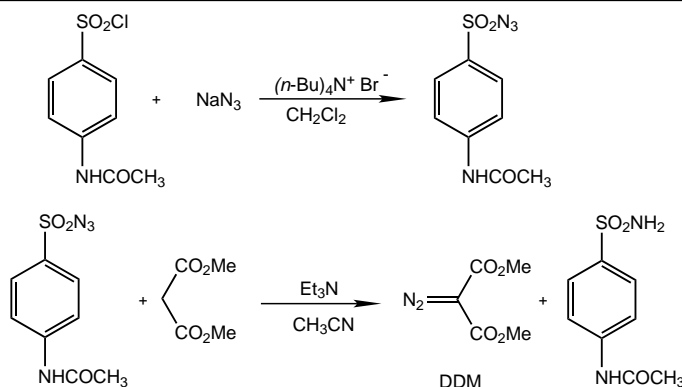
Scheme 9: Synthesis of dimethyl diazomalonate (DDM)

To insert DDM into the NH bond of bis(4,4-dimethyl-3,5-dioxanyl)amine, dirhodium tetraacetate was used as a catalyst of the decomposition of DDM since it is well-known to form strong complexes with Lewis bases. This would lead to the tertiary amine-dimethyl 2-(N,N-bis(4,4-dimethyl-3,5-dioxanyl)amino)malonate. However, according to Porter and his coworkers [72, 73], the catalytic activity of $Rh_2(OAc)_4$ is totally inhibited by primary amines (Scheme 10). If the secondary bis(4,4-dimethyl-3,5-dioxanyl)amine has some impurities containing primary amine, the catalyst will be poisoned immediately when added. The solution would then become red-brown instead of the normal green color. Hence, bis(4,4-dimethyl-3,5-dioxanyl)amine must be very pure when used. Fortunately, we obtained very white pure crystals from the previous step. Therefore, a slight excess of DDM and 8 mol% of catalyst $Rh_2(OAc)_4$ were added into a toluene solution of acetonide amine at room temperature. The mixture was heated to

reflux (110 °C) for one night. The solvent was removed by rotary evaporator and the product was purified by chromatography passing it on a silica column with ethyl acetate: hexane (1:3 / v:v) as an eluent to afford the tertiary amine dimethyl 2-(N,N-bis(4,4-dimethyl-3,5-dioxanyl)amino)malonate.

Lithium aluminum hydride ($LiAlH_4$) was then used to reduce the ester groups. 6 Equivalents of LAH were dissolved in 20 ml of THF to give a gray suspension which was injected drop wise into 10 ml of tertiary amine in THF solution under argon at 0 °C. The whole suspension was kept stirring overnight at room temperature. Then were added sequentially water (0.9 ml), 15% sodium hydroxide (0.9 ml) and water (3×0.9 ml). The mixture was filtered and the filtrate was evaporated to obtain a light yellow transparent liquid, 2-(N,N-bis(4,4-dimethyl-3,5-dioxanyl)amino)-1,3-propanediol. Yield 50%.
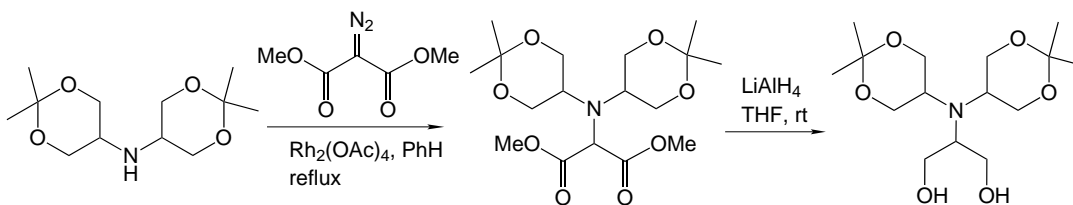
Scheme 10: Synthesis of 2-(N,N-bis(4,4-dimethyl-3,5-dioxanyl)amino)-1,3-propanediol

Trifluoroacetic acid in aqueous THF was employed to cleave the acetal groups of 2-(N,N-bis(4,4-dimethyl-3,5-dioxanyl)amino)-1,3-propanediol, affording deprotected tertiary amine as trifluoroacetate salt. This mixture was flushed through an ion-exchange resin column, Amberlite, IR-120, H^+. The column was eluted with water first, and then with a solution of 1 M aqueous ammonia. A yellow oil was obtained. The oil was kept under high vacuum overnight, and it became a yellow solid tris(1,3-dihydroxy-2-propyl)amine (Scheme 11). The product was obtained in 72% yeild.

Tris(1,3-dihydroxy-2-propyl)amine

^1H NMR (300 MHz, D_2O, 298K): δ_H: 3.521 (12H, m, CH_2O), 3.146 (3H, m, NCH); ^{13}C NMR (75 MHz, D_2O, methanol, 298K): δ_C: 57.1, 61.3.
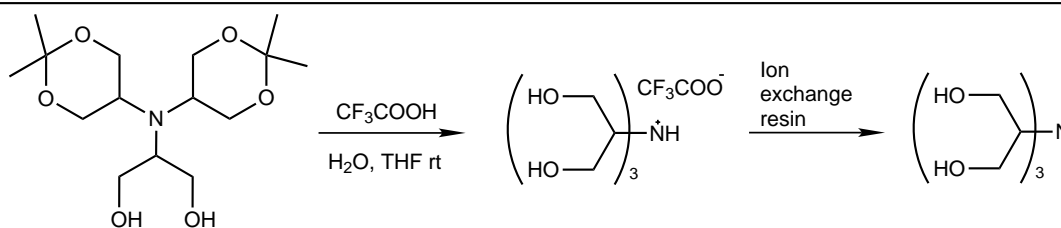
Scheme 11: Synthesis of tris(1,3-dihydroxy-2-propyl)amine.

Using this tris(1,3-dihydroxy-2-propyl)amine, we synthesized 3 new silatranes which have two atrane structures sharing the same nitrogen atom and three adjacent carbon atoms. The silatranes were synthesized by transesterification of tris(1,3-dihydroxy-2-propyl)amine with the corresponding organotrialkoxysilane. The transesterification method is wildly used in silatrane synthesis. In the thesis of Yuan Pingjie [71], it was mentioned that they obtained two triptych-silatranes, di(phenyl)- and di(methyl)-bi-silatrane using this method. In our case, we used mixed solvents DMF and toluene instead of single solvent DMF. DMF was used as a good solvent to dissolve tris(1,3-dihydroxy-2-propyl)amine and toluene was used to provide a lower reflux temperature, thus preventing the product from thermal decomposition (Scheme 12).

R = CH$_2$CH$_3$, C$_6$H$_5$CH$_2$, C$_6$H$_5$

Scheme 12: Synthesis of bisilatranes.

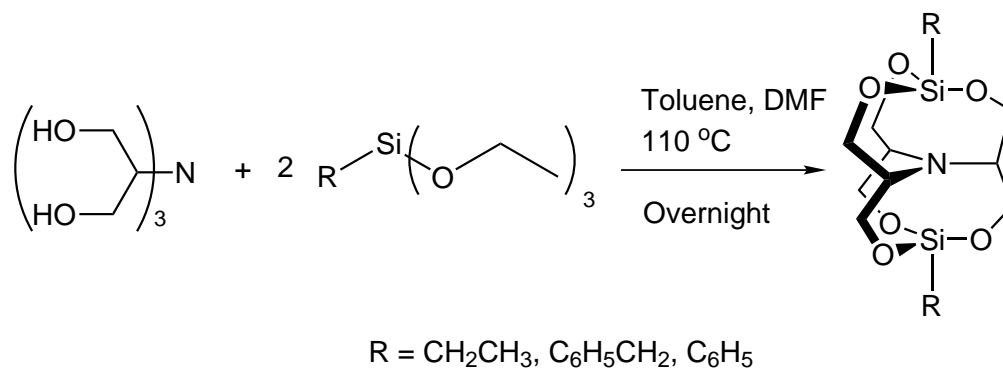**Di(phenyl)-bi-silatrane.** Phenyltriethoxysilane (0.49 mL, 2.016 mmol) was added to the solution of tris(1,3-dihydroxy-2-propyl)amine (80 mg, 0.336 mmol) in DMF (1 mL) and toluene (4 mL). Under argon, the solution was heated (oil bath 110 °C) for 12 h. TLC was employed to follow the reaction. At the beginning of the reaction there were two new spots on the TLC plates. The relatively polar spot of the two gradually disappeared. Finally, there was only one new spot left. The solvent and excess of phenyltriethoxysilane were removed under reduced pressure and the residue was purified by recrystallization from CH$_3$CN to afford white crystal (126 mg, 85%).

^1H NMR (300 MHz, $CDCl_3$, 298K): δ_H: 7.704 (4H, m, C$_6$H$_5$ **24, 25, 29, 30**), 7.380 (6H, m, C$_6$H$_5$ **23, 27, 26, 28, 31, 32**), 3.813 (6H, dd, J = 4.568, 11.58, CH$_2$ **3, 7, 11, 13, 15, 18**), 3.744 (6H, t, J = 11.520, CH$_2$ **3, 7, 11, 13, 15, 18**), 3.509 (3H, m, CH **4, 6, 9**); ^{13}C NMR (75 MHz, $CDCl_3$, 298K): δ_C: 134.3, 131.9, 130.5, 128.0, 61.1, 57.6.
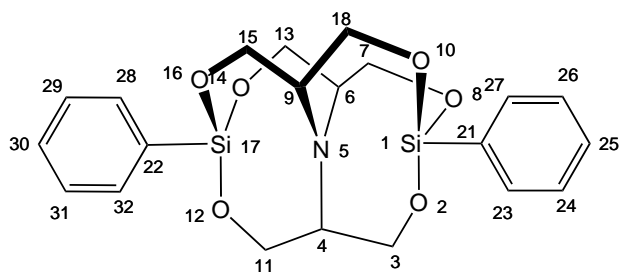
Di(ethyl)-bi-silatrane. The procedure is the same as described for di(phenyl)-bi-silatrane, with ethyltriethoxysilane (0.43 mL, 2.016 mmol) and tri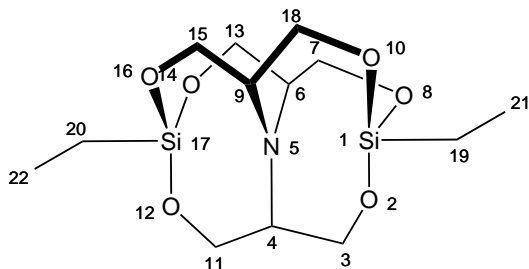s(1,3-dihydroxy-2-propyl)amine (80 mg, 0.336 mmol) as starting materials. Crystallization from hexane gave 60 mg of di(ethyl)-bi-silatrane (51% yield) as colorless needle-shaped crystals.

^1H NMR (300 MHz, $CDCl_3$, 298K): δ_H: 3.664 (6H, dd, J = 4.375, 11.48, CH_2 **3, 7, 11, 13, 15, 18**), 3.524 (6H, t, J = 11.146, CH_2 **3, 7, 11, 13, 15, 18**), 3.283 (3H, m, CH **4, 6, 9**), 0.967 (6H, t, J = 7.887, CH_3 **21, 22**), 0.582 (4H, q, J = 7.94, 15.76, $SiCH_2$ **19, 20**); ^{13}C NMR (75 MHz, $CDCl_3$, 298K): δ_C: 60.62, 57.17, 6.63, 3.90;

Di(benzyl)-bi-silatrane. The procedure is the same as described above, with benzyltriethoxysilane (0.52 mL, 2.016 mmol) and tris(1,3-dihydroxy-2-propyl)amine (80 mg, 0.336 mmol) as starting materials. Crystallization from toluene gave 116 mg di(benzyl)-bi-silatrane (78% yield) as colorless crystals.

^1H NMR (300 MHz, $CDCl_3$, 298K): δ_H: 7.125 (10H, m, C_6H_5 **23-32**), 3.637 (6H, dd, J = 4.263, 11.49, CH_2 **3, 7, 11, 13, 15, 18**), 3.483 (6H, t, J = 11.219, CH_2 **3, 7, 11, 13, 15, 18**), 3.238 (3H, m, CH **4, 6, 9**), 2.129 (4H, s, $SiCH_2$ **19, 20**); ^{13}C NMR (75 MHz, $CDCl_3$, 298K): δ_C: 137.71, 128.83, 128.10, 124.56, 60.70, 57.18, 21.42.

40
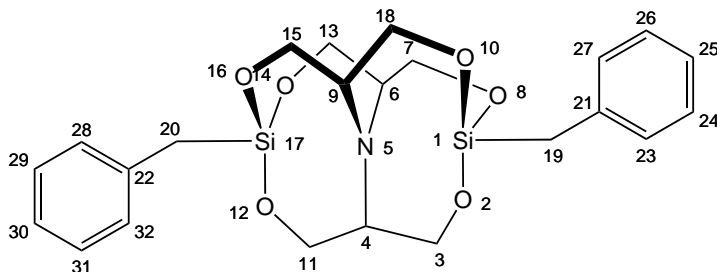
4.7 Electrosynthesis of di-stannatrane

In the two-compartment electrolytic cell described above, 0.049 g of stannatrane chloride and 0.48 g of lithium perchlorate were dissolved into 30 mL of acetonitrile under argon. A tension of -1.94 V was then applied to the system for 1 hour and the current changes were recorded. At the end of the electrochemical reaction, the solvent was evaporated on a rotary evaporator. The resulting product was re-dissolved in hexane, creating a suspension of $LiClO_4$ that was filtered off. The remaining impurities were purified by column chromatography (eluent: hexane) to afford pure di-stannatrane. In the series of repeated electrolyses, the material yield was between 5% and 30%.

Bi-stannatrane.

^1H NMR (500 MHz, $CDCl_3$, 298K): δ_H: 1.608 (12H, s, $2 \times 3(\mathrm{NCH_2})$ **4, 6, 11, 15, 17, 22**), 1.345 (36H, s, $2 \times 6(\mathrm{CH_3})$ **23-34**); ^{13}C NMR (125 MHz, $CDCl_3$, 298K): δ_C: 72.075, 69.197, 31.104, 29.263; ^{119}Sn NMR (186 MHz, $CDCl_3$, 298K): δ_{Sn}: -639.72.
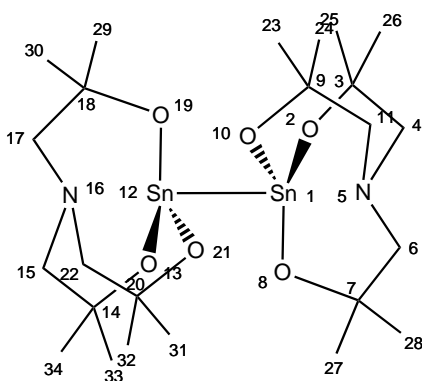
RESULTS AND DISCUSSION

5 Results and discussion

Analysis of bonding and electronic interactions in aryl, benzyl and alkyl silatranes allows us to outline several conjugative schemes involving transannular interactions (both axial and lateral) which might be found in metallatrane-based reaction series. Main building block in these systems is the 3c-4e unit. As it was revealed above, most interesting feature of the 3c-4e system in silatranes is that upon one-electron withdrawal (providing a 3c-3e system), it forms an odd-electron system with axial symmetry in which the unpaired electron occupies internal axial orbital (mostly, $p_z(N)$). Extension of such structure by further axial (/lateral) conjugation (/hyperconjugation) can open the route to formation of more conjugated systems like 4c-6e, 5c-6e, 6c-8e *etc*.

Their efficiency of conjugation and stability might be quite different but those identified as stable energy minima can then be envisaged to be used for designing molecular systems with long-term transmission of electronic effect, i.e. a limiting nc-(n+1)e scheme which might start a new generation of molecular wires.

From this standpoint, we considered several systems and attempted their synthesis and study of their electrochemical behavior. Selected structures and their bonding schemes are shown in figure 21.

5c-6e

bi-silatranes

$n+2\sigma^*$

2σ

5c-8e

di(silatranyl)ether

$2(n+\sigma^*)$

2σ

6c-8e

1,2-bis-(silatranyl)ethane

$2n+2\sigma^*$

$2(n+\sigma^*+\sigma)$

$\sigma+\sigma$

44

6c-8e

1,4-bis-(silatranyl)benzene

$2(n+\sigma^*)$

2σ

7c-8e

1,1-bis-(silatranyl)methane

$(n+\sigma^*+\sigma)\times2$

$(\sigma+\sigma^*)\times2$

$n+\sigma^*$

σ

$\Big\}\times2$

$(\sigma+\sigma)\times2$
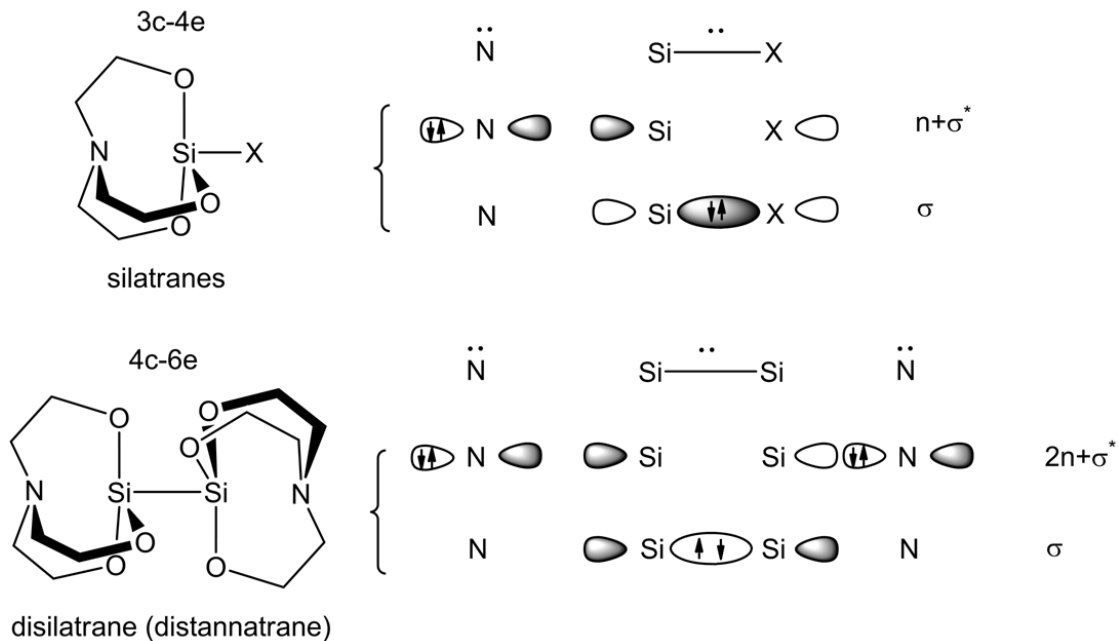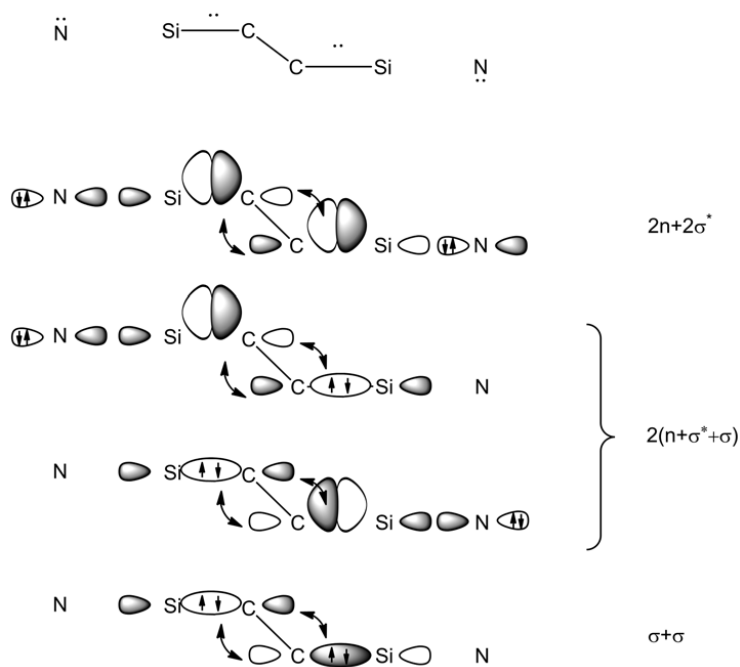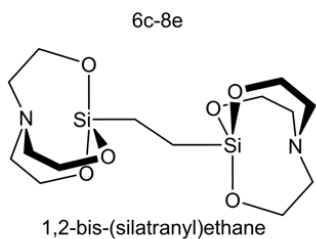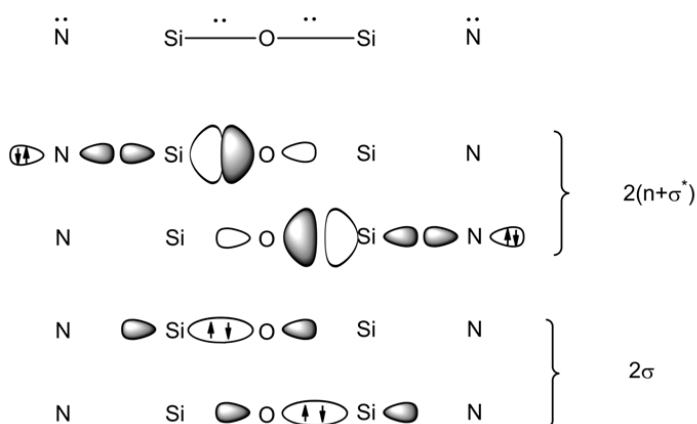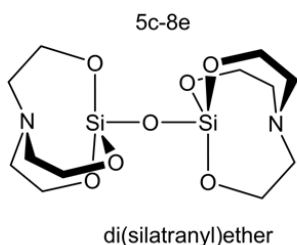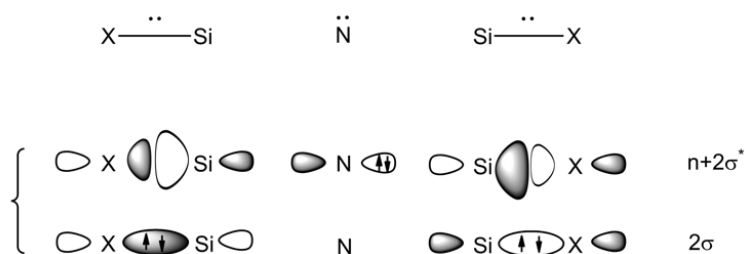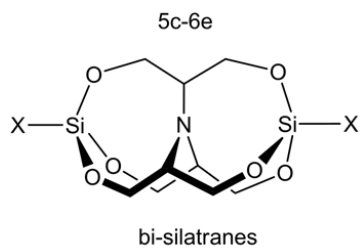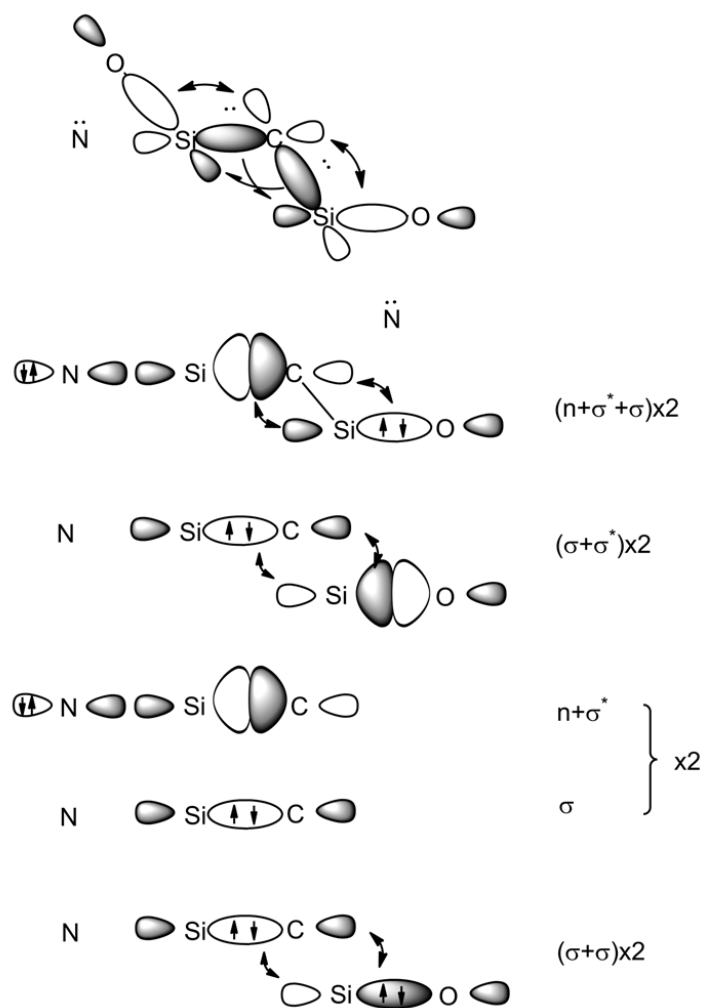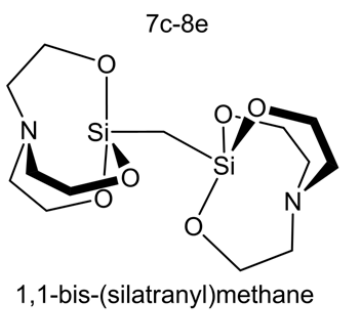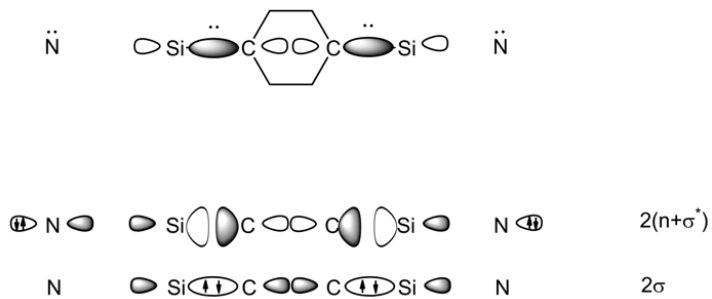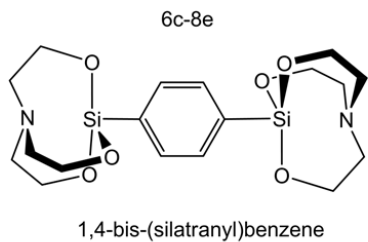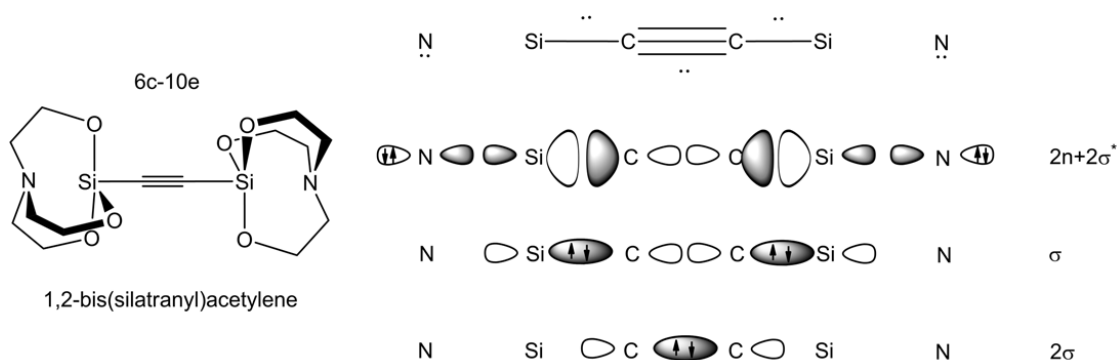
Figure 21: Selected metallatrane-based structures and their bonding schemes.

5.1 Simple 1-R-silatranes

5.1.1 Introduction

Though the family of known 1-R-silatranes is extremely large, it has been very poorly studied by electrochemistry [74, 5]. Comparison of the few available data on the electrooxidation of this class of compounds with the works on electrochemistry of homologous germatranes [49, 33, 34] allowed to suppose that electronic structure on the cation radicals of Si-substituted aromatic and aliphatic derivatives on one hand, and benzylic derivatives on the other, should have different nature and therefore, would result in a different electrochemical behavior. This difference is intrinsically related to the nature of bonding interactions in neutral silatranes.
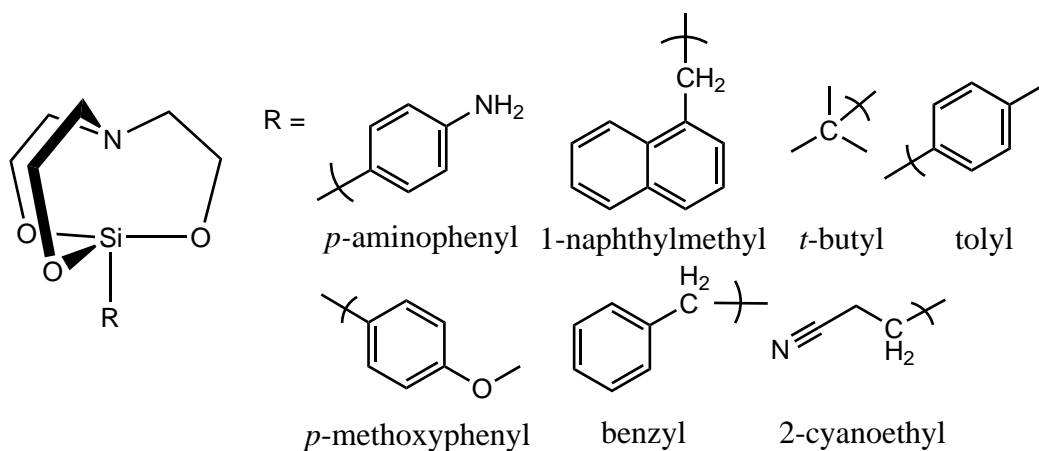
Figure 22: 1-R-silatranes

In order to elucidate the specific features of these effects and the possibility of incorpora-

46

tion of a simple 3c-4e system into more extended 5c-6e or higher $(5c\text{-}6e)_n$ electronic systems, we first synthesized and studied several model silatranes (Figure 22).

5.1.2 Structure

Seven 1-R-silatranes structures, studied in the next section were prepared according to previously reported methods, as described in the experimental section.

Although they all are already known and their crystal structure was even released in several publications [1, 28, 29], we found that these structures were neither deposited at CCDB, nor the details on their structure were really published. So we found it useful to consider more this missing aspect. The crystal structures of four silatranes were obtained by X-ray single crystal diffraction. The structure of *p*-aminophenylsilatrane, 1-naphthylmethylsilatrane, *p*-methoxyphenylsilatrane and benzylsilatrane are the first we characterized. Their molecular structures are shown in figures 23-26, the crystallographic data are listed in the table 4 and the selected bond lengths and angles are listed in table 5.

Table 4: Selected crystallographic data and details of refinement for *p*-aminophenylsilatrane, 1-naphthylmethylsilatrane, *p*-methoxyphenylsilatrane and benzylsilatrane.

R	*p*-aminophenyl	1-naphthylmethyl	*p*-methoxyphenyl	benzyl
Empirical formula	$C_{12}H_{18}N_2O_3Si$	$C_{17}H_{21}NO_3Si$	$C_{13}H_{19}NO_4Si$	$C_{13}H_{18}NO_3Si$
Formula weight	266.37	315.44	281.38	265.38
Crystal system	Orthorhombic	Orthorhombic	Monoclinic	Monoclinic
Space group	$Pc2_1n$	$Pbca$	$P2_1/n$	$P2_1/n$
a (Å)	6.6141 (4)	13.8928 (5)	10.4799 (8)	10.3529 (2)
b (Å)	11.8122 (8)	14.5060 (6)	10.4219 (8)	11.5350 (2)
c (Å)	16.1752 (11)	15.0774 (6)	12.5058 (10)	11.0310 (2)
$\alpha(^o)$				
$\beta(^o)$			99.275 (4)	102.224 (1)
$\gamma(^o)$				
V ($Å^3$)	1263.72 (14)	3038.5 (2)	1348.03 (18)	1287.46 (4)
Z	4	8	4	4
$D_{\mathrm{calcd}}(\mathrm{Mg/m^3})$	1.400	1.379	1.386	1.369
Radiation (MoKα)	$\lambda = 0.71073$Å	$\lambda = 0.71073$Å	$\lambda = 0.71073$Å	$\lambda = 0.71073$Å
T (K)	150	150	423	150
θRange (^{o})	2.5–27.5	2.4–27.5	2.4–27.5	2.7–27.4
Total reflections	14009	46767	10522	10430
Unique reflections	2496	3488	3091	2919
Parameters	163	199	173	163
R_1, w$R2$ ($I > 2\sigma(I)$)^a	0.023, 0.064	0.045, 0.119	0.037, 0.097	0.032, 0.087
Goodness-of-fit on F^2	1.04	1.06	1.06	1.05

$$^a R_1 = \sum ||F_0| - |F_c|| / \sum |F_0|; \; wR_2 = \{\sum [w(F_0^2 - F_c^2)^2] / \sum [w(F_0^2)^2]\}^{1/2}$$

The silatrane structure can be seen as a distorted trigonal bipyramid with N atom and C atom in the axial positions, three oxygen atoms occupying the equatorial sites and the Si atom in the body center. The N-Si-C atoms are almost aligned (177.61(7)–179.29(6)°) in all these compounds. The values of the distance between Si and N in these four molecules lie within the typical range for silatranes (1.964–2.420 Å) which clearly verifies the existence of Si–N transannular bond [75].

Table 5: The main geometrical parameters for *p*-aminophenylsilatrane, 1-naphthylmethylsilatrane, *p*-methoxyphenylsilatrane and benzylsilatrane

Compound	$d(\text{Si}\cdots\text{N})$ (Å)	d (Si–C) (Å)	d Si–O (Å)	$\angle$N–Si–C (°)
p-aminophenylsilatrane	2.1665(13)	1.8831(14)	1.6710(11) 1.6718(10) 1.6727(11)	179.29(6)
1-naphthylmethylsilatrane	2.1393(14)	1.9020(17)	1.6663(13) 1.6676(13) 1.6698(12)	177.61(7)
p-methoxyphenylsilatrane	2.1523(13)	1.8958(15)	1.6702(11) 1.6713(10) 1.6631(11)	178.20(6)
benzylsilatrane	2.1215(11)	1.8990(13)	1.6685(9) 1.6700(9) 1.6733(9)	178.50(5)

d Si$_1\cdots$(O$_4$–O$_7$–O$_{10}$) (Å)	d N$_1\cdots$(C$_2$–C$_5$–C$_8$) (Å)
0.2031	0.3782
0.1884	0.3786
0.1897	0.3735
0.1761	0.3821

The silicon atom is displaced from the plane formed by three oxygen atoms towards the carbon atom on the apical position, whereas the nitrogen atom is displaced from the plane of three carbon atoms in α-positions inward the atrane cage thus adopting an *endo*-configuration. Concerning the five-membered side branches of the rings of silatrane skeleton in these four compounds, they adopt an "envelope"-like conformation, the carbon atoms in α-positions to the N atom being like the "flap" sites.

As shown in the table 5, in the atrane structure N atom is not on the plane of the three C atoms (C2, C5 and C8) but is sunk inward by a distance around 0.37-0.38 Å. According to the VSEPR (valence shell electron pair repulsion) theory, the lone-pair-electron of N and the other three valence electrons should repel each other as much as possible to reach a stable status. From this theory it is as well proved that the lone pair electrons of N are pointed right to the

Si atom.

The Si atom is ∼0.18 Å off the plane formed by O4, O7 and O10 which is also explained by VSEPR theory. We notice that the distance between Si and three oxygen atoms has a slight difference. This could be caused by the substituents because the angle ∠N–Si–C in those four silatranes is not 180° (Table 5).

For the silatranes shown in figure 23 and figure 25, the aromatic substituents are connected to the silicon atom directly. As the carbon atoms in the aromatic substituent have sp^2 hybridization, the delocalized π bonds are on the both sides of the aromatic plane and are perpendicular to the orbital of Si and N atoms in the atrane structure. Thus there is not interaction between the N→Si bond and the π-system of aromatic substituents. On the other side, there are amino- and methoxy- groups at the para-position of the aromatic substituent (Figure 23 and figure 25, respectively). The lone pair electron on the N and O atom participate in the formation of delocalized π bond and the conjugated system even if they are not exactly on the same plane.
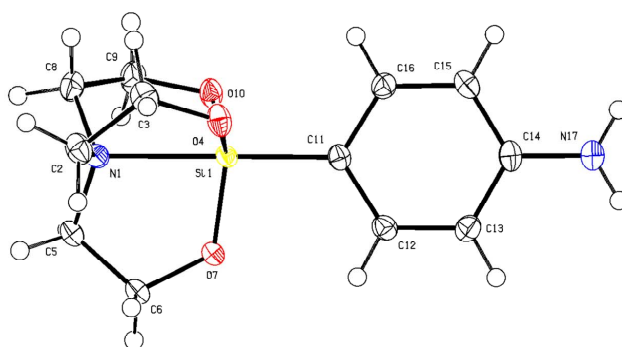
Figure 23: ORTEP drawing of the molecular structure of *p*-aminophenylsilatrane.
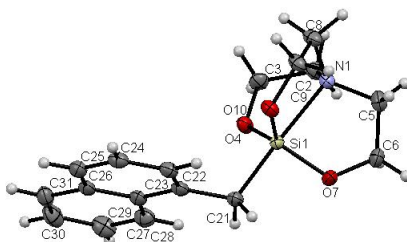
Figure 24: ORTEP drawing of the molecular structure of 1-naphthylmethylsilatrane.

For 1-naphthylmethylsilatrane and benzylsilatrane (Figure 24 and figure 26), the Si atom connected the CH_2 bridge by a σ bond (with C in the sp^3 hybridization). The σ bond is symmetrical with respect to rotation about the bond axis which cause the angle ∠Si–C21–C22 (Figure 24) to be equal to 118.37° and ∠Si–C11–C12 (Figure 26) equal to 116.07°. On the

other hand, the carbon atoms C22 (Figure 24) and C12 (Figure 26) of the aromatic substituent, either phenyl or naphthyl, are in sp^2 hybridization. The electrons from this σ bond and the adjacent C atom π^* orbital can interact via hyperconjugation mechanism which leads to the shortening of the single bond length (d (C11–C12) = 1.5057 Å and d (C21–C22) = 1.518(2) Å). For naphthyl substituent, the conjugated system is weaker than in phenyl, hence the hyperconjugation is not that notable which makes the single bond length much closer to the normal C–C length ($\sim$1.520 Å).
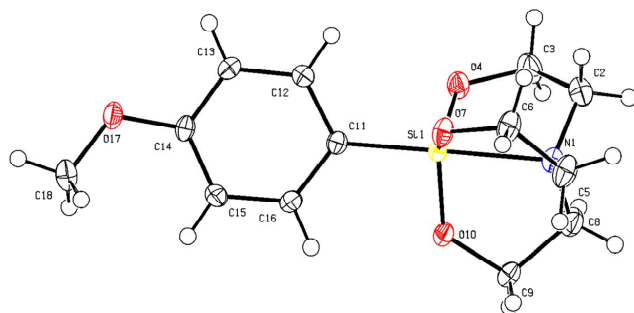
Figure 25: ORTEP drawing of the molecular structure of *p*-methoxyphenylsilatrane
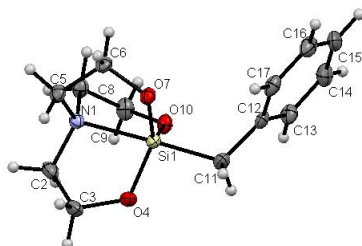
Figure 26: ORTEP drawing of the molecular structure of benzylsilatrane

5.1.3   Cyclic voltammetry

The oxidation of seven Si-substituted silatranes was studied in 0.1 M tetrabutylammonium hexafluorophosphate (TBAPF$_6$) acetonitrile (CH$_3$CN) solutions at a Pt electrode. A Pt microdisk electrode was used as the working electrode as it yielded voltammograms better shaped than those obtained with other electrodes (glassy carbon was also tried). The oxidation peak potentials of these compounds are in the range 0.78-1.45 V (vs. SCE), depending on the nature of substituent R (Table 6). Upon oxidation, three out of seven silatranes show a distinct reversible peak (Figure 27). We observed direct proportionality between the oxidation peak current (i_p) and the concentration of the electroactive substance. Direct proportionality was observed as well between the peak current and the square root of the scan rate ($i_p/v^{1/2}$ = const.) at sufficiently fast scan rates *(v > 0.5 V/s)*. These two results suggest a diffusion

control of the process. The number of electrons transferred at this oxidation step has been determined using the method proposed by Malachesky [40] which is based on the following relations. Peak current i_p for a linear sweep voltammogram of a reversible redox system can be expressed as follows:

$$i_p = 2.68 \times 10^5 n^{3/2} ACD^{1/2} v^{1/2}$$

On the other side, for potentiostatic chronoamperometry [66]:

$$it^{1/2} = nFACD^{1/2}\pi^{-1/2}$$

Combining these two equations, one obtains the following relationship:

$$R = \frac{i_p/v^{1/2}}{it^{1/2}} = 4.92n^{1/2}$$

which allows one direct evaluation of the absolute electron stoichiometry. This method is free of the uncertainty due to the different diffusion coefficient *D*, concentration and electrode surface, contrary to the method based on the comparison of i_p with a standard compound like ferrocene. Now applying this relationship to the oxidation of sever silatranes, we found that all of them undergo mono-electronic process at E'_p (Table 6).

Table 6: Parameters of electrochemical oxidation of silatranes at a platinum disk electrode at $v = 1V/s^a$

R	E_p^a(V)	E_p^c(V)	E^o(V)	n	$E_p^a - E_{p/2}^a$ (mV)	$\Delta E_p^a/\Delta lg(V)$ (mV)	α^b
p-aminophenyl	0.78	–	–	1	93	14	0.50
1-naphthylmethyl	1.10	–	–	1	88	28	0.50
t-butyl	1.22	1.14	1.18	1	91	10	0.50
tolyl	1.35	1.26	1.30	1	72	14	0.65
p-methoxyphenyl	1.37	–	–	1	66	40	0.72
benzyl	1.42	–	–	1	150	40	0.32
2-cyanoethyl	1.45	1.30	1.38	0.9	81	23	0.58

[a] Cyclic voltammetry was carried out in CH_3CN / 0.1 M $TBAPF_6$. All the voltammograms are brought to the SCE scale.
[b] Transfer coefficient estimated as a mean of α from $E_p - E_{p/2} = 1.85RT/\alpha F$ [41].

As mentioned previously, the electronic effects of the substituents R affect significantly the

oxidation potentials of the silatranes [5]. Amongst seven silatranes, *t*-butyl and tolyl silatranes show a distinct reversible electrooxidation signal even at low scan rate ($v = 0.5$ V/s). Tolyl-silatrane has an oxidation peak at $E_p = 1.35$ V (vs. SCE), with the corresponding cathodic counterpart at 1.26 V (vs. SCE). As for the *t*-butyl derivative, it is a substituent with a strong electron-donating inductive effect which leads to a relatively easy oxidation of this silatrane (1.22 V vs. SCE).
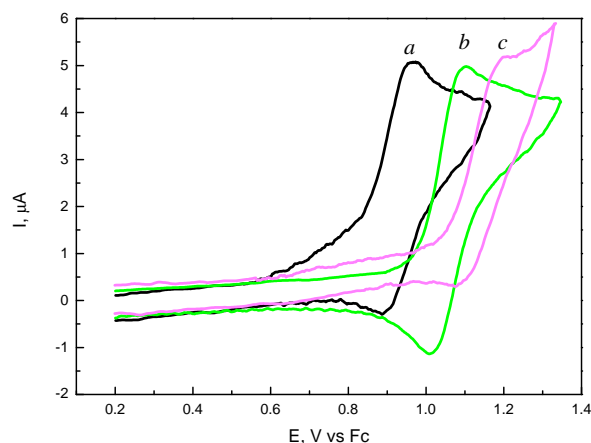
Figure 27: Cyclic voltammetry of *a, t*-butylsilatrane; *b,* tolylsilatrane; *c,* 2-cyanoethylsilatrane ($C = 0.1$ mmol/L) in $CH_3CN/0.1M$ Bu_4NPF_6 at a 1 mm Pt electrode. $v = 1$ V/s; $T = 25$ ^{o}C.

Quite surprisingly at first sight but perfectly in agreement with our hypothesis on electronic interactions as main factor of the stability of cation radicals of metallatranes, 2-cyanoethly-silatrane exhibits reversible oxidation at $E_p = 1.45$ V vs. SCE (Figure 27). The corresponding cathodic peak is less pronounced compared to *t*-butylsilatrane and formal E_0 is anodically shifted (Table 6). Both facts supposedly arise from the electron-withdrawing inductive effect of the CN group.

The other four silatranes (Figure 28) showed a different electrochemical behavior under the same conditions. Their oxidation peaks (Table 6) are irreversible even at higher scan rates ($v = 10$ V/s). In order to rationalize these data, electronic structure and possible mechanisms of transmission of electronic effects in these systems were considered in more details.

For the methoxyphenyl silatrane, phenyl substituent is in principle a mesomeric π-donor, but it does not have the expected effect on E_p and stability of cation radicals because the π orbital system of the phenyl ring is perpendicular to the σ orbital of the bond between Si and C atoms (Figure 30). Thus the inductive effect of the substituent must be considered in this case. According to Hammett equation [76]:

$$\log \frac{K}{K_o} = \sigma \rho$$

52

For a given equilibrium reaction with substituent R, K is relating the equilibrium constant and the reference K_o constant when R is a hydrogen atom to the substituent constant σ which depends only on the specific substituent R and the reaction constant ρ which depends only on the type of reaction but not on the substituent used. Here the constant σ reflects all the combination of field, inductive and resonance effects influencing the reaction rates. However, in our case, we only consider the inductive influence of the substituent. Thus we use σ_I constants (Taft's modification) indicating the electronic effect of a substituent (Table 7).

Table 7: Substituent field/inductive parameters for selected substituents

R	$\sigma_I = 0.45\sigma^*$ CH_2X Taft[a]	σ_F Taft[b]	σ_I Taft[c] (F NMR)
C_2H_5	-0.05	0.00	0.06
C_6H_4Me	0.11	0.12	0.14
H	0.00	0.00	0.00
C_6H_4OMe	0.14	0.13	0.08
Cl	0.47	0.45	0.43
C_2H_4CN	0.33	0.17	0.53
$C(CH_3)_3$	-0.09	0.00	0.09

[a] [77, 78]; [b] [79]; [c] Calculated from the meta-substituted fluorobenzene F NMR shift (felative to fluorobenzene) [80].
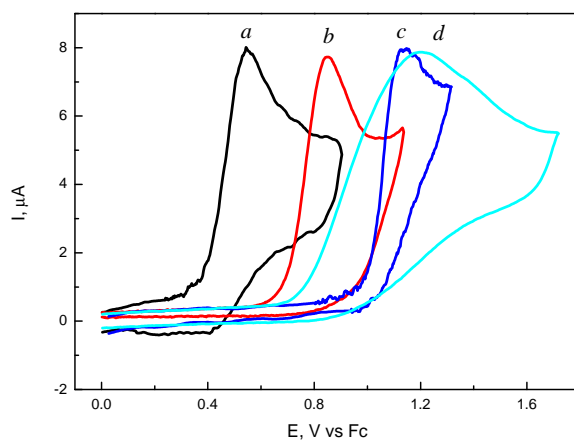
Figure 28: Cyclic voltammetry of *a, p*-aminophenylsilatrane; *b,* naphthylsilatrane; *c, p*-methoxyphenylsilatrane; *d,* benzylsilatrane (C = 0.1 mmol L^{-1}) in CH_3CN/0.1M Bu_4NPF_6 at a 1 mm Pt electrode. v = 1 V/s; T = 25 ^oC.

It can be seen that the oxidation peak E_p of *t*-butyl, tolyl, methoxyphenyl and 2-cyanoethyl-silatrane correlate well with inductive σ_I constants (Figure 29), with a slope of 1.78 (R-square

= 0.97). The fact that inductive effect affects the oxidation peak is not surprising in itself; most important is that the points for aromatic subsituents fit the same correlation as aliphatic groups. This is perfectly in agreement with the 3c-4e character of the HOMO in these compounds.
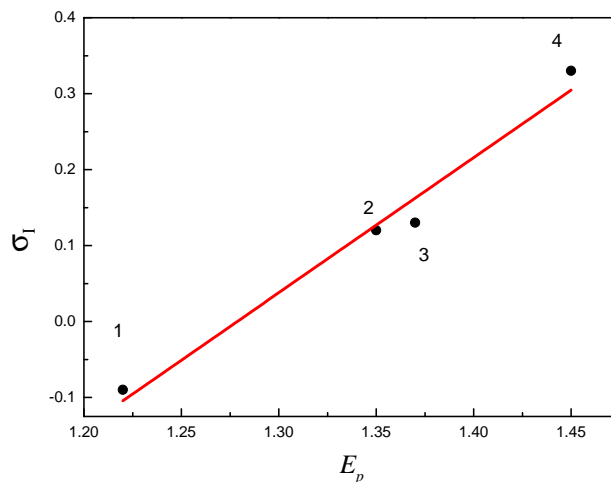
Figure 29: Oxidation peak of selected silatranes vs. σ_I constants. 1. *t*-butylsilatrane; 2. tolylsilatrane; 3. *p*-methoxyphenylsilatrane and 4. 2-cyanoethylsilatrane.
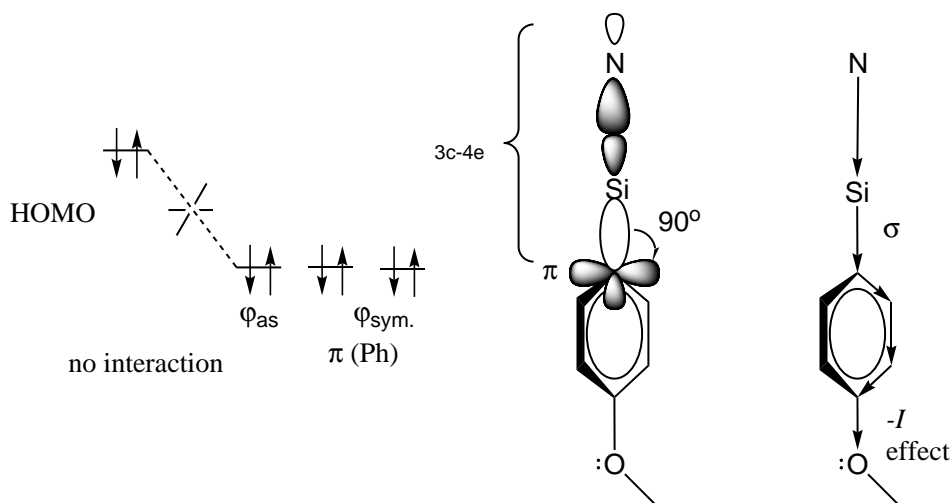
Figure 30: Molecular orbital of methoxyphenylsilatrane and inductive effect in this system (the atrane cage is not shown).

From the table we can see that the electron-withdrawing effect of phenyl is stronger than that of akyl substituents which makes methoxyphenyl group a σ-acceptor; in accordance with this, this silatrane has a relatively higher E_p = 1.37 V vs. SCE (Table 6). In fact comparing to C_{sp^3} in akyl substituents with C_{sp^2} linking atom in phenyl, the latter has stronger electron-withdrawing properties. Moreover, Pauling electronegativity of Si atom (1.90) is less than

that of C atom attaching the substituent. Aryl substituents therefore, are simply σ-acceptors with respect to the silatrane moiety, leading to the lowering of the HOMO of such compounds which is another reason why they have a high electrooxidation potential. Inductive effect fades out very rapidly with distance (Figure 30); so there must not be a big difference in an overall inductive effect of phenyl and anisyl groups in the corresponding silatranes (Table 7). The p-methoxyphenylsilatrane, on its part, has a very sharp oxidation peak (the value $E_p^a - E_{p/2}^a =$ 66 mV is close to those for purely Nernstain systems), and might therefore become reversible for $v \to \infty$ (Figure 31).
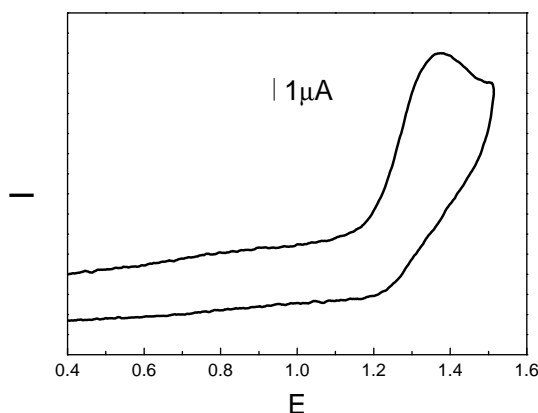
Figure 31: Cyclic voltammogram of *p*-methoxyphenylsilatrane oxidation at *v* = 10 V/s.

One can see that methoxyphenylsilatrane has an oxidation peak potential $E_p =1.37$ V vs. SCE, (Table 6) higher than that of the naphtylmethylsilatrane ($E_p =1.10$ V). Indeed, 1-naphtylmethylsilatrane -contrary to tolyl- and anisyl derivatives- exhibits an overall π-donor effect of the naphtyl group. Remarkably, π-system from naphtyl and the σ(C–Si) fragment from the 3c-4e bond are in the hyperconjugation which leads to the electron delocalization (Figure 32).
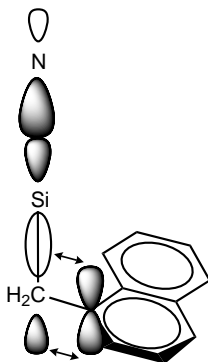
Figure 32: Hyperconjugation of 3c-4e bond with the π-system in 1-naphtylmethylsilatrane.

Same conjugative mechanism also allows spin delocalization in the cation radical from N atom to naphthyl π-system. The unpaired electron, localized on N atom and isolated inside the atrane cage in the case of alkyl or aryl silatranes, becomes visible from outside by external radicalophilic species due to its presence on naphtyl rings, primarily at 4-position. Thus the observed lowering of the oxidation potential of this silatrane is due to two factors: electron donating thermodynamic contribution of the substituent, and fast ensuing reaction of electrogernerated cation radicals (kinetic shift of E_p). Therefore, it unsurpisingly has one of the lowest oxidation peak potentials in Table 6, at E_p =1.10 V vs. SCE.

The benzylsilatrane is very similar to 1-naphtylmethylsilatrane. However, it has a more positive oxidation peak E_p = 1.42 V vs. SCE (Table 6), which supposedly results from the hyperconjugation interplay of the same factors as in 1-naphtylmethylsilatrane, plus -probably- some contribution of heterogeneous interactions with the electrode. Indeed, different from other voltammograms, benzyl silatrane exhibits a rather large irreversible oxidation peak. Although the oxidation of benzylsilatrane begins at close potentials (foothill part of the voltammogram, figure 28), the peak potential is located at 1.42 V vs. SCE. The peak width, $E_p - E_{p/2}$ of benzylsilatrane is 150 mV, which is remarkably larger than for the other compounds of the reaction series (Table 6). Since its oxidation is supposed to be electrochemically reversible, as in general is expected in the silatrane family, one could think of adsorptional interactions of its aromatic system with Pt as a possible reason of this abnormally large peak. However, naphtyl silatrane, which has a similar (and even more developed) aryl moiety, does not show this feature which thus remains quite unclear.
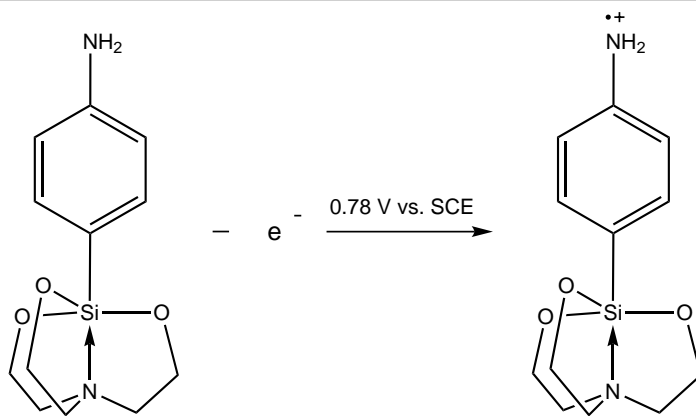
Scheme 13: *p*-Aminophenylsilatrane oxidation.

Finally, *p*-aminophenylsilatrane has the less anodic oxidation potential (0.78 V vs. SCE) which falls out of the silatrane electrooxidation range. This might be explained by the ease with which the amino substituent itself can be oxidized. The oxidation peak at 0.78 V would then arise from the oxidation of the aniline fragment (Scheme 13), since the p_z(N) electrons, contributing the most to the HOMO of this compound have lowest ionization potential and

therefore this atom would be the first that would become electrooxidized. The voltammogram of the aminophenylsilatrane might become reversible at high scan rates (Figure 33).
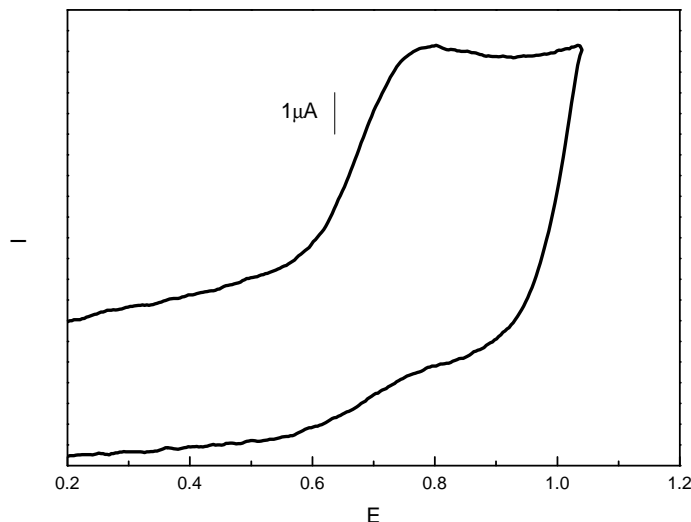
Figure 33: Cyclic voltammogram of *p*-aminophenylsilatrane oxidation at higher scan rate $v = 10$ V/s

Compared to the voltammograms of triethylamine ($E_p = 0.582$ V) and triethanolamine ($E_p = 1.126$ V [33]) in which the nitrogen atom is not involved in any coordinating interactions, silatranes have higher oxidation potentials. This anodic shift is explained by the transannular interaction between nitrogen and silicon atoms. This effect causes a strong transmission of electron density from N to Si atom which could be considered as an internal donor-acceptor charge transfer. This anodic shift is clearly seen in the results shown in Table 6. In general, the potentials of electrooxidation of the silatranes were 0.52-0.87 V higher than that of triethylamine.

Thus, the potential of electrooxidation of silatranes reflects the combined effects of the N→Si transannular bonding and the electronic effects of the substituent R attached to the silicon atom.

5.1.4 EPR spectroscopy

Reversibility of the oxidation of phenylsilatrane (reverse peak of reduction of the cation radicals is seen already at $v = 0.2$ V/s allowed us to study this silatrane by EPR-spectroelectrochemistry. When phenylsilatrane was oxidized at microelectrode in an EPR cell, a signal of electrogenerated odd-electron species appeared at E = 0.7 V. The spectrum has a characteristic feature 9

group of repeating pattern, the separation between them going to the baseline.

EPR spectrum of the cation radical of phenylsilatrane (Figure 34) has a large end-to-end width (~160 G) and consists of more than 184 well-resolved lines. Given its large spectral span, the high field part of this spectrum shows some distortion by second-order effects, which makes it difficult to reconstruct it with the simple tools included into Bruker Symphonia package. Nevertheless, the following parameters have been extracted from low-field part allowing a 99.8%-quality reconstruction of this spectrum: g = 2.0037; aN = 18.41 G; $3 \times a^{\alpha}H_{ax}$ = 37.93 G; $3 \times a^{\alpha}H_{lat}$ = 0.23 G; $6 \times a^{\beta}H$ = 1.8 G. This spectrum corresponds to a species with practically planar N atom, carrying the major part of the free electron density, which has strong interaction with three axially-oriented α-protons. The C-H bonds of the other three α-protons are practically orthogonal to the axes of this molecule so that their interaction with magnetic field is about 160 times weaker compared to that of axial α-protons.
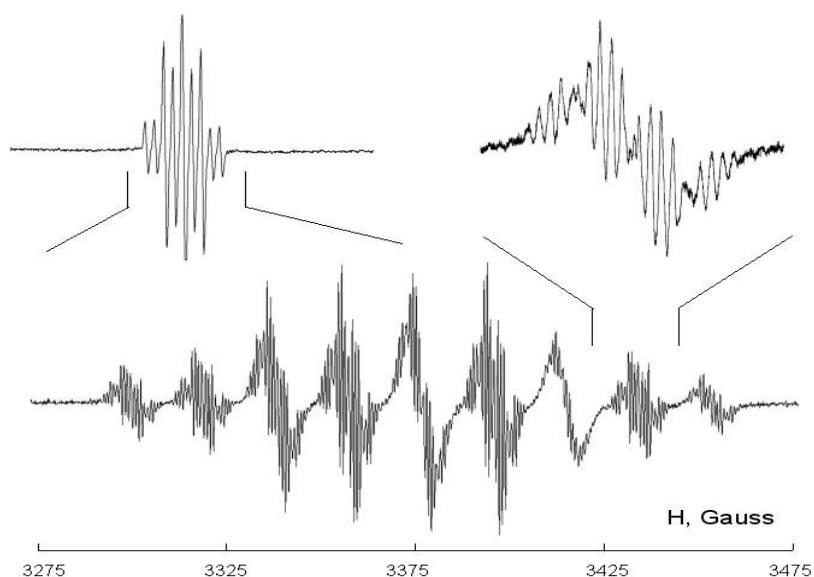
Figure 34: EPR spectrum of the cation radical of phenylsilatrane. Pt microplate electrode. Microwave frequency f = 9.46 GHz; modulation amplitude a = 0.25 G. T = 223 K. E = 0.7 V.

The oxidation of *p*-methoxyphenylsilatrane (Figure 35) under similar conditions also resulted in an EPR spectrum of electrogenerated cation radical though less resolved than in the case of phenylsilatrane (Figure 35). The spectrum is also split into 9 groups with the same integral intensities and has a similar end-to-end width. These facts indicate similar spin distribution in these two species. It is to be noted that very similar spectra were observed for the cation radicals of 1-organogermatranes [34], attesting that in these two families of metallatranes, the unpaired electron is mostly residing on N-atom, with relatively strong spin-orbital interactions with the elements (C–H bonds) parallel to the axes of the atrane cage.

Upon the oxidation of 1-naphtylsilatrane at Pt electrode in the EPR spectroelectrochemical

cell, the signal of paramagnetic species-cation radicals produced by 1e at E_p = 1.25 V was observed (Figure 36). The spectrum of the cation radical of naphthylsilatrane was reconstructed using the following parameters: g = 2.0051, *hfc* a_N = 6.152, 3x$a_{H-\alpha}$ = 3.633, 2x$a_H(CH_2)$ = 2.326, ~ a_{H-p} = 2.595, ~2xa_H = 1.509, ~ a_H = 0.34. LW = 0.28 G. In the whole it corresponds to a radical strongly delocalized over naphthyl moiety with only small contribution from N atom and from three α-protons of the silatrane cage.

Anisylsilatran

3266.78	3322.80	3378.82	3434.84	3490.86

H, Gauss
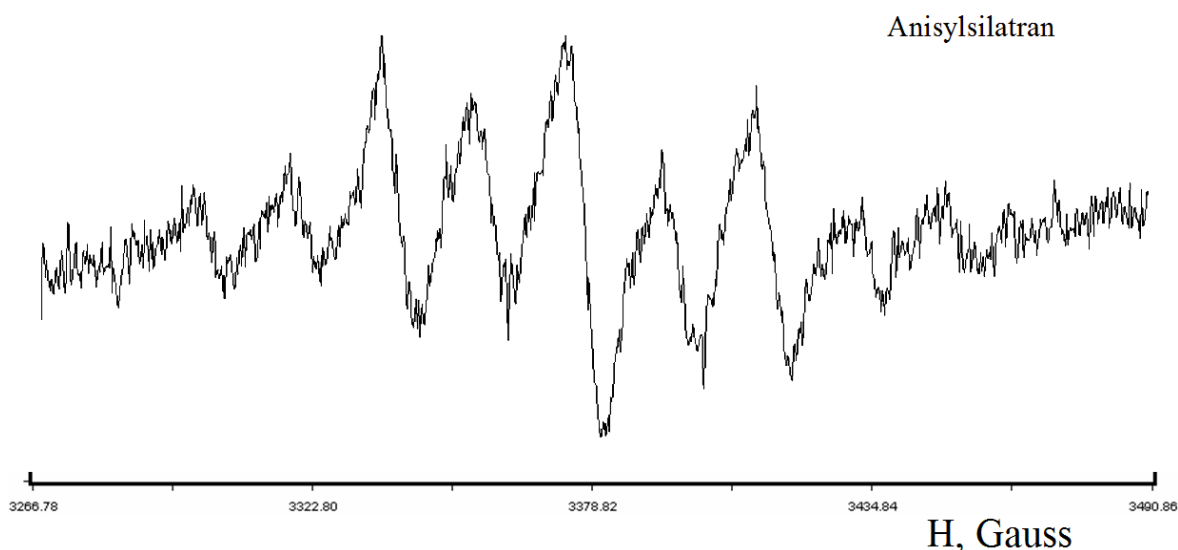
Figure 35: EPR spectrum of electrogenerated cation radicals of *p*-methoxyphenylsilatrane. Oxidation in CH_3CN/0.1M $TBAPF_6$ at a Pt microspiral electrode. E = 1.35 V, T = 224 K.

Oxidation of *p*-aminophenylsilatrane in the cavity of the EPR spectrometer also allowed detecting the electrogenerated cation radicals. The spectrum (figure 37) was then reconstructed using the following parameters: g = 2.003, a_N = 11.73 G, a_{o-H} = 7.309 G, a_{m-H} = 0.65 G, a_{NH} = 5.718 G. The *g*-factor corresponds to a purely organic radical, apparently with no contribution from the Si atom. The coupling with only one nitrogen is present which, based on own ionization potentials of aminophenyl and silatranyl fragments, was assigned to the NH_2-group nitrogen. The spectrum of this cation radical is therefore, the one of the silatranyl-substituted aniline cation radical. Because comparing to the aniline, atrane fragment has higher HOMO and needs more energy to be oxidized. Therefore, the oxidation potential E_p of *p*-aminophenylsilatrane has approximate value as aniline as well as similar spin EPR spectrum. This observation is perfectly in line with the results of DFT calculations of this and NEt_2-substituted compounds.
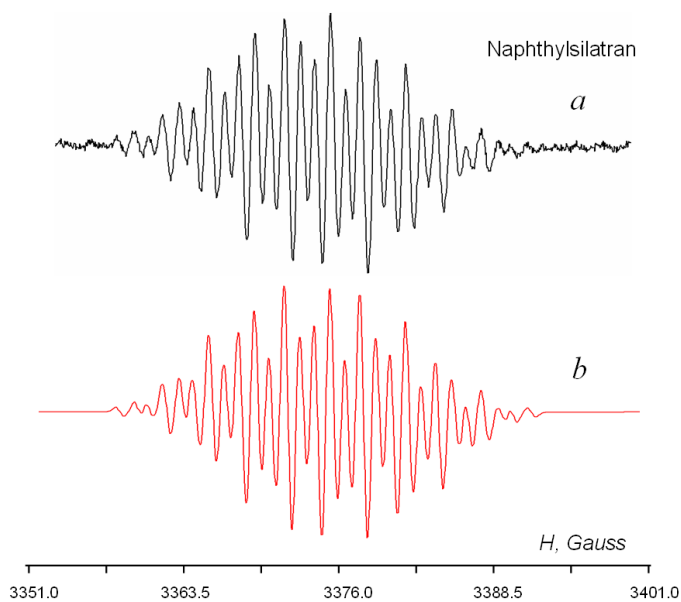
Figure 36: EPR spectrum of electrogenerated cation radicals of naphthylsilatrane. *a*. experimental; *b*. Simulated. Oxidation in CH_3CN/0.1M $TBAPF_6$ at a Pt microspiral electrode. E = 1.25 V, T = 224 K.
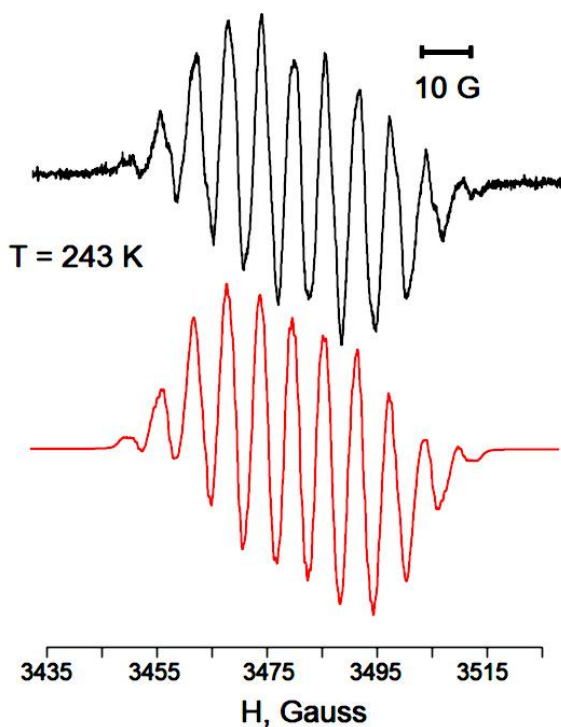
Figure 37: EPR spectra of *p*-aminophenylsilatrane. Upper – experimental, lower – simulated. Oxidation in CH_3CN/0.1M $TBAPF_6$ at a Pt microspiral electrode. E = 0.7 V, T = 234 K.
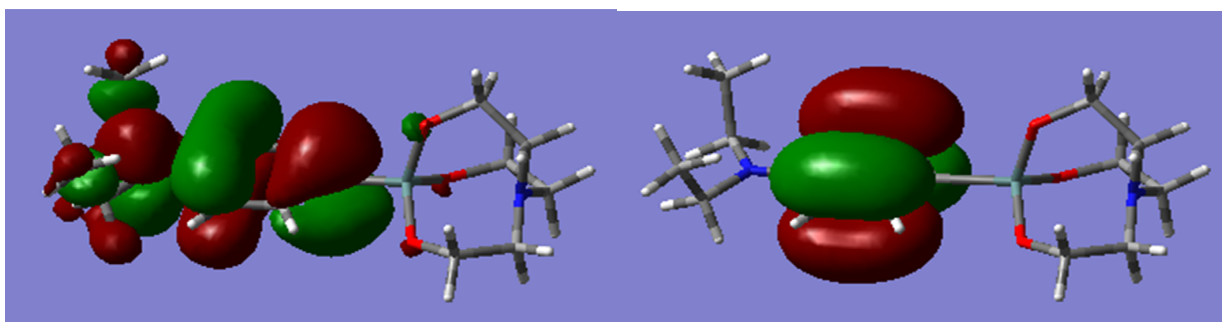
Figure 38: HOMO and HOMO-1 of diethylanilinesilatrane by DFT B3LYP/Lanl2DZ calculations.

5.1.5 UV-vis spectroscopy

Voltammetric stability of the electrogenerated cation radicals of silatranes are allowed to study their UV absorbance using in situ UV-vis spectroelectrochemistry the spectrum of neutral t-butylsilatrane and of its cation radicals are shown in figure 40. Compared to phenylsilatrane (Figure 39), the maximal absorbance of the cation radicals of t-butylsilatrane lies at longer wavelenths, $\lambda = 362$ nm.
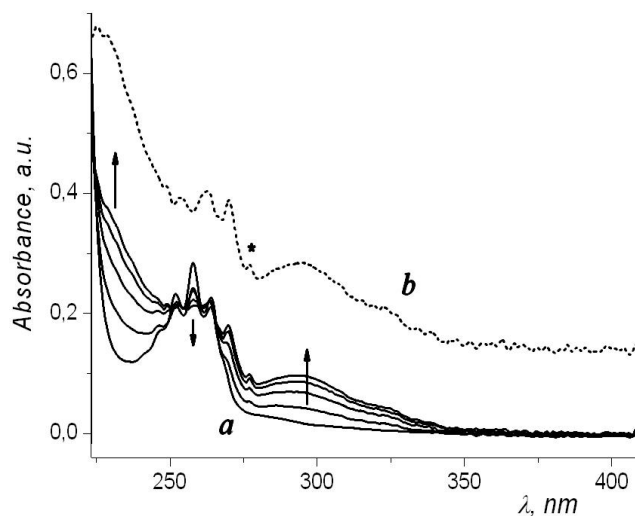
Figure 39: Solvent-subtracted UV spectra of phenyl silatrane a. and of its electrogenerated cation radical (dotted line, b). CH_3CN/0.1M $TBAPF_6$. $E_w = 1.2$ V, Pt micro grid electrode. $\lambda_{max} = 295$ nm. The star shows a UV transition which is symmetry-forbidden in the neutral molecule and which becomes allowed in the cation radical.
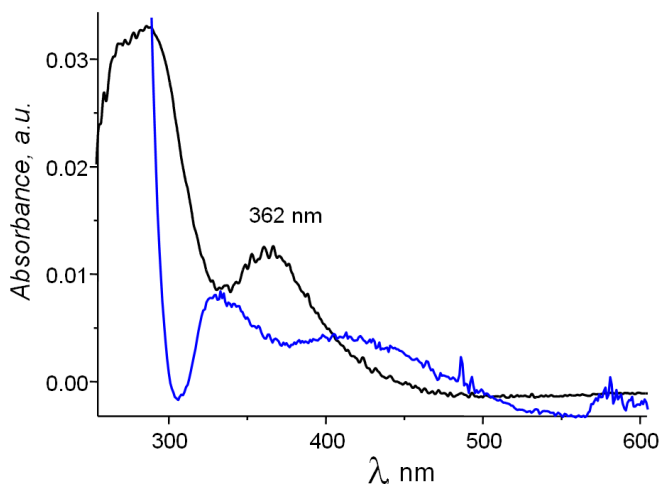
Figure 40: Solvent-subtracted UV spectra of *t*-butylsilatrane (blue) and of its electrogenerated cation radical (black). DME/AN (1:2 v/v) + 0.1 M TBAPF6. Ew = 1.2 V, Pt micro grid electrode. T = 270 K.

Donor inductive effect of three Me groups of the *t*-butylsilatrane substituent at Si rises the level of σ(C–Si) component of the 3c-4e bond thus reducing the LUMO-SOMO gap in the cation radical compared to that in the cation radical of methyl or phenyl silatrane. This effect accounts to the bathochromic shift of the maximum of UV-absorbance of this species (sf. Figure 40).

5.1.6 DFT calculations

The geometry and electron density of phenyl- and benzyl- silatrane as well as their cation radicals were adjusted first at HF/6-311G level then the structures were optimized by DFT B3LYP/Lanl2DZ level for long-term and delocalizing electronic interactions. The same level was used for NBO analysis and to check the optimized structures for the absence of imaginary vibrations.

In a total agreement with the results of EPR and qualitative orbital considerations, DFT calculations reveal that the HOMO of the "proper" silatranes (i.e. those not carrying an easy to oxidize substituent, like $H_2NC_6H_4-$) is mainly built of the n(N) orbital at the atrane nitrogen (Figure 41) upon withdrawal of one electron, transforming a 3c-4e system into a 3c-3e, the localization and symmetry of the highest (singly) occupied molecular orbital is conserved: main contribution to the SOMO still comes from the p_z(N) orbital. Axial C–H bonds, parallel to the main spin-carrying orbital, participate in spin stabilization in these species and determine the specific pattern of the EPR spectra of "proper" metallatranes.
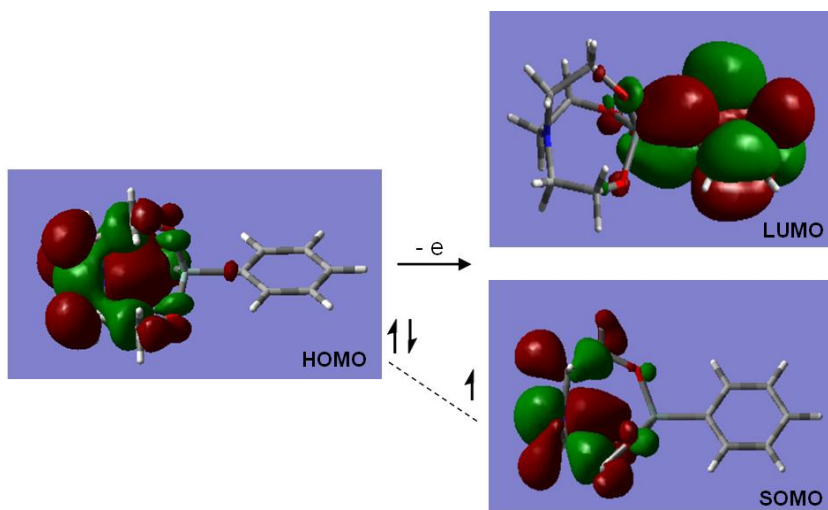
Figure 41: HOMO of phenylsilatrane and N-localized SOMO of its cation radical by DFT B3LYP/Lanl2DZ calculations.
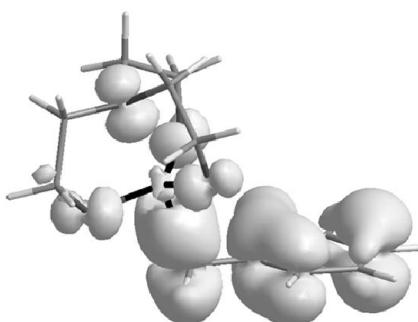
Figure 42: SOMO of the cation radical of benzylsilatrane by DFT B3LYP/Lanl2DZ.

The silatranes with benzyl- and 1-naphthyl substituents have similar HOMO (main contribution from $n(N)$ electrons) but their cation radicals show a quite different structure of highest frontier orbital (Figure 42) As is shown in figure 42 by DFT B3LYP/Lanl2DZ calculations, spin density in the cation radical of benzylsilatrane is mostly delocalized over benzyl fragment, with only small part still residing on N atom (For HOMO of this type of molecules, see figure 32 above). The contribution of the σ(C-Si) orbital, playing the key role in 3c-4e bonding and in the "spin-leakage" mechanism is clearly seen. Supposedly, this feature must be typical for all benzylic (CH_2-aryl) type substituents.

5.2 Bis-(silatranyl)alkanes

In this chapter we will present the results of three products bis-(silatranyl)methane, bis-(silatranyl)hexane and bis-(silatranyl)octane including the cyclic voltammetry and DFT calculations analyses.

5.2.1 Cyclic voltammetry

Three bis-(silatranyl)alkanes were studied in acetonitrile (CH_3CN) solutions containing 0.1 M tetrabutylammonium hexafluoro- phosphate ($TBAPF_6$). Several drops of dichloromethane were added to help dissolving these products. A glassy carbon (GC) working electrode was used to carry out the voltammetry of these compounds because it gave better peak shape than Pt in this case. All these compounds of this reaction series exhibit either one or two oxidation peaks (Figure 43). The oxidation peak current has a good relation with measured scan rate ($i_p/v^{1/2}$ = const.) which implies the electrooxidation reactions follow a diffusion controlled process. In the same electrolyte the chronoamperometry was measured, then this result was combined with the value of the peak current to calculate the absolute electron stoichiometry.
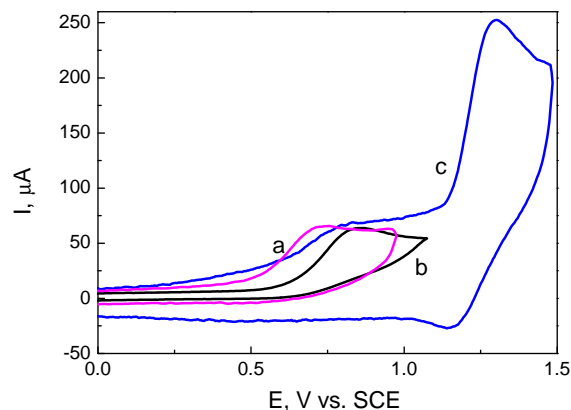
Figure 43: Cyclic voltammetry of *a,* bis-(silatranyl)hexane; *b,* bis-(silatranyl)methane; *c,* bis-(silatranyl)octane (C = 1 mmol/L) in CH_3CN/0.1 M Bu_4NPF_6 (several drops of CH_2Cl_2 was added to help dissolving the product) at a 2 mm GC electrode. v = 1 V/s; T = 25 ^{o}C.

Table 8: Parameters of Electrochemical Oxidation of Silatranes at a GC Disk Electrode at v=1V/s

R	E_p^c(V)	E_p^a(V)	E^o(V)	n	$E_p - E_{p/2}$ (mV)	$\Delta E_p/\Delta lgV$ (V)	α^b
bis-(silatranyl)methane	0.85	–	–	1	117.13	0.18	0.41
bis-(silatranyl)hexane	0.78	–	–	1	114.63	0.08	0.21
bis-(silatranyl)octane	1.30	1.14	1.22	2	87.44	–	0.24

The cyclic voltammetry was carried out in acetonitrile, with 0.1 M of $TBAPF_6$ as the supporting electrolyte. All the voltammograms are corrected by SCE.
Transfer coefficient estimated as a mean of α, from $E_p - E_{p/2} = 1.85RT/\alpha nF$

In this series of three compounds, the oxidation peak of bis-(silatranyl)hexane is the lowest, at E_p^c = 0.78 V, and the peak is irreversible at low scan rate. Similarly the peak of bis-

(silatranyl)methane is very close to bis-(silatranyl)hexane $E_p^c = 0.85$ V as well as the first peak of bis-(silatranyl)octane ($E_p^c = 0.79$ V). If it is the atrane moiety that gets oxidized, the oxidation potential should be higher than this value (less than 1 V). Moreover the measured value of the peak current should be much larger, at such concentrations as the ones presented in the conditions, and at the respective scan rate. On the other hand, this potential corresponds to the oxidation of one of the reactants, namely triethanolamine. It is therefore credible that the peak observed at less than 1 V for the three products represents the oxidation of triethanolamine.

Apart from the first peak shown on its cyclic voltammograms, the bis-(silatranyl)octane displays peaks showing a reversible reaction (Figure 43), at $E^o = 1.22$ V even at low scan rate. It shows a normal peak current value, compared to the previous peak, each recorded in the same conditions respectively. Bis-(silatranyl)octane displays a reversible peak even at low scan rate ($v = 0.5$ V/s) and has the oxidation peak ($E_p - E_{p/2} = 87.44$ mV) (Table 8), but the apparent peak width is too large to correspond to a perfect reversible redox process. As briefly mentionned above, during the experiment, several drops of dichloromethane were added to the solution to help dissolve the compound. However, the quantity of added CH_2Cl_2 was somewhat different for the three compounds. Compared to acetonitrile, dichloromethane is less polar ($\varepsilon = 9$ vs. 37 for acetonitrile) so the voltammograms in such binary solvent are subject to higher distortion due to uncompensated ohmic drops, iR. This could lead to the observed deformation, a broadening and anodic shift of the voltammogram.

5.2.2 DFT calculations

DFT calculations were carried on with the molecule bis-(silatranyl)methane as an example. Compared to the other bis-(silatranyl)alkanes with long chains, bis-(silatranyl)methane has only one CH_2 between two atrane moieties. The CH_2 between the two atrane structures forms 2 σ bonds, with the C_{sp3} atom connected with each of the two Si atoms. Taking into account the lone electron pairs on two N atoms, this structure can be seen as two 3c-4e bonds, one on each side of the atrane molecule.
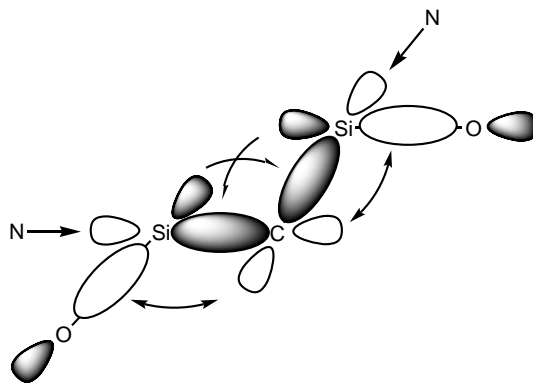
Figure 44: Molecular orbital of bis-(silatranyl)methane lateral σ(Si–O)-σ(Si–C) conjugation.

65

Compared to the silicon atom, each of the two N atoms on the terminal positions and the C atom on the center are more electronegative elements. This is the right condition to form a 5c-6e bond. However, the geometry of the central CH_2 means the two σ bonds form an angle between two atrane parts, instead of being aligned whereas the orbital between Si and O atoms would approach to the two H atoms from CH_2 and form a W shape moleculare orbital which is demostrated in the figure 44. This is supported by the DFT result (Figure 45). Either the neutral or the cation radical form shows clearly that the carbon atom connecting two atrane forms an angle with the two silicon atoms. This angle $\angle$Si–C–Si' $\approx$ 118° (Table 9).
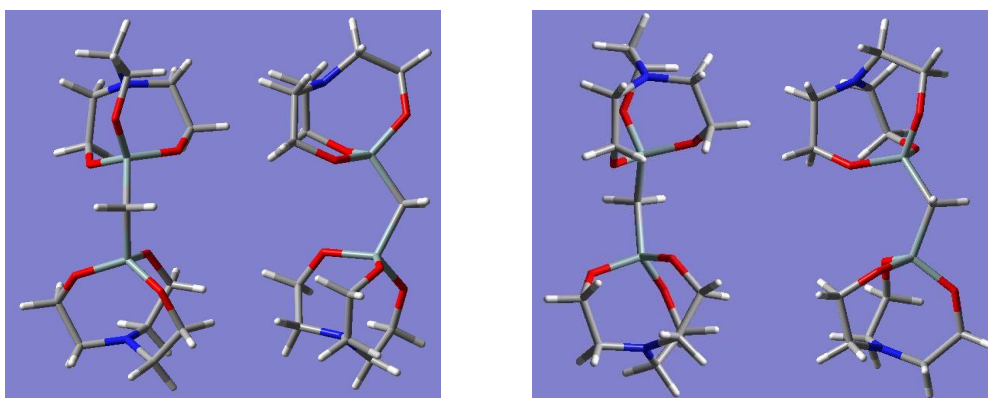
Figure 45: Geometry of neutral (left panel) and cation radical (right panel) of bis-(silatranyl)methane optimized by DFT B3LYP/Lanl2DZ

The result ofthe DFT calculations of the SOMO of bis-(silatranyl)methane when it forms a cation radical is shown figure 46. It is clearly seen that the two parts of the atrane molecule present 2 independent 3c-4e hypervalent bonds instead of one 5c-6e bond. From all the evidences and analyses above, it can be concluded that the hypervalent structure of bis-(silatranyl)methane is established by 2 3c-4e bonds, and not 5c-6e bond, because sp3 hybridization of the central carbon atom and the attraction force between the central hydrogen atom CH_2 and the molecular orbital between Si and O.
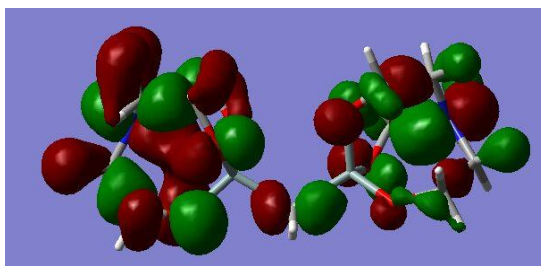
Figure 46: SOMO of the cation radical of bis-(silatranyl)methane from DFT B3LYP/Lanl2DZ calculations. Two crossing 3c-4e moieties are well seen.

Table 9: Selected geometrical parameters (bond lengths in Å, angles in degrees°) and charges in bis-(silatranyl)methane and its cation radical according to DFT B3LYP/Lanl2DZ calculations.

	l(Si–N)	l(Si–C)	∠Si–C–Si'	Mulliken			(NBO)charges	
				N	Si	C	O	O'
Neutral	2.708	1.862	118.43	-0.219	1.623	-1.297	-0.616	-0.625
	2.737	1.863		-0.212	1.656		-0.612	-0.624
							-0.605	-0.602
Cation radical	3.031	1.853	118.44	-0.094	1.629	-1.273	-0.619	-0.628
	3.046	1.853		-0.089	1.646		-0.636	-0.638
							-0.604	-0.600

Table 10: Selected geometrical parameters (bond lengths in Å, angles in degrees°) and charges in bis-(silatranyl)acetylene and its cation radical according to DFT B3LYP/Lanl2DZ calculations.

	l(Si–N)	l(Si–C)	l(C≡C)	∠Si–N–Si'	Mulliken			(NBO)charges	
					N	Si	C_{sp}	O	O'
Neutral	2.669	1.839	1.204	180	-0.839	2.093	-0.408	-0.936	-0.936
	2.668	1.839			-0.839	2.093	-0.408	-0.951	-0.964
								-0.964	-0.951
Cation radical	3.008	1.814	1.229	180	-0.092	1.582	-0.342	-0.628	-0.615
	3.008	1.814			-0.092	1.582	-0.342	-0.615	-0.628
								-0.599	-0.599

Table 11: Selected geometrical parameters (bond lengths in Å, angles in degrees°) and charges in di(methyl)bisilatrane and its cation radical according to DFT B3LYP/Lanl2DZ calculations.

	l(Si–N)[a]	l(Si–C$_{Me}$)	l(N–C)	∠Si–N–Si'	∑(∠C–N–C')	∠O–Si–O'	Mulliken		(NBO)charges	
							N	Si	C(Me)	O
Neutral	3.026	1.850	1.471	180	360	108.17	-0.807	2.374	-1.027	-1.015
	3.027	1.850					(-0.004)	(2.359)	(-1.073)	(-0.996)
Cation radical	3.025	1.850	1.471	180	360	108.17	-0.423	2.321	-1.015	-0.984
	3.027	1.850					(-0.037)	(2.321)	(-1.065)	(-0.975)

[a]Total Si↔Si separation is 6.054 Å in both species.

5.2.3   6 center-8 electron hypervalent bonding

Both bis-(silatranyl)hexane and bis-(silatranyl)octane have long alkyl chains linking the two atrane moieties. This leads us to think that the flexibility displayed by such a long chain would allow two atrane moieties to approach each other when it forms the cation radicals and establish a new hypervalent bonding: 6c-7e. However, for these two compounds, even the length of $(CH_2)_8$ chain is not enough to allow the required axial arrangement of the two terminal silatranyl groups, which finally form two independent 3c-4e bonds (Figure 47). Probably, if the number of carbons on the alkyl chain was higher than 12, such interamolecular arrangment could be observed (Figure 48).
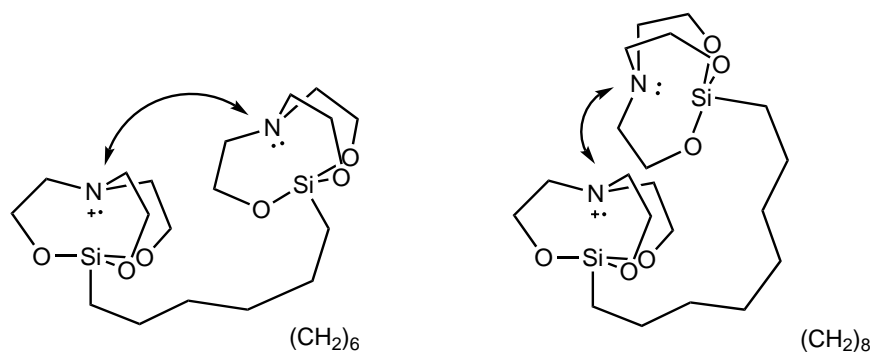
Figure 47: Two independent 3c-4e bonds in molecule bis-(silatranyl)hexane and bis-(silatranyl)octane.
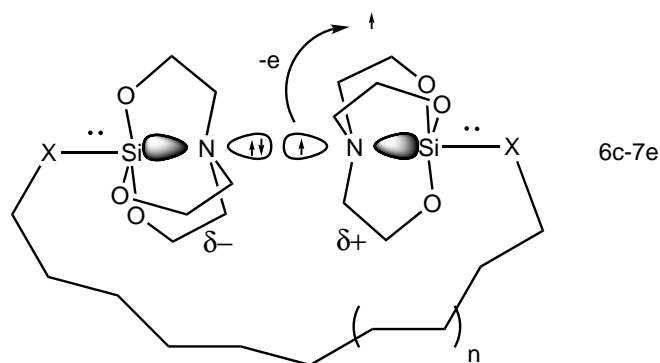
Figure 48: 6c-7e hypervalent bonding in cation radicals when number of carbon on the alkyl chain is more than 12.

5.3   Bi-silatranes

In the previous section we saw the hypervalent bonding in bis(silatranyl)methane. In fact, in classical 5c-6e bond, the central and terminal ligands are highly electronegative with respect to Si. In the case of bis(silatranyl)methane, these positions (the central carbon atom and two

terminal atoms N) are indeed occupied by more electronegative elements. In this section, a series of compounds with two merged silatrane structures were also synthesized, different from bis(silatranyl)methane. In a way, nitrogen atom is now the central atom in the 5c-6e bond (perfectly linear in these molecules), and the two carbon atoms from the substituents act as the terminal atoms. The electrochemical behavior of these new compounds will be discussed in the following section.

5.3.1 Structure

Two novel structures of bi-silatranes were obtained and analyzed by XRD. To complete our research, a known structure di(phenyl)-bi-silatrane was synthesized as well but its structure is not shown in this section.

We started by characterizing the structure of the newly prepared di(ethyl)- and di(benzyl)-bi-silatranes. Their molecular structures are shown in figures 50 and figure 52, the crystallographic data is listed in table 12 and the selected bond lengths and angles are listed in table 13.

Table 12: Crystallographic data and details of structure refinement for di(benzyl)-bi-silatrane

Crystal	di(benzyl)-bi-silatrane
Empirical formula	$C_{23}H_{29}NO_6Si_2$
Formula weight	471.65
Crystal system	Monoclinic
Space group	$P2_1/c$
a (Å)	12.3388(3)
b (Å)	10.6408(2)
c (Å)	18.0121(4)
$\alpha(^o)$	
$\beta(^o)$	99.0570(10)
$\gamma(^o)$	
V (Å^3)	2335.41(9)
Z	4
D_{calcd}(Mg/m^3)	1.341
Radiation (MoKα)	$\lambda = 0.71073$Å
T (K)	150
θRange (^{o})	2.99–27.47
Total reflections	17784
Unique reflections	5275
Parameters	319
R_1, w$R2$ ($I > 2\sigma(I)$)^a	0.0563, 0.1465
Goodness-of-fit on F^2	1.055

$^a R_1 = \sum ||F_0| - |F_c||/ \sum |F_0|; wR2 = \{\sum[w(F_0^2 - F_c^2)^2]/ \sum[w(F_0^2)^2]\}^{1/2}$

The structure of bi-silatranes can be seen in two ways. First, two atrane parts can be considered like two distorted bipyramids with two Si atoms in the body center with three O atoms, one C atom from the substituent and the sharing N atom on the vertexes (Figure 49 *a*). Second, bi-silatrane can be seen as one distorted bipyramid formed by N atom in the body center with three adjacent C atoms and two Si atoms on the vertexes (Figure 49 *b*).

| *a* | *b* |
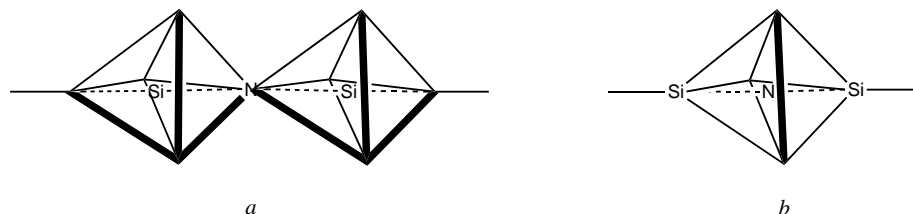
Figure 49: Structure of bi-silatranes *a.* two distorted bypyramids with two Si atoms in the body center; *b*. one non-distorted bipyramid with N atom in the body center.

Notably, in the structure of bi-sialtrane, the nitrogen atom is located on the plane formed by the three carbon atoms in α-positions to the nitrogen atom (as can be seen since the sum of these C–N–C angles is 360°). This is very different from the classic silatranes that we studied until now where nitrogen in *endo*-configuration always kept some tetrahedrality due to its sp^3 hybidization. Both silatrane moieties in this molecule are perfectly symmetric in relation to a plane containing the central N atom and the 3 carbon atoms around it. The Si1–N–Si2 axes is close to linear (Table 13) in both compounds.

Table 13: Main geometrical parameters for di(ethyl)-bi-silatrane and di(benzyl)-bi-silatrane

Compound	$d(\text{Si}\cdots\text{N})$ (Å)	$d(\text{Si–C})$ (Å)	$d(\text{Si–O})$ (Å)	
di(ethyl)-bi-silatrane	2.9766 2.8408	1.985(1) 1.964(4)	1.583(3) 1.643(7) 1.656(9)	1.643(9) 1.712(2) 1.600(6)
di(benzyl)-bi-silatrane	2.9214 2.8996	1.860(2) 1.858(2)	1.617(2) 1.621(3) 1.665(2)	1.576(3) 1.649(2) 1.668(3)

$\angle$N–Si–C (°)	$\angle$Si1–N–Si2 (°)
169.927 169.362	176.01
179,486 178,427	179.91

From these two ways it is obvious that all three atoms Si1, N and Si2 are contorted to an extracoordinating geometry so we can analyze its structure like coordination complex. Apparently being the center atom in a pentacoordination the atom should be electron pair acceptor.

However in the second propose of pentacoordination structure (Figure 49 *b*) that N atom being the center atom of pentacoordinating molecule is not very suitable, thus it is not very interesting for us. On the other hand, being pentacoordinating center Si atom is perfect because not only it is electron pair acceptor but also in first structure propose (Figure 49 *a*) the atoms on the vertexes are more electronegative elements. The substituent of the C atom is positioned on the axial positions, three oxygen atoms at each atrane structure are occupying the equatorial sites and the two Si atoms are in the body centers of each of two pyramidal bodies. This proposal has similar geometry as simple silatrane structure.

For the di(ethyl)-bi-silatrane, the complete crystallographic data could not be obtained successfully since there are more than one molecular structure in one unit lattice - in fact, twelve - and they all point to different directions (Figure 53). This would be caused by the conformationnally fluctuating ethyl substituent on the both sides of this molecule (Figure 51). The Si–C σ bonds of the ethyl fragments allows the rotation about it leading to different orientations of substituents and cause a variety of molecular structures with different mutual orientations of the Et groups (Figure 53).
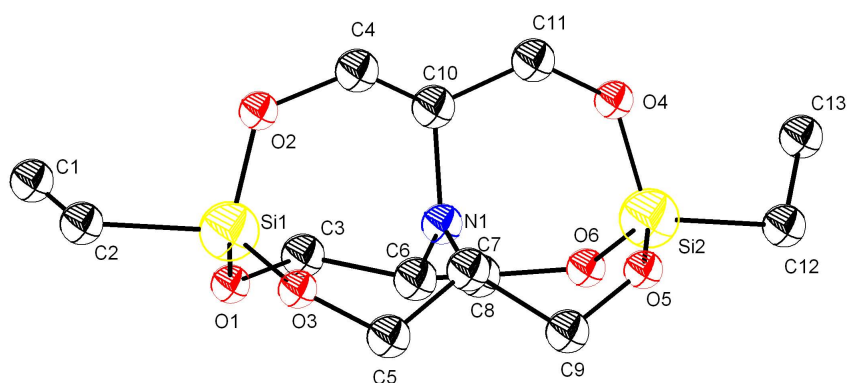
Figure 50: ORTEP drawing at the molecular structure of di(ethyl)-bi-silatrane. H atoms are omitted for clarity.

The silicon atom (Si1 and Si2 from figure 50) is displaced from the plane established by three oxygen atoms towards the carbon atom (C2 and C12 from figure 50) on the apical substituents. The distance between N atom and two Si atoms is practically the same on the both sides though there is a slight difference of 0.1358 ($\mathring{A}$) (4.5%) for di(ethyl)-bi-silatrane. This difference does not seem meaningful in terms of pentacoordination of N but rather relates to the inhomogeneity caused by crystal field during the package of the elementary blocks.
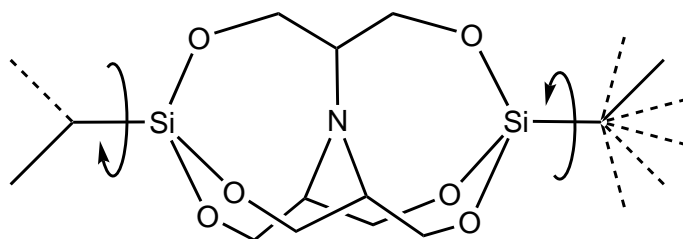
Figure 51: Conformational ambiguity of di(ethyl)-bi-sialtrane depending on the orientation of ethyl substituents.
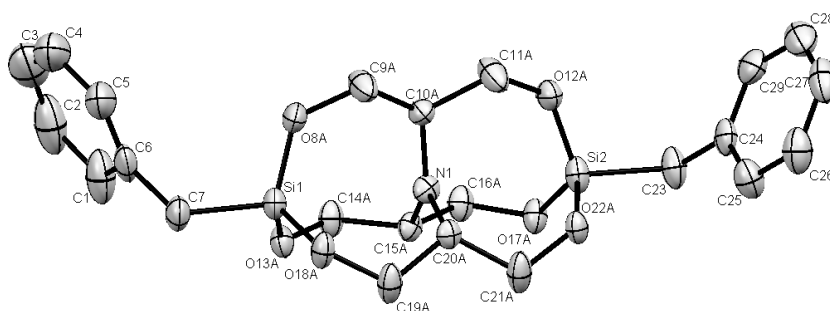
Figure 52: ORTEP drawing of the molecular structure of di(benzyl)-bi-silatrane. Thermal ellipsoids are drawn with 50% probability.
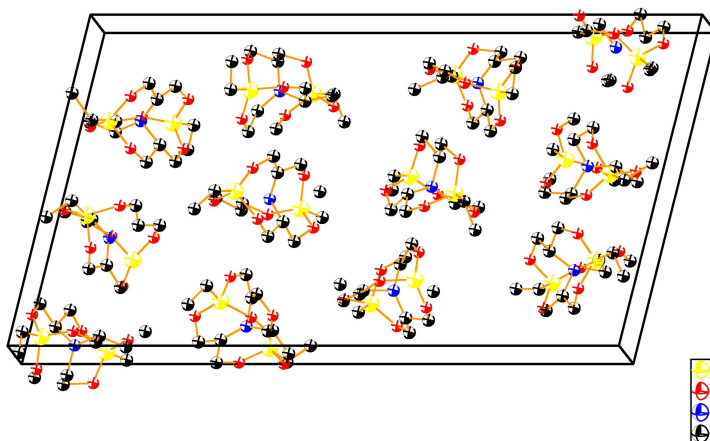
Figure 53: A unit cell molecular structure of di(ethyl)-bi-silatrane.

The crystallographic data for di(benzyl)-bi-silatrane is listed in table 13. It has the similar structure on the atrane part. The difference of the distances between N1 to Si1 and to Si2 is 0.0218 $\mathring{A}$ (0.7%) which is not large enough to be meaningful so we can consider the atom N1 is in the middle of Si1 and Si2.

5.3.2 DFT calculations

The geometry of the bi-silatranes as well as their cation radicals were optimized using by a combined treatment: firstly, geometric parameters were done at HF/6-311G level, and then the structures and NBO analysis were optimized at the DFT B3LYP/LANL2DZ level.
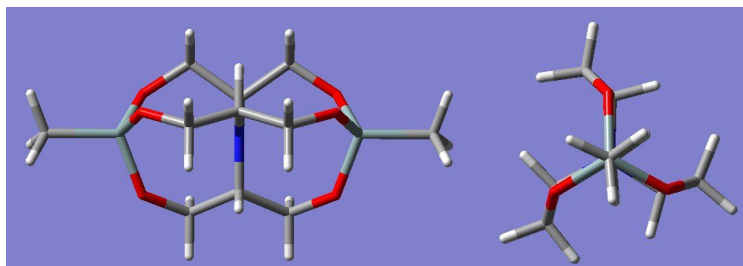
Figure 54: A DFT B3LYP/Lanl2DZ-optimized geometry of neutral di(methyl)-bi-silatrane. Lateral and axial views.
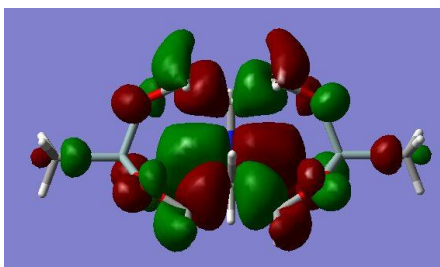
Figure 55: HOMO of di(methyl)-bi-silatrane from DFT B3LYP/Lanl2DZ calculations. Axial 5c-4e bonding system is clearly seen.
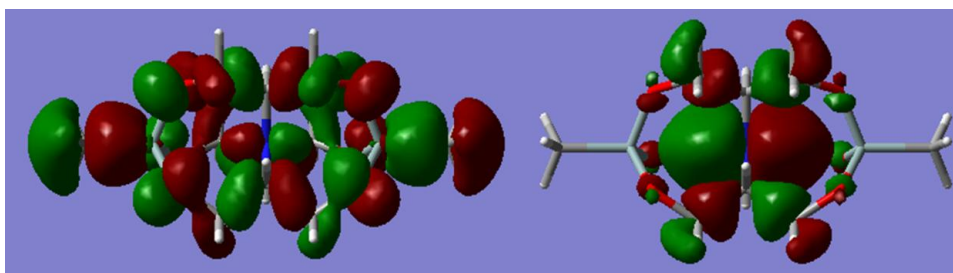
Figure 56: SOMO of di(methyl)-bi-silatrane. Left: one-electron populated (α-orbital) part; right: empty level (β-orbital). DFT UB3LYP/Lanl2DZ calculations.

Unrestricted mode of consideration of the electron configuration of di(methyl)-bi-silatrane allows one to visualize that main contribution to the HOMO of this molecule is constituted of n-electrons of N atom: after the electron removal, its empty part (seen as β-orbital, figure 56) is mostly on N p_z-orbital, whereas remaining unpaired electron (seen as α-orbital) is delocalized over the axial 5c-6e system (which became 5c-5e in the cation radical). A remarkable

participation of parallel elements of the bi-atrane cage (C–C and C–O bonds σ-orbital) is also seen.

5.3.3 Cyclic voltammetry of bi-silatranes and of the model tris(1,3-dihydroxy-2-propyl)-amine

For a better understanding of the electrochemical oxidation of the bi-silatranes, we carried out a series of cyclic voltammetry experiments on these bi-silatranes, and compared these results to the precursor tris(1,3-dihydroxy-2-propyl)amine. The cyclic voltammetry was carried out on the glassy carbon electrode either in acetonitrile (for bi-silatranes) containing 0.1M of Bu_4NPF_6 or in the mixture of DMF and acetonitrile (for tris(1,3-dihydroxy-2-propyl)amine) containing 0.1M of Bu_4NPF_6. The peak currents for all four compounds are linear with the square root of the scan rate ($i_p/v^{1/2}$ = const.), thus suggesting diffusional control of the process. The electron stoichiometry was determined by combining voltammetry parameter $i_p/v^{1/2}$ with the Cottrell slope obtained from chronoamprometry at the same electronde and the same solution.

The electrooxidation is proceeding by one-electron transfers in all four cases (Table 14). As is shown in figure 58, di(ethyl)- and di(phenyl)-bi-silatranes reveal a distinct reversible electrooxidation step even at low scan rate (v = 0.5 V/s). Di(ethyl)-bi-silatrane has an oxidation peak at 1.62 V (vs. SCE) with the cathodic counterpeak at E = 1.49 V (vs. SCE). Di(phenyl)-bi-silatrane has an electrooxidation peak at 1.68 V (vs. SCE) and cathodic peak at 1.59 V (vs. SCE). The width ($\Delta E = E_p - E_{p/2} \approx 65 - 80$ mV) for these three compounds is somewhat larger than 58 mV, the theoretical value for an electrochemically reversible electron transfer. For di(benzyl)- and di(ethyl)-bi-silatranes, the E_p increases with the scan rate slightly more than expected for a first-order electrochemical follow up process of the cation radicals (first-order increase with the slope of 30 mV per decade of the scan rate would be expected). The oxidation peak width of di(phenyl)-bi-silatrane is the smallest of the three compounds (Table 14) which implies that it is closer to a pure Nernstian system. Moreover, the $\Delta E_p/\Delta lg(v)$ slope is close to 20 mV instead of 30 mV which seems to reflect a reversible electron transfer and meaning that the cation radicals of this compound undergo a fast second-order reaction in contrast to the other compounds of this reaction series.

Both di(ethyl)-bi-silatrane and di(phenyl)-bi-silatrane have reversible oxidation peak even at low scan rate (v = 0.5 V/s) which attests a good stability of the cation radicals. There is a slight difference between di(ethyl)-bi-silatrane and di(phenyl)-bi-silatrane in E_p. This slight difference is caused by the electronic properties of the substituents on two sides of bi-silatrane. The C_{sp^2} linking atom from phenyl has higher value of σ_I which makes it more electron-withdrawing as an electron acceptor than ethyl-substituent which has sp^3 hybridization of linking C atom. This slight difference on the hybirdization was reflected in the peak potentials:

74

di(phenyl)-bi-silatrane has 60 mV higher E_p compared to di(ethyl)-bi-silatrane (E_p = 1.62 V).
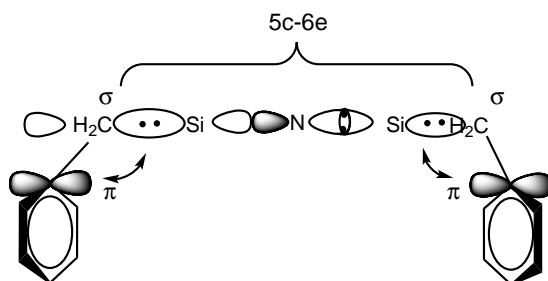
Figure 57: Hyperconjugation effect in di(benzyl)-bi-silatrane

The oxidation peak of di(benzyl)-bi-silatrane is irreversible even at high scan rate (> 5 V/s) which means the cation radical of di(benzyl)-bi-silatrane is unstable at least at room temperature. It has the lowest oxidation value ($E_p^c = 1.45$ V vs. SCE) in all three bi-silatranes which can be explained from two aspects. First of all, both sides of this molecule have the electron donating substituents which for the reasons discussed above for benzyl derivatives in metallatrane series, can manifest some of its π-donnor ability through hyperconjugative mechanism. In fact, similar to the 1-naphthylmethyl silatrane, the σ(C–Si) fragment from the 3c-4e bond and π-system from phenyl are boned by hyperconjugation. At the stage of the cation radical, this effect can cause the spin delocalization from N atom to the π-system of phenyl (Figure 57). Along with the increase HOMO energy (thermaldynamic facilitation of oxidation by lowering the E_o), the increased reactivity of electrogenerated cation radicals also contribute to the lowering of the apparent oxidation E_p through the kinetic shift of E_p with respect to E_o. Based on these two reasons, di(benzyl)-bi-silatrane has the lowest E_p = 1.45 V in three bi-silatranes.

Table 14: Cyclic voltametry data for the oxidation of bi-sialtranes. All samples are taken at v = 1V/s and potentials are corrected to SCE

Compound	E_p^c(V)	E_p^a(V)	E^o(V)	n	$E_p - E_{p/2}$(mV)
Tris(1,3-dihydroxy-2-propyl)amine	0.84	0.69	0.76	1	72
di(benzyl)-bi-silatrane	1.45	–	–	1	81
di(ethyl)-bi-silatrane	1.62	1.49	1.55	1	81
di(phenyl)-bi-silatrane	1.68	1.59	1.63	1	67

$\Delta E_p/\Delta lgV$(mV)	α^a
34	0.7
33	0.6
36	0.6
18	0.7

Transfer coefficient estimated as a mean of α from $E_p - E_{p/2} = 1.85RT/\alpha nF$.

Figure 58: Cyclic voltammetry of *a,* tris(1,3-dihydroxy-2-propyl)amine (C = 0.1 mmol/L) in CH_3CN/DMF, 4:1 v/v 0.1M Bu_4NPF_6 at a 2 mm GC electrode; *b,* di(ethyl)-bi-silatrane; *c,* di(benzyl)-bi-silatrane; *d,* di(phenyl)-bi-silatrane (C = 0.1 mmol/L) in $CH_3CN/0.1M$ Bu_4NPF_6 at a 2 mm GC electrode. v = 1 V/s; T = 25 ^{o}C.
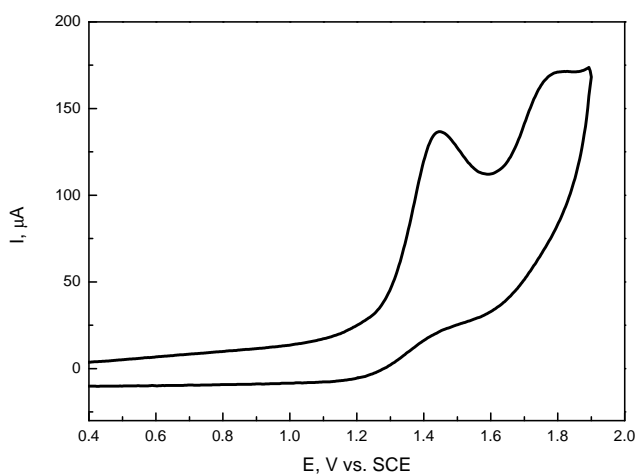
Figure 59: Cyclic voltammetry of the di(benzyl)-bi-silatrane (C = 0.1 mmol/L) in $CH_3CN/0.1M$ Bu_4NPF_6 at a 2 mm GC electrode. v = 1 V/s; T = 25 ^{o}C.

Thus one-electron oxidation of bi-silatranes results in the corresponding silatrane cation radicals. Potential-determining deprotonation of the cation radicals of di(benzyl)- and di(ethyl)-bi-silatranes can be limited at relatively slow scan rates, which creates favorable conditions for stabilizing these species at low temperatures and studying them by EPR spectroscopy. Cation radicals of di(phenyl)-bi-silatrane seem to follow a bimolecular way of reactivity, the feature more typical for delocalized or low energy intermediates.
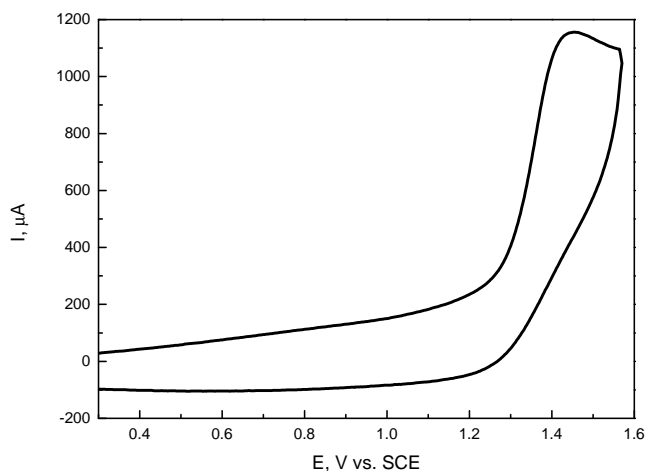
Figure 60: Cyclic voltammetry of di(benzyl)-bi-silatrane at a 2 mm GC electrode. v = 10 V/s; T = 25 ^{o}C.

For comparison, the voltammogram of tris(1,3-dihydroxy-2-propyl)amine was recorded under the similar conditions as the three bi-silatranes. The only difference was that the solvent was mixed with 20% DMF to help dissolving the tris(1,3-dihydroxy-2-propyl)amine completely. Obviously the molecule has only one atom which can be directly involved in electrooxidation (the nitrogen). In this sense, all these compounds have similar reaction center of electron transfer. It is seen (Figure 58) that bi-silatranes have 0.61-0.84 V higher oxidation potentials than tris(1,3-dihydroxy-2-propyl)amine. At the same time the oxidation potentials of the bi-silatranes are higher than those of homological simple silatranes: for instance, di(phenyl)-bi-silatrane has E_p = 1.68 V whereas tolylsilatrane and phenylsilatrane have oxidation peak potentials at 1.35 V and 1.55 V [5], respectively; similarly di(ethyl)-bi-silatrane has 200~400 mV more anodic value (E_p = 1.62 V) comparing to *t*-butylsilatrane (E_p = 1.22 V) or ethylsilatrane (E_p = 1.42 V) [5]. This anodic shift would be correlated with the specific position of nitrogen atom. As the molecules are symmetric, N atom is located in the center of bi-silatrane. Unlike the structure of simple silatrane, N atom in bi-silatrane was on the plane of three carbon atoms on the α-position. From the point of view of electronic effects, there are two acceptors on both sides of N atom forming two axial bonds with two Si atoms and three 2p orbital of N atom as well as three equatorial σ-bonds from sp^3 hybridized with carbon atoms on the α-position (Figure 61). N atom is forced to have a planar configuration so as its p$_z$ orbital (4-electrons) is equally available for donor-acceptor interaction with both Si-fragments. As a result, its energy is remarkably lowered, which is reflected in the increased oxidation potentials.
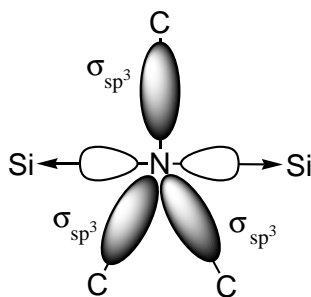
Figure 61: Bonding structure of N atom in bi-silatranes

5.4 1-R-Stannatranes

From the previous studies of metallatranes by various physical chemical methods there follows that dative N→M interactions are stronger when going down the group 14, in the order $Si < Ge < Sn$ [43]. It is expected more than the availability of the lone pair of nitrogen must decrease in the same order and hence the electron withdrawal in the homological metallatranes must become more and more difficult. No data on electrochemistry of stannatranes was reported so far, so we considered the oxidation of several selected stannatranes under the same conditions as described above.

5.4.1 Cyclic voltammetry

To obtain an insight into the intermolecular electronic interactions in the new stannatranes we worked with, their electrochemical behavior was considered. Depending on their solubility, cyclic voltammetry of compounds **12, 13, 14** and **15** (Figure 62) was carried out in acetonitrile (CH_3CN), CH_2Cl_2 or in a binary mixture (CH_3CN/CH_2Cl_2, 1:1 v/v) containing Bu_4NPF_6 (0.1 M) as supporting salt.

Contrarily to silatranes [74, 5] and germatranes [33], the stannatranes **12** and **13** show distinct oxidation signals only at a Pt electrode. The limiting currents i_p of stannatranes **12** and **13** are both diffusion controlled ($i_p/v^{1/2}$ =const; $\lg(i_p)/\lg(v)$ = 0.45 and 0.46 for **12** and **13**, respectively) and, as was shown using $i_p/v^{1/2}$ ratio along with Cottrell slope from chronoamperometry at the same electrode [40], the number of electrons transferred at this step is $n = 1$ (Table 15). Temperature dependence of $\lg(i_p^1)$ of **13** provides E_a = 2.46 kJ/mol (2.85 kJ/mol for second peak), corresponding to the activation energy of the diffusion flow of solvent. The peak half-widths $E_p - E_{p/2}$ of **12** and **13** are too large for simple one-electron reversible processes, supposedly because of the adsorption interactions or substantial structural reorganization accompanying electron transfer.

In a less polar solvent such as CH_2Cl_2, the oxidation of **13** proceeds via two steps (Figure

63), with the second one being reversible already at $v = 0.5$ V/s. With the vertex potential set before the onset of the second oxidation peak ($E_v = 1.45$ V), the first peak also starts showing cathodic counterpart (at $v > 50$ V/s). Thus, both oxidation signals arise from electrochemically reversible processes.
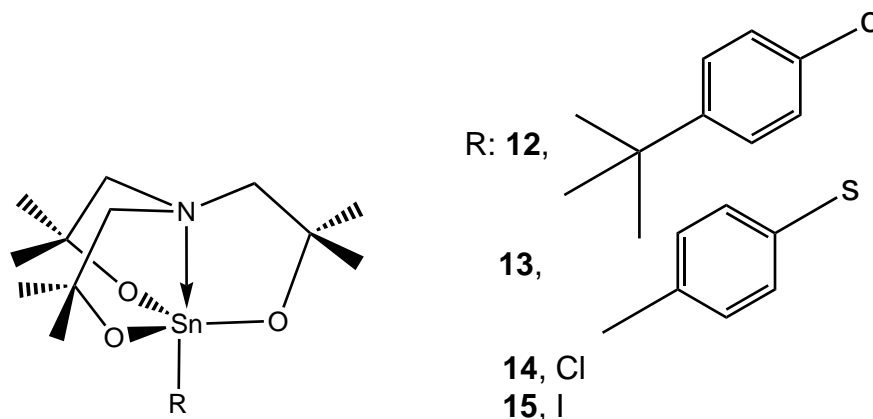
Figure 62: 1-R-stannatranes **12**, **13**, **14** and **15**

Table 15: Parameters of electrochemical oxidation of stannatranes **12, 13, 14** and **15** at a platinum disk electrode

Cpd	Solvent	E_p, V^a	$E_p - E_{p/2}$, V	$\Delta E_p / \lg(v)$, mV	n	IP, eV
12	CH_3CN	1.47	0.171	30	0.94	5.569
12	CH_3CN/CH_2Cl_2	1.46	0.115	48	0.94	
12	CH_2Cl_2	1.33	0.127	43	0.97	
13	CH_3CN	1.41	0.119	25	1.40	5.959
13	CH_3CN	$1.41(1.47)^d$	0.098	49	1.18	
13	CH_3CN/CH_2Cl_2	1.40(1.53)	0.082	58	1.03	
14	CH_2Cl_2	>2.2				7.338
15	CH_2Cl_2	>2.3				

Cpd	Solvent	α^b	$\Delta E_p / \lg(v), \mathrm{mV}^c$
12	CH_3CN	0.3	23
12	CH_3CN/CH_2Cl_2	0.4	19
12	CH_2Cl_2	0.4	17
13	CH_3CN	0.4	22
13	CH_3CN	0.5	25
13	CH_3CN/CH_2Cl_2	0.6	26

^{a} Peak potentials at $v = 1$ V/s. ^{b} Formal transfer coefficient, found from $(E_p - E_{p/2})/1.85 = RT/\alpha F$. ^{c} Two peaks merged. ^{d} Second of two peaks.

The *i-t* curve with the hold at E_p^1 (Figure 63) allowed to subtract the diffusion limited

current of the first peak i_p^1 (the baseline for the second peak [66] and to quantify the current of the second oxidation step, i_p^2. The latter was shown to have an electron stoichiometry of $n = 0.4$, caused by self-reactions involving cation radicals, as it was observed in the case of oxidation of Ar_2S or $ArSM$ [81] with the HOMO localized on the ArS fragment. Thus, the similarity in the oxidation pattern of **13** and of aryl sulfides suggests that the p-$CH_3C_6H_4S$ fragment in **13** is most probably the reaction site that accounts for the first oxidation peak. The E_p of compound **13** is about 150-200 mV higher than those of diaryl or arylalkyl sulfides [82], due to the electron acceptor effect of the stannatranyl substituent. The possibility of oxidation of the stannatranyl moiety at E_p^2 should obviously be ruled out because not only the HOMO but also the lower lying HOMO-1 in **13** is mostly built of sulfur atom orbital.

Moreover, considering orbital energies (as IP $= -\varepsilon_{HOMO}$ in Koopman's approach, by B3LYP/LANL2DZ) of HOMO-1 in **13** (6.655 eV) and of SOMO in $\mathbf{13}^{+\bullet}$ (6.094 eV), it is more probable that a second electron withdrawal affects the cation radical, like in the case of aryl sulfides. In contrast to the trend in E_p^{ox} of diaryl and arylalkyl thioethers, which are easier to oxidize than parent ethers [82], the order of E_p values for oxygen- and sulfur-containing stannatranyl derivatives is reversed (Table 15). This is supposedly because of stronger Sn–S versus Sn–O bonding and a stronger acceptor effect of the stannatranyl moiety on the E_p of **13** compared to the E_p of **12**.
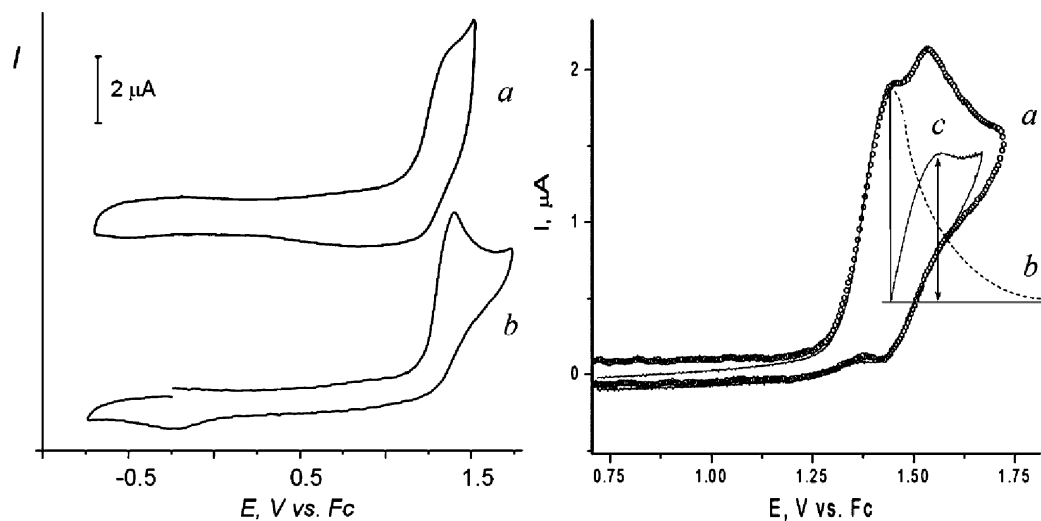
Figure 63: Cyclic voltammograms for the oxidation of stannatranes. Left: (a) − **12** and (b) − **13** (10^{-3} mol/L) in CH_3CN/0.1 M Bu_4NPF_6 at a Pt disk electrode; $v = 5$ V/s. Right: I–E curve of **13** (1.1×10^{-3} mol/L) in CH_2Cl_2/0.1 M Bu_4NPF_6 at a Pt disk electrode. (a) normal scan; (b) $I-t$ curve after the hold at E_p. (c) diffusion limiting current of the second oxidation step. $v = 0.5$ V s^{-1}; T $= 22$ °C.

The stannatranes **14** and **15** did not show any distinct oxidation peaks up to the media limits. As was pointed out by Broka *et al.* [5], the chloro-substituted silatrane $N(CH_2CH_2O)_3SiCl$

cannot be oxidized. No such data exist for the chloro-substituted germatrane $N(CH_2CH_2O)_3GeCl$ but one can expect even higher E_p since germatranes are more difficult to oxidize than silatranes [33, 83]. From a simple correlation of E_p with calculated IPs of the stannatranes **12, 13** and **14**, the oxidation potential of the chloro-substituted derivative **14** should be above 2.3 V which corroborates the results of its voltammetry.

On the contrary, compound **14** shows a well-shaped reduction peak at E_p = -1.5 V; the reduction process results in elimination of Cl^- anions whose oxidation peak at $\sim$1 V is detected by voltammetry during the second cycle. The peak at -1.5 V falls into the range of reduction potentials of known chloridostannanes [84] and might have arisen from the dissociative reduction of Sn–Cl bond in **14**. Similarly, the oxidation peak of the iodide anion I^- appears after the reduction of **15**. This is in agreement with the conductivity measurements of **14** in CH_3CN/CH_2Cl_2 (50:50 v/v), which have only shown residual solvent conductance and no contribution from any ionic conductivity due to the possible Sn–Cl dissociation prior to the reduction. A practically identical conductivity curve was observed for the phenolatosubstituted stannatrane **12**. Therefore the chloridosubstituted stannatrane **14**, just as **12**, remains a covalent compound in solution, at least in this media.

5.4.2   EPR-spectroelectrochemistry

Since the oxidation of the phenoxy-substituted stannatrane **12** shows partial reversibility (Figure 63), it was studied by real-time EPR-coupled electrochemistry. The solution of **12** (10^{-3} mol/L) in $CH_3CN/0.1$ M Bu_4NPF_6, initially ERP-silent, has shown the signal of paramagnetic species when the potential 1.23 V was applied (Figure 64).

The visible end-to-end span of the observed spectrum ($\Delta = 23 - 24$ G) corresponds to the coupling constants from 2 sets of equivalent protons and to some contribution from $^{117/119}$Sn nuclei. The *g*-factor (g = 2.0036) is slightly increased relative to that of pure organic radicals because of the interaction with oxygen and tin and falls into the range of the values for known phenoxyl radicals [85, 86]. The triplet of triplets pattern with 1:2:1 intensities is rather straightforward and fits well with two pairs of practically equivalent protons (*o,o´*- and *m,m´*-) in the supposed phenoxyl species. Though the ends of the spectrum are not well enough resolved to allow extracting exact $Sn^{117/119}$ coupling constants, its symmetry permits to suppose two values a^{119}Sn = 6.7 G and a^{117}Sn = 7.4 G. The set of 2H with the *hfc* constant of $a\mathrm{H_o}$ = 6.22 G can be substituted with two large proton *hfc* constants ($a\mathrm{H_{o-}}$-= 6.27 G and $a\mathrm{H'_{o-}}$ = 6.03 G), assigned to two slightly different ortho-protons of the phenyl ring (see Figure 63).
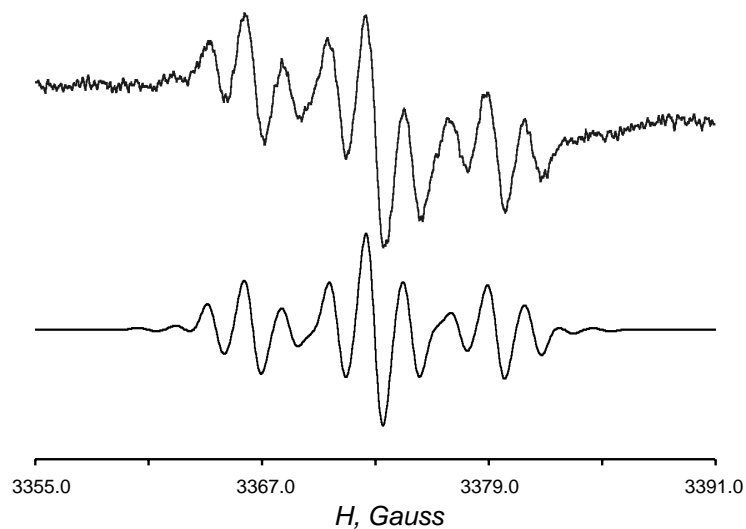
Figure 64: EPR spectrum from the oxidation of stannatrane **12** in CH_3CN/0.1 M Bu_4NPF_6 at a Pt microspiral electrode. Upper, experimental; lower, simulated using the parameters in the text. T = 233 K, E = 1.23 V.

This substitution provides a better fitting but in any case, this difference is at the level of the (possible) contribution from the protons of the *t*-Bu group. Two *m*-protons account for a smaller constant, aH_m = 1.85 G (2H). It appears as there is no coupling with the atrane cage nitrogen atom or, if any, its contribution is very small. In general, the presence of d-metals often results in strong spin-orbital interactions [87] broadening the spectral lines and making it difficult to observe well resolved hyperfine structure. Thus the cation radical of stannatrane **12** has the spin distribution as an O-substituted *t*-Bu-phenoxy radical and not as a proper metallatrane, similarly to the cation radicals of germatranes in which the 1-substituent has lower own ionization potential than the atrane nitrogen atom [83].

5.4.3   DFT calculations

The geometry of the stannatranes **12**, **13** and **14** and of their cation radicals was optimized using a combined treatment: primary adjustment was done at HF/6-311G level, and then the structure was optimized at DFT B3LYP/ DGDZVP level, better accounting for long-term and delocalizing electronic interactions. The same level was used for NBO analysis and to check the optimized structures for the absence of imaginary vibrations.

The N–Sn distance is affected very little by electron withdrawal. It becomes slightly longer in **12**$^{+•}$, slightly shorter in **13**$^{+•}$ and remains practically unchanged in **14**$^{+•}$ (Table 16). Meanwhile, other geometrical parameters of these stannatranes show remarkable configurational change when forming the cation radical. Thus, for the neutral stannatrane **12**, the dihedral

angle $\varphi(\angle$Co-Ar–Ci-Ar–O–Sn) is 93.63°, while it becomes 3.81° in the cation radical (Figure 65) showing that the atrane moiety twists around the O–Sn bond by the right angle (55° for the couple $\mathbf{13/13^{+\bullet}}$).
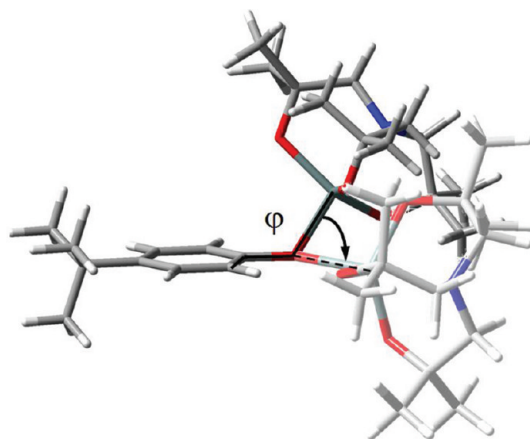
Figure 65: B3LYP/DGDZVP optimized geometry of stannatrane **12** and of its cation radical (see text).

The driving force of this remarkable twist is the interaction of p_z-orbital of the O and S atoms with the $\pi-$systems of the aromatic fragments, destabilizing the HOMO in the neutral molecules and stabilizing the corresponding CRs. The stabilization of the phenoxy system in $\mathbf{12^{+\bullet}}$ is stronger than of the arylthio fragment in $\mathbf{13^{+\bullet}}$: while the couple $\mathbf{12/12^{+\bullet}}$ clearly switches between two most stable forms, orthogonal and planar, (both corresponding to global minima on the corresponding energy surface), the bulkiness of the S atom and the poorer match in the size of overlapping orbital in $\mathbf{13^{+\bullet}}$ force the latter to adopt a compromise half-eclipsed configuration. It implies that the nuclear frames of **12** and **13**, following the redistribution of the electron density upon oxidation (electrochemical electron transfer is adiabatic by its nature), exist in two fixed geometries: those of neutral and of the oxidized forms (**12** vs $\mathbf{12^{+\bullet}}$ and **13** vs $\mathbf{13^{+\bullet}}$).

This fact precludes the formation of pure Nernstian reversible redox systems for these compounds which accounts for small apparent transfer coefficient α for **12** and **13** (Table 15). There is no contribution of the nitrogen atom to the spin−orbital interactions in $\mathbf{12^{+\bullet}}$ since the 3c-4e system has lower energy than SOMO (Figure 66) and is doubly populated. The $\mathbf{12^{+\bullet}}$ is thus a phenoxyl radical; it agrees very well with its EPR spectrum that has no characteristic pattern of a nitrogen-centered radical. Fermi contact couplings at the nitrogen and tin atoms (Table 16), and at the atoms of the phenoxy fragment, obtained from B3LYP/DGDZVP calculations, agree well with this feature. Contrary to cation radicals of germatranes, showing no unpaired spin density on the germanium atom and no coupling with it [34], the spectrum of the iodido-substituted stannatrane **15** shows the $^{117/119}$Sn satellites which is also consistent

with the nonzero FCT on the Sn atom (Table 16).

Table 16: Selected geometrical parameters (distances in Å, angles in degrees), fermi contact terms (FCT, MHz), and NBO charges for stannatranes **12**, **13**, **14** and their cation radicals from DFT B3LYP/DGDZVP calculations

Cpd	l(Sn–N)	l(Sn–X)^a	$\angle$N–Sn–X	$\angle$X–Sn–O^b	$\angle$O–Sn–O^b
12	2.240	2.030	171.66	102.46 (89.07)	126.77 (101.43)
12$^{+\bullet}$	2.265	2.121	177.84	96.32 (98.93)	118.73
13	2.402	2.442	175.94	101.72	116.02
13$^{+\bullet}$	2.273	2.582	173.82	99.99 (91.72)	118.46
14	2.374	2.373	179.97	100.60	116.69
14$^{+\bullet}$	2.376	2.332	164.89	105.72 (90.45)	126.34 (111.03)

Cpd	N		Sn	
	FCT	q(NBO)	FCT	q(NBO)
12		-0.348		1.296
12$^{+\bullet}$	0.0000	-0.342	-0.3056	1.307
13		-0.326		1.171
13$^{+\bullet}$	0.0003	-0.342	-2.6584	1.196
14		-0.327		1.195
14$^{+\bullet}$	0.7022	-0.327	104.5738	1.163

^{a} X is first atom of the 1-substituent. ^{b} for two Sn-symmetrical O$_{eq}$ atoms, the value given in the parentheses is for the remaining nonsymmetrical O$_{eq}$.

Upon oxidation of the chlorido-substituted stannatrane **14**, the tin atom also undergoes substantial reorganization: instead of a trigonal bipyramid it adopts the configuration of the pyramid with a rhombic base, when one oxygen atom is at the apical position and the long diagonal of the base is formed by nitrogen and chlorine atoms (Figure 67); in general it resembles to Berry pseudorotation transition state. The calculated Sn–O$_{eq}$ bond length is 1.994 Å in average, whereas the third Sn–O$_{eq}$ distance (for which $\angle$Cl–Sn–O$_{eq}$ = 90°) is 2.244Å. The N–Sn–Cl angle being 180° in the neutral molecule is smaller by about 15°, bringing closer the nitrogen and chlorine atoms (Table 16).

The structure of the HOMO of the chloro-substituted stannatrane **14** is rather complex (Figure 67). Contrary to the HOMOs of lighter metallatranes (M = Si, Ge) the 3c-4e bonding system of which involves the easiest to ionize orbital (n-electrons of N) [33, 34, 88], the HOMO of **14** only contains it to a small extent (at least, at the B3LYP/DGDZVP theory level) suggesting that upon electron withdrawal, the whole orbital system involved must be very perturbed with no possibility of delocalizing stabilization of the cation radical.
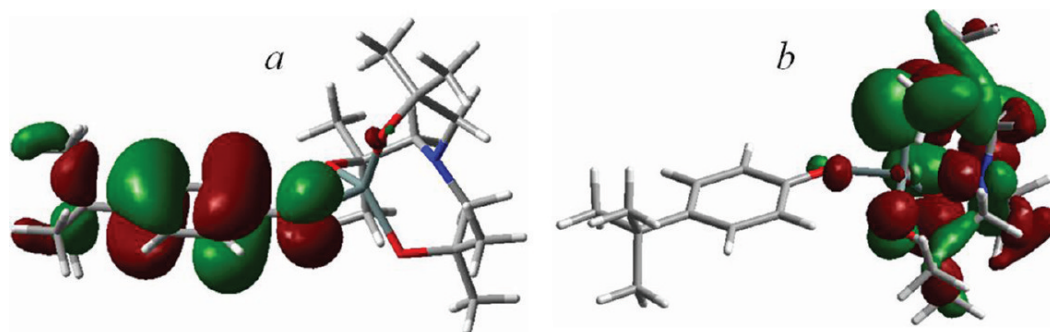
Figure 66: Unpaired electron density (SOMO) delocalization on the phenoxy fragment in the cation radical $12^{+\bullet}$ by B3LYP/DGDZVP (*a*), and doubly populated (SOMO−1) orbital (*b*) with small contribution of 3c-4e N–Sn–O bonding.
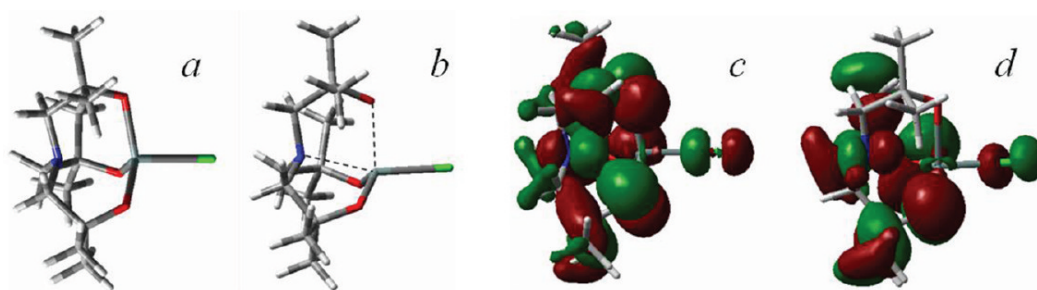
Figure 67: Geometry and FMOs for $14/14^{+\bullet}$ from B3LYP/DGDZVP optimization: (*a*) neutral, (*b*) cation radical, (*c*) HOMO of **14** and (*d*) SOMO of $14^{+\bullet}$. The contribution of intramolecular N–S–O (3c-4e) bonding is clearly seen, though with moderate orbital coefficients.

The spin-bearing orbital in $14^{+\bullet}$ is mainly localized on the tin atom (sf. Table 16), and is neither sterically shielded nor involved into conjugation as in germatranes [33, 34]. On this reason it is probably much more difficult to observe this species in solution, since it is closer to R_4Sn or R_5Sn radicals [89] than to known cation radicals of sila- or germatranes with N-centered spin-carrying orbital [33, 34]. The importance of surrounding Sn O_{eq}-atoms in the HOMO suggests a strongly perturbed Sn environment upon electron removal leaving few chances for observing such cation radical under conventional conditions. It is then rather questionable whether it is possible to observe these species in solution, above the freezing point of common electrochemical solvents. Also, **14** has high value of the ionization potential (Table 15) which, using the approximate E_p – IP correlation, leads to the E_p of about 2.4–2.6 V, meaning that the oxidation of this stannatrane could not be observed under the conditions employed. However, these estimations are based on the gas phase data and bonds polarization in the solution might lower the actual oxidation potential, so a broad shoulder observed at ∼2.2–2.3 V for **14** and **15** in CH_2Cl_2 might actually stem from this oxidation. In any case, high oxidation potential of **3** and **15** excludes the use of spin traps because many of them

undergo oxidation much before these potentials.

5.5 Distannatrane from electroreduction of halostannatranes

Because of their low lying HOMO, halostannatranes are hardly oxidizable. On the contrary, they have a LUMO localized on antibonding σ^*(Sn–X) orbital which can relatively easily accept an extra electron and therefore allow electroreduction.

Alkyl and even aryl chlorostannanes have similar LUMO, therefore one can expect that the reduction of halostannatranes would follow a similar way. Electrochemical reduction of chlorostannanes was reported by several authors who provided a lot of information on this process, albeit quite contradictory [90, 91, 92]. Most important conclusion that one can draw from these studies, is that -whatever the exact mechanism- electroreduction of tin chlorides in aprotic media results in the corresponding distannane products. With this in mind, we examined cathodic reduction of the above halostannatranes (X = Cl, Br, I) in view of obtaining so far unknown distannatrane.

This molecule, containing central Sn–Sn bridge, corresponds to the 4c-6e bonding scheme and therefore it would be very tempting to prepare it in view of exploring its behavior in electron-withdrawal processes.

5.5.1 Cyclic voltammetry of electroreduction of halostannatranes

Before creating the Sn–Sn bond by electrochemical reaction of halostannatranes, it is required to reveal the mechanism of the electrochemical reduction of these compounds. We studied electroreduction of the halo stannatranes (X = Cl, Br, I) and compared it with model tin compounds, Ph_3SnCl and Bu_3SnCl.

All three halostannatranes, chloride, bromide and iodide have well-shaped reduction peaks (Figure 68, 69). Although the peak shape is somewhat deformed -probably by adsorptional interactions-, their reduction peak currents are linear with concentration and with square root from the scan rate $(\Delta\lg(i)/\Delta\lg(\sqrt{v}))$; these tests confirm the diffusional character of the process at these potentials. To determine the calculate the electron stoichiometry of electroreduction of these hoalstannatranes, we used three methods whose results are presented in table 17. First, absolute n was obtained by combination of i_p from the linear sweep voltammetry and of Cottrell relationship. Second, known amount of ferrocene was added to the solution at the end of every experiment and the voltammogram was recorded with ferrocene; n was then calculated from the proportion between i_p of the stannatrane and i_p of ferrocene. Third, n was obtained from the comparison of i_p of stannatranes with those of Cl^- or Br^- ions, added as corresponding salts LiCl and Et_4NBr. All these methods converge in that the process at E_p^1 corresponds to the transfer of 1-electron.
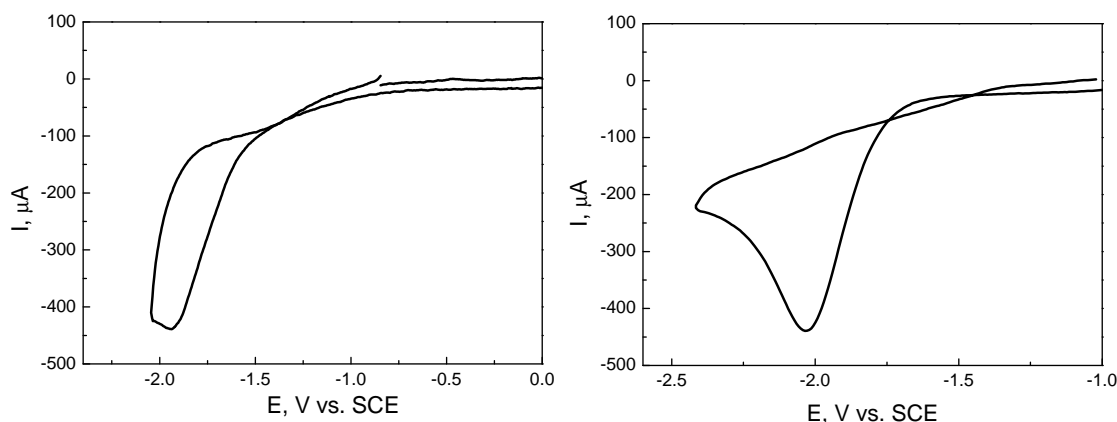
Figure 68: Cyclic voltammetry of electroreduction of left, stannatrane chloride; right, stanna-trane bromide (C = 0.1 mmol/L) in CH_3CN/0.1M Bu_4NPF_6 at a 2 mm GC electrode. v = 1 V/s; T = 25 ^oC.
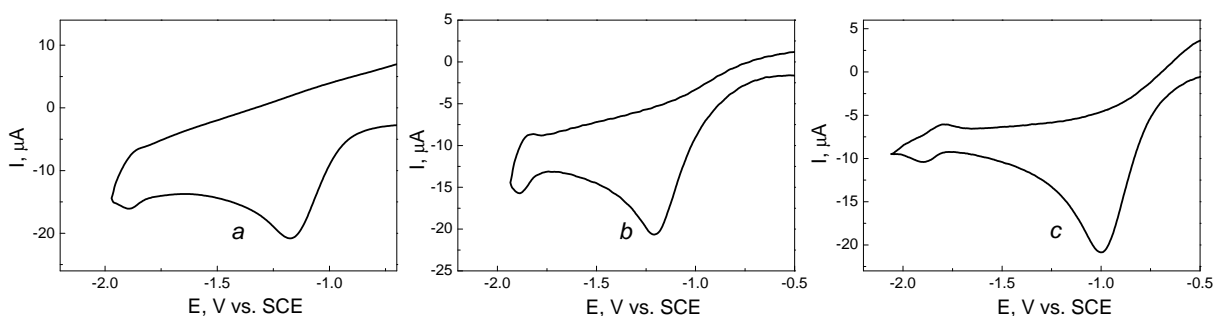
Figure 69: Cyclic voltammetry of electroreduction of a, stannatrane chloride; b, stannatrane bromide (C = 0.1 mmol/L) in CH_3CN/0.1M Bu_4NPF_6 at a 1 mm Pd electrode; c, stannatrane iodide (C = 0.1 mmol/L) in CH_3CN/0.1M Bu_4NPF_6 at a 1 mm Pt electrode. v = 1 V/s; T = 25 ^oC.

Table 17: Parameters of electrochemical reduction of stannatrane chloride, stannatrane bro-mide, tributyltin chloride and triphenyltin chloride at a GC electrode.

Cmpd	$E_p(V)^a$	$\Delta E_p - E_{p/2}(V)$	n^b	n^c	n^d
Stannatrane chloride	-1.94	0.19	1	1	1
Stannatrane bromide	-2.04	0.15	1	1	1
Stannatrane iodide	–	–	–	–	–
Tributyltin chloride	-2.14	0.16	2	1	-
Triphenyltin chloride	-2.55	0.11	2	1	-

[a] Peak potentials (E_p) at v = 1 V/s; [b] n is obtained from chronoampermetry; [c] n is from compar-ison with i_p of ferrocene; [d] n is from oxidation currents of Cl^- and Br^- ions, in CH_3CN/0.1 M Bu_4NPF_6 v = 1 V/s; T = 25 ^oC.

Several articles have reported the reduction process of Ph_3SnCl. A. Savall *et al.* claimed

Table 18: Parameters of electrochemical reduction of stannatrane chloride, stannatrane bromide, tributyltin chloride and triphenyltin chloride at a transition metal electrode.

Cmpd	E_p^1(V)	E_p^2(V)	$\Delta E_p^1 - E_{p/2}^1$(V)	n
Stannatrane chloride	-1.17[a]	-1.90[a]	0.13[a]	2
Stannatrane bromide	-1.20[a]	-1.89[a]	0.16[a]	2
Stannatrane iodide	-1.00[b]	-1.90[b]	0.15[b]	2
Tributyltin chloride	-1.60[c]	-2.90[c]	–	2
Triphenyltin chloride	–	–	–	–

[a]The values are measured at a 1 mm Pd electrode; [b] the values are measured at a 1 mm Pt electrode; [c] [93].

that the reduction of Ph_3SnCl at -2.2 V vs. Ag/Ag^+ is a two-electron process leading to Ph_3Sn^- via $Ph_3Sn^\bullet$ and thereafter to $Ph_3SnSnPh_3$ by chemical steps [91] whereas R. E. Dessy *et al.* [93] found that the reduction of triphenyltin chloride exhibits two well-defined waves. The reduction step at -1.6 V vs. $AgClO_4$/Ag, shown to require one electron per mole of triphenyltin chloride, yielded quantitatively hexaphenylditin. The second reduction wave at -2.9 V vs. $AgClO_4$/Ag could represent the uptake of two electrons per mole to lead directly to Ph_3Sn^- then to the dimer $Ph_3SnSnPh_3$ [93]. By the other side, Holm *et al.* [94] reported $E_{1/2}$ potentials of $E_{Ph_3Sn^\bullet/Ph_3Sn^-}$ and $E_{Bu_3Sn^\bullet/Bu_3Sn^-}$, which are -0.54 V and -0.93 V vs. SCE respectively [94]. The discrepancy one can note in the bibliographic data stems on the reduction of Ph_3SnCl is caused by the fact that the reduction has been carried out on cathodes made of different materials. More precisely, some electrodes were made of transition (Pt) or post-transition (Hg) metals while others were made of graphite or glassy carbon (GC).

At a GC electrode, a proper reduction of the Sn–X bond whose σ^* component corresponds to the (LUMO of the molecule) takes place. On the contrary, on a Pt or Hg electrodes, a preceding oxidative addition of the Sn–X compound to the surface-located metal atoms might occur. Consequently, it is not a Sn–X but Sn–Pt–X or R_3–Sn–X intermediates who undergo electroreduction under these conditions (Figure 69). The electron uptake to such metallo-organic species requires much less cathodic potentials than the direct reduction of cation radicals to the R_3Sn–X σ^* orbital (LUMO). The reduction potentials of such R_3Sn–M–X species are less negative than those of known $E_{1/2}$ of reductuion of $Sn^\bullet$-centered radicals [94]. Therefore, it is not surprising that one-electron reduction of R_3Sn–M–X surface-located intermediates is followed by second one-electron step at more negative potentials, corresponding to the formation of R_3Sn^- anions (the step being less cathodic and hence usually absorbed in an overall two electron reduction peak if the reduction is carried out at a GC electrode).

Difference in the observed n values for Ph_3SnCl and Bu_3SnCl on the one hand, and for halo- stannatranes on the other, might arise from different steric hindrance in these systems in

homobimolecular reactions like S_N2 or radical dimerization: $Ph_3Sn > Bu_3Sn >$ Stannatrane. Unlike parent Si or even Ge derivatives, stannatrane is bulky because of the inner d-orbital of Sn. Sn atom forms longer bonds with its environment and is much more available for external reagents steric hindrance from the phenyl groups is comparable with that of three *i*-Pr substituents; *n*-Bu, though normally, create more steric hindrance than three O-Alk groups in stannatrane, because the latter are attached to the back N-atom and fixed in one direction.

Therefore, the rates of S_N2 attack of stannatranyl anion on chlorostannatrane or of the radical dimerization of stannatranyl radicals are supposedly higher than for the corresponding Ph_3Sn-species.

In the case of a two-electron process ($n = 2$), the mechanism could be the following:

$$R_3SnCl + e \xrightarrow{\quad -Cl^- \quad} R_3Sn^{\bullet} \xrightarrow{\quad + e \quad} R_3Sn^-$$
$$ E_1 \phantom{\xrightarrow{-Cl^-}} E_2 \quad |E_1| > |E_2|$$

$$R_3Sn^- + R_3SnCl \xrightarrow{\quad -Cl^- \quad} R_3SnSnR_3$$
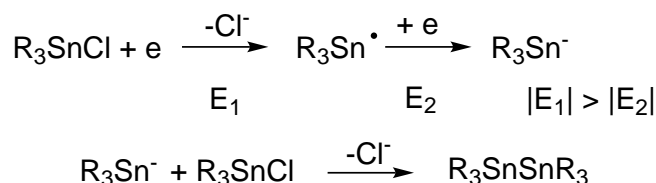
Scheme 15: Two-electron reduction process of chlorostannanes (R = Ph, Bu).

Halogenostannane has associated one electron and lost Cl^- at the first step, leading to the radicals $R_3Sn^{\bullet}$; then these unstable radicals were reduced (addition of another electron) and formed R_3Sn^- at the potential of their formation.

Then the R_3Sn^- anions would attack the unreduced molecule R_3SnCl to substitute one Cl^- and to form the dimeric organotin (Scheme 15). If there is a proton source in the system, HD, the R_3Sn^- anions could be protonated to form R_3SnH:

$$R_3Sn^- + HD \xrightarrow{\quad -D^- \quad} R_3SnH$$
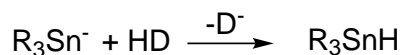
Therefore, Q_{Total} in a large scale reduction must be 1 F/mol, since two electrons per mole are needed for the reduction of one Sn–Cl bond (Scheme 15) but the R_3Sn^- anions, reacting with neutral molecule R_3SnCl, consume second equivalent of the chlorostannane thus leading to the overall stoichiometry of 2e/2 molecules = 1 F/mol. However, from the cyclic voltammetry of R_3SnCl the electron stoichiometry is $n = 2$. This probably because of the slow rate of the nucleophilic displacement (Scheme 15) in a short time scale ($t \to 0$), which does not occur to a substantial extent during the voltammetric experiment but is accomplished during much longer preparative electrolysis. Thus there is a disagreement on the electron stoichiometry between the results of cyclic voltammetry and large scale reduction analysis.

On the contrary, for halo-stannatranes the n value is unity even in the conditions of voltammetry. This is supposedly because of higher rate of nucleophilic substitution at these compounds for the steric reasons discussed above.

The order of E_p of halo-stannatranes is seemingly inversed with respect to the usual easiness of the series Cl < Br < I. However, the values of their $\Delta E_p - E_{p/2}(V)$ are quite large (Table 17), so the observed difference in E_p (stannatrane chloride) and E_p (stannatrane bromide) is not really meaningful.

5.5.2 Electroreduction of halostannatranes at transition metal cathodes

From the analysis above it is supposed that for stannatrane chloride, during the electroreduction at a transition metal working electrode (Pt, Pd or Hg), the radical intermediate $R_3Sn^\bullet$ is formed at less negative potential:
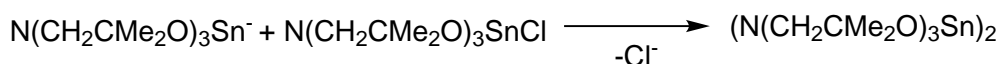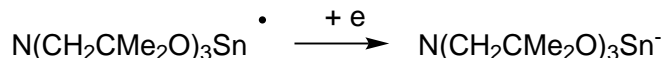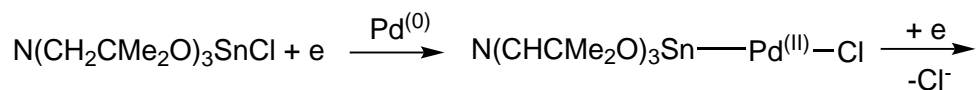
To prove the existence of these intermediate stannatranyl radicals, spin trapping with α-phenyl-N-*tert*-butyl-nitrone (PBN) was applied. Because the reduction potential of PBN is more negative than the potential of forming atranyl radicals $Sn^\bullet$, this spin trap can be used under the condition of reduction of R_3Sn–Pt–Cl intermediates:
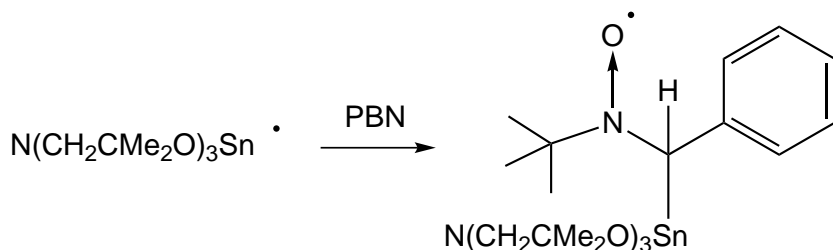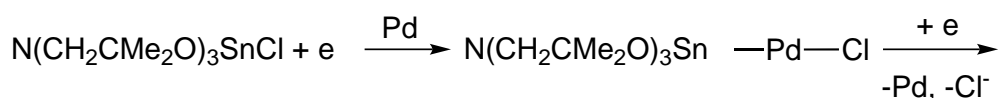
During the electroreduction of the corresponding halostannatranes (table 19) it is confirmed the formation of Sn-centered radicals during the reduction process in this range of weakly cathodic potentials and hence the occurrence of a different mechanism of reduction at transition metal electrodes. Under these conditions, similar species were as well trapped with model chlorostannanes, Ph_3SnCl and Bu_3SnCl (Figure 70). Small proton *hfc* constants

in these adducts attest bulky character of the trapped radical addend and the values of a_H are reciprocate to the steric demand of the concerned species: Ph_3Sn > Bu_3Sn > stannatrane. In the case of stannatrane iodide (Figure 73), only the nitrogen triplet spectrum was obtained, arising from the spin-adduct without α-proton. As was mentioned before, this stannatrane is light-sensitive, its decomposition probably involving radical species. In addition, it has higher Lewis acidity than the other stannatranes. Since the concentration of PBN in the catholyte is inferior to that of the iodostannatane, the nitrone was supposedly all reacted with these decomposition-induced radicals via hydrogen abstraction or simply via deprotonation.

Table 19: Spin trapping of electrogenerated stannyl radicals with PBN[a]

Halostannane	g-factor	hfc, G	Ratio
Ph_3SnCl	2.0065	a_N: 14.687, a_H: 2.732	50%
	2.0067	a_N: 13.815, a_H: 2.333	50%
Bu_3SnCl	2.0065	a_N: 14.625, a_H: 3.129	75%
	2.0067	a_N: 13.854, a_H: 2.286	23%
	2.0073	a_N: 16.183	2%
Stannatrane chloride[b]	2.0083	a_N: 14.596, a_H: 3.357	92%
Stannatrane bromide	2.0065	a_N: 14.543, a_H: 2.760	79%
	2.0067	a_N: 13.846, a_H: 2.329	18%
Stannatrane iodide	2.0064	a_N: 15.704	98%

[a] Electrolyses at a Pd electrode in CH_3CN/0.1 M $TBAPF_6$; [b] Electrolysis in THF/0.1 M $TBAPF_6$.
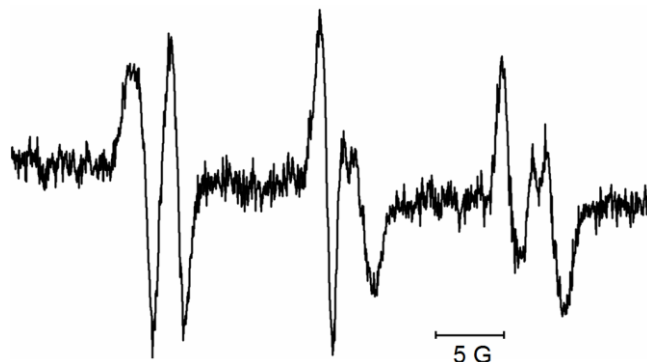

Figure 70: EPR spectrum from ex-cell spin-trapping experiments with PBN during the reduction of Bu_3SnCl. Electrolysis at a Pd cathode in CH_3CN/0.1 M $TBAPF_6$, E = -0.9 V. T = 293 K.

Besides major spin-adduct, in all experiments run in acetonitrile, there is also a signal from an extra radical species (with g = 2.0067 and $a_N \cong$ 13.83 G, $a_H \cong$ 2.3 G), supposedly the
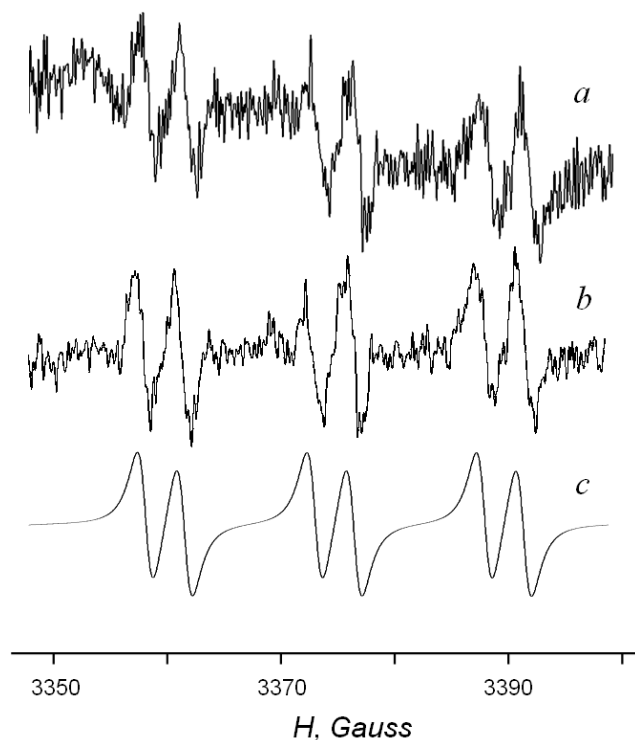
Figure 71: EPR spectrum from ex-cell spin-trapping experiments with PBN during the reduction of chlorido stannatrane. (a) Experimental, (b) baseline-corrected, (c) simulated. Electrolysis at a Pd cathode in THF/0.1 M $\mathrm{TBAPF_6}$, E = -1.0 V. T = 293 K.

spin-adduct from the trapping of solvent-related radical by PBN. In similar experiments using THF as solvent, this signal was not observed. In case of reduction of $\mathrm{Bu_3SnCl}$ in the presence of PBN, trace amounts of a spin-adduct without α-proton (spectrum as simple triplet with single nitrogen constant, g = 2.0073 and a_N = 16.183 G) was registered, the species issued of a two-step trapping, which involves H-abstraction by $\mathrm{Bu_3Sn^\bullet}$ and first stannyl-radical addition providing an even-electron stannylated adduct which then acts as a trap for second $\mathrm{Bu_3Sn^\bullet}$ radical.

Therefore we tried to obtain the dimer of stannatrane by electroreduction. The result was shown in the figure 74: *a* is the cyclic voltammogram of stannatrane chloride before the electrolysis and *b* is after 1 h electrolysis. It is obvious that the reduction peak of stannatrane chloride disappeared after the electrolysis which indicates that there is no more stannatrane chloride in the solution (distannanes are not reducible [93]). After separation purification, and we obtained dimer of stannatrane chloride. We did the same electrolyse with two model organotin chlorides (triphenyltin chloride and tributyltin chloride) and also obtained corresponding the dimers. Table 20 shows the chemical shifts of $^{119}\mathrm{Sn}$ NMR. There are large shifts to higher fields from the monomer to dimer (Table 20). The result of GC-MS also proved that the dimer was obtained after electrolysis in the case of triphenyl- and tributyl tin chloride. However it
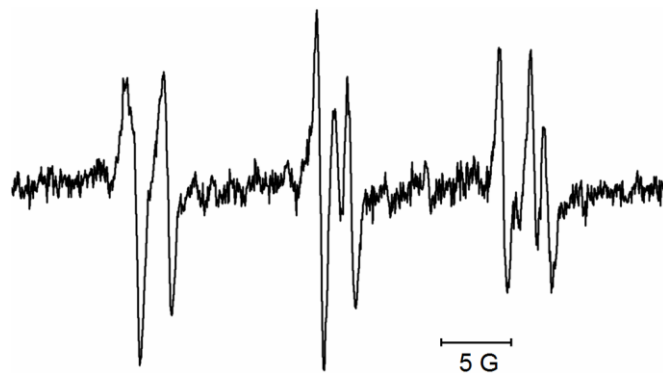
Figure 72: EPR spectrum from spin-trapping with PBN during the reduction of bromo stanna-trane. Electrolysis at a Pd cathode in CH_3CN/0.1 M $TBAPF_6$, E = -0.9 V. T = 293 K.

Figure 73: EPR spectrum from spin-trapping experiments with PBN during the reduction of iodo stannatrane. Electrolysis at a Pd cathode in CH_3CN/0.1 M $TBAPF_6$, E = -0.7 V. T = 293 K.

cannot detect the dimer of stannatrane chloride.

Table 20: dimer SnSn (Result of GC-MS)

Compound	$\delta^{119}Sn$ (ppm)	E (V)	Product	$\delta^{119}Sn$ (ppm)
Triphenyltin chloride	-44.90	-0.54	Tris(n-phenyl)distannane	-143.27
Tributyltin chloride	156.88(144)^a	-0.93	Tris(n-butyl)distannane	-82.66
Stannatrane chloride	-243	-1.94	Bis-stannatrane	-639.72

^{a}[95, 96]

5.5.3 Oxidation of distannatrane

Besides the above proofs obtained from chemical analysis, the cyclic voltammetry of electrooxidation of distannatrane was examined as well as compared with the oxidation of dimer $Bu_3SnSnBu_3$.

On the anodic branch of voltammogram of the solutions electrolyzed at 1.34 V vs. SCE, new peaks appeared, as shown in figure 75. Since neither stannatrane chloride nor tributyltin chloride are oxidizable at these potentials, one can suppose these peaks to arise from the oxidation of the corresponding distannane products.

However, other candidates for the oxidation at these potentials should be considered as

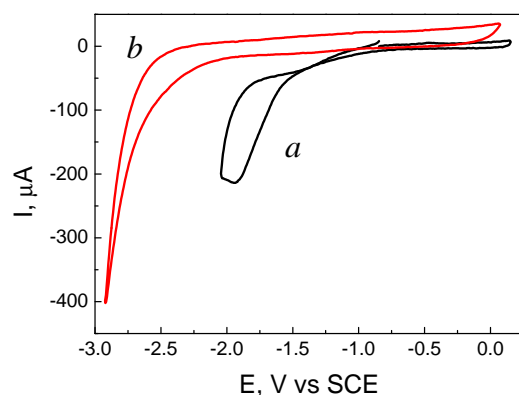Figure 74: Voltammetric monitoring of the electrolysis of stannatrane chloride E = -1.94 V at GC electrode in CH_3CN/0.1 M $LiClO_4$ *a*. electroreduction before electrolysis; *b*. after 1 h

well. A very easy oxidation of Ph_3SnH was reported, $E_p = -0.3$ V vs. SCE [97] or $E_p = -0.4$ V vs. SCE [98], though in more recent accounts it was confronted with much higher value of $E_p = 0.8$ V vs. SCE [99]. It was mentioned above that the $E_{1/2}$ of the redox couple $Ph_3Sn^+/Ph_3Sn^\bullet$ was reported, $E_{1/2} = 0.2$ V vs. SCE [94]. ($E_{1/2}(Ph_3Sn^\bullet/Ph_3Sn^-) = -0.46$ V in CH_3CN vs. SCE and $E_{1/2}(Bu_3Sn^\bullet/Bu_3Sn^-)$ = -0.93 V in DMSO vs SCE).
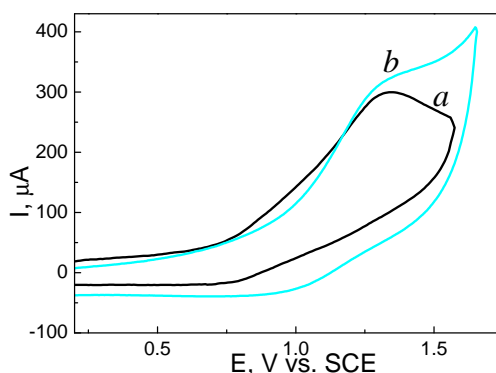
Figure 75: Cyclic voltammetry of *a* bis-stannatrane (C = 0.1 mmol/L) in CH_3CN/0.1M $LiClO_4$ at a 2 mm GC electrode v = 1 V/s T = 25 ^oC; *b* tris(*n*-butyl)distannane (C = 0.1 mmol/L) in CH_3CN/0.1M $TBAPF_6$ at a 2 mm GC electrode v = 1 V/s, T = 25 ^oC.

Moreover it is reported that the oxidation dimer of $Me_3SnSnMe_3$ and $Et_3SnSnEt_3$ occurs at 1.28 V and 1.24 V vs. Ag/AgCl (Ag/AgCl = 1.99 V vs. NHE), respectively, in CH_3CN at GC electrode [100] these values are close to those observed in our cyclic voltammetry expressions of dimers. Thus one can believe that the oxidation peaks at the potential 1.34 V and 1.33 V vs. SCE (Figure 75) are dimer $Bu_3SnSnBu_3$ (*b*) and distannatrane (*a*) respectively even though the peaks are not reversible and the values of peak width ($E_p - E_{p/2}$) are much larger to correspond to a perfect redox process.

94

5.6 New non-coordinating fluoride encapsulating silsesquioxane-based supporting electrolyte

Weekly coordinating anions mostly used in supporting electrolytes can be arbitrarily divided into four groups (Figure 76): those with a Lewis acid central atom carrying additional electron-acceptor substituting atoms (a: BF_4^-, PF_6^-, AsF_6^-, SbF_6^-), those with bulky delocalizing organic groups (b: Ph_4B^-), those combining both features (c: bulky delocalizing groups with electron-withdrawing substituents, $(C_6F_5)_4B^-$, $[(CF_3)_2C_6H_3]_4B^-$, $[(CF_3)_3CO]_4Al^-$), and relatively recently introduced icosahedral carboranes CB_{11} containing no π-orbital (d: $CB_{11}H_6X_6^-$ with X = Cl or Br).

On the other hand, many "rattle-like" systems (e) are known, in which an atom or an ion is entrapped inside of a hollow cavity, with no covalent bonding between them. Metals inside of fullerenes ($M@C_{60}$), hydrogen atom in octahedral silsesquioxanes ($H^\bullet@T_8$), and fluoride anion in zeolites provide such examples. Recently, Bassindale et al [101] discovered a new class of silsesquioxane structures, with F^- anion encapsulated inside of the T_8Ph_8 cage. Negative charge in these systems is hidden in the center of an inert siloxane box cutting off direct coordination with external electrophiles in favor of purely electrostatic interactions.
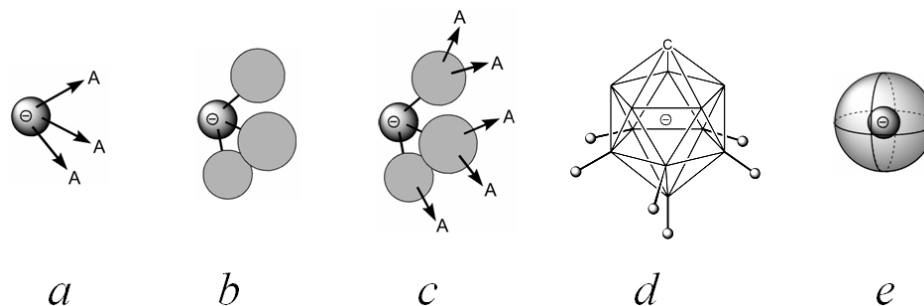
Figure 76: Different types of low-coordinating supporting electrolyte anions

It was pointed out that such compounds could not be prepared with non-acceptor substituents at Si [101, 102]. Since the LUMO of T_8R_8 structures lies inside of the T_8 cage [103], the electron-withdrawing substituents should raise its level, so if it worked with R = Ph, then all substituents whose inductive electron-withdrawing effect (Taft's σ_R) is stronger than that of Ph (Figure 77), in principle must permit the formation of such anions. Based on this consideration, we prepared TBA salts with F^- encapsulating T_8R_8 cages choosing the R groups bordering the silsesquioxane cage which would be potentially compatible with the electrochemical environment (R = Ph, CH_2CN, CH_2CH_2CN, $CH_2CH_2CF_3$).
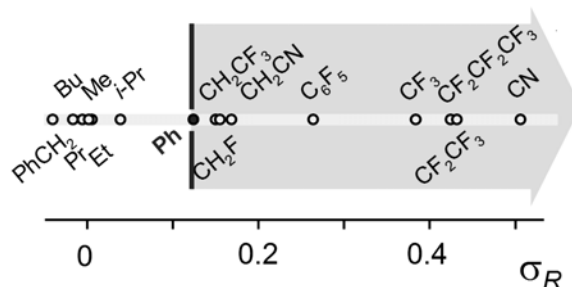
Figure 77: The substituents with Taft inductive constants σ_R suitable for the formation of fluoride-encapsulated silsesquioxane salts TBA[F$^-$@T$_8$R$_8$].

In the meantime other structures, all with the substituents R satisfying $\sigma_R > \sigma_{Ph}$ requirement, have been prepared: R = p-R-Ph, $(CH_2)_2(CF_2)_mCF_3$ (m = 0, 3, 5, 7 [104]), Vin, CH=CH$_2$Ph and CH$_2$CH$_2$(CF$_2$)$_n$CF$_3$ (n = 0, 3, 5) [105].

As was shown by DFT B3LYP/6-311G(d,p) calculations, there is no substantial charge transfer from the central F$^-$ anion to the surrounding atoms of the silsesquioxane cage: NBO charge on F$^-$ changes from -1 to -0.89 when passing from free to the T$_8$-entrapped form. Given that F$^-$ ion can enter and leave the T$_8$ cage [104, 105], the use of polar solvents should rather be precluded, as they will destabilize the F$^-$@T$_8$ systems by solvation of the cage-escaped F$^-$ anion.
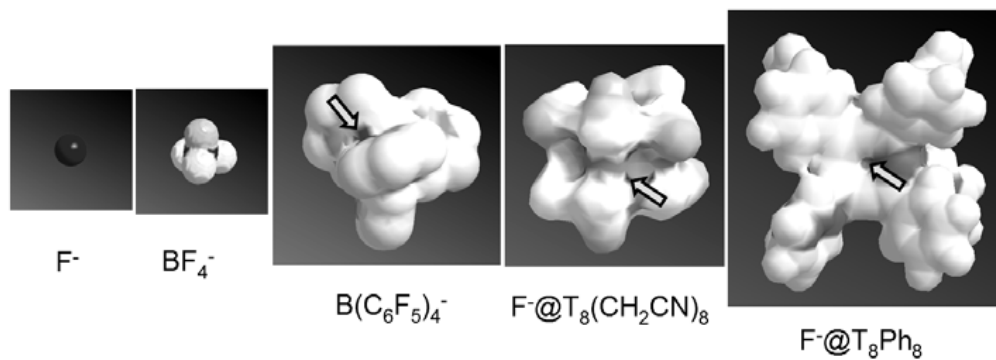
Figure 78: Negative charge (dark areas for F$^-$ and BF$_4^-$, and those marked with the arrows for the other anions) mapped on solvent available surface for low-coordinating anions (DFT B3LYP/6-311G(d,p) calculations); F$^-$ and BF$_4^-$ are given for comparison.

$$\lambda^\circ = eFx/r_h\eta\{0.5y(y/x)^2[1 + r_S + 4r_S\sqrt{2}/(r + r_S)^2(1 + M_W/M_S)^{1/2}]\}$$

5.6.1

Negative charge, mapped on the solvent available surface and visible by external elec-

trophiles, is shown in figure 78 for $F^-@T_8R_8$ (with R = CH_2CN and Ph), and is compared to several common anions. Whereas free F^- anion is 100% available from all sides, only small electrophiles (H^+, Li^+, Na^+) can approach the zones of a meaningful nucleophilicity in $F^-@T_8(CH_2CN)_8$ and $F^-@T_8Ph_8$.

In aprotic solvents like CH_3CN and THF, the TBA($F^-@T_8R_8$) salts undergo ionic dissociation. Limiting values of molar conductivity of these anions, λ_o, have been estimated (table 21) using Stokes equation $\lambda_o = N_A e^2/(6\pi\eta r)$ and within the more advanced model of Kuznetsova (Eq 5.6.1) taking into account solvent holes fluctuation, radius of the solvation sphere and frontal resistance to the movement of a bulky ionic complex in this media [106].

Here x is a mean distance between solvent molecules, r_h and r_S are "hole" and solvent radii, y is the radius of the moving ionic complex, M_W and M_S are ion and solvent masses, respectively, and η is solvent viscosity.

Table 21: Limiting molar conductivites of $F^-@T_8$ anions and their TBA salts

R	$M_W(F^-@T_8R_8)$, g/mol	$r(F^-@T_8R_8)$, Å[a]	$\lambda_o(F^-@T_8R_8)$, S cm^2/mol	Λ_o[b], S cm^2/mol
Ph	1033	6.70	27.15 (29.75)	69.45 (71.87)
$(CH_2)_2CF_3$	1212	6.40	29.75 (30.96)	72.05 (73.26)
$(CH_2)_2CN$	867	6.34	29.97 (31.25)	72.27 (73.55)

[a] From DFT B3LYP/6-311G(d, p) optimized geometry.
[b] $\Lambda^o = \lambda^o(F^-@T_8R_8) + \lambda^o(Bu_4N^+)$; in parenthesis, the values form Stokes model are given.
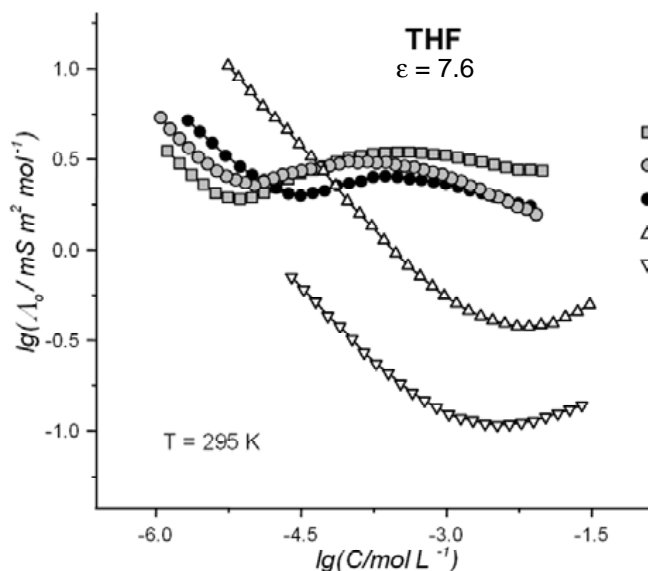

Figure 79: Molar conductivity of THF solutions of: ($\square$)TBA[$F^-@T_8(CH_2CH_2CF_3)_8$], ($\circ$)TBA[$F^-@T_8(CH_2CN)_8$], ($\bullet$)TBA[$F^-@T_8Ph_8$], ($\triangle$)TBABF$_4$, ($\triangledown$)TBAF.

In THF solutions, the conductivity of $TBA(F^-@T_8R_8)$ salts are about 10 times higher than that of $TBABF_4$ (Figure 79); in CH_3CN it is slightly lower, even for the anion with CH_2CN substituent, mimicking acetonitrile itself. Interestingly, that in THF ($\varepsilon = 7.8$) the $F^-@T_8R_8$ anions all show a shallow minimum due to ion pairing, which occurs at the concentrations much below those practically used ($C \cong 5^{-10}$ M) beyond which the conductivity remains stable. For $TBABF_4$, such minimum is observed at the values close to practical concentrations ($C \cong 2^{-10}$ M). In perfluoroisopropanol, $TBA(F^-@T_8Ph_8)$ shows a deep minimum corresponding to the formation of ion pairs and then the conductivity regains the same values as in CH_3CN (Figure 80).
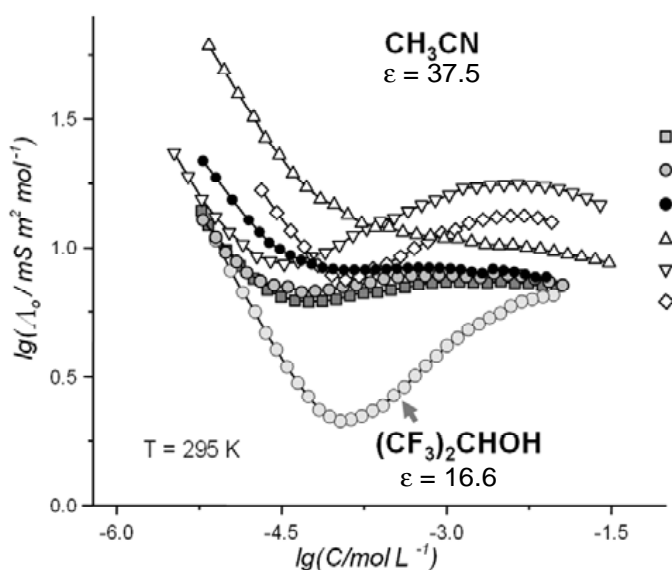
Figure 80: Molar conductivity of CH_3CN solutions of: ($\square$)$TBA[F^-@T_8(CH_2CH_2CF_3)_8]$, ($\circ$)$TBA[F^-@T_8(CH_2CN)_8]$, ($\bullet$)$TBA[F^-@T_8Ph_8]$, ($\triangle$)$TBABF_4$, ($\triangledown$)TBAF, ($\lozenge$)TMAF, ($\blacksquare$)$TBA[F^-@T_8Ph_8]$ in$(CF_3)_2CHOH$.

In the same solvent, the difference of potentials between two consecutive electron transfers of an electrochemically stable redex system, $\Delta E = E_o^1 - E_o^2$, is a good criterion for assessing the energy of ion pairing between the electrogenerated ionic species and the counter ion of the supporting electrolyte; this aspect was considered in details in many papers, both for reduction and oxidation processes, see e.g. [56, 57, 58]. We used the reversible one-electron oxidation of phenothiazine (Scheme 16), followed by formation of unstable dication, as a probe for comparing the ion-pairing ability of $F^-@T_8R_8$ anion with that of several common electrochemical anions.
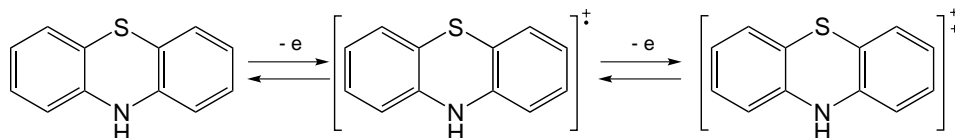
Scheme 16: Reversible one-electron oxidation of phenothiazine

Table 22: Difference in potentials of first and second oxidation peaks of phenothiazine with different supporting salt anions TBAX in CH_3CN

X	E_o^1, V[a]	ΔE_o^1, V[b]	E_p^2, V	$E_p^2 - E_o^1$, V
BF_4^-	0.269	0	0.869	0.600
PF_6^-	0.281	0.012	0.925	0.644
$B(C_6F_5)_4^-$	0.325	0.056	1.188	0.863
$F^-@T_8Ph_8$	0.325	0.056	1.316	0.991

[a] *vs.* Ag/0.1 M $AgNO_3$ in CH_3CN
[b] *vs.* $E_o^1(BF_4^-)$

Table 23: Difference in potentials of first and second oxidation peaks of phenothiazine with different supporting salt anions TBAX in CH_2Cl_2

X	E_o^1, V[a]	ΔE_o^1, V[b]	$E_p^2(E_o^2)$, V	$E_p^2 - E_o^1(\Delta E_o)$, V
BF_4^-	0.258	0	1.018	0.760
PF_6^-	0.258	0	0.986(0.873)	0.728(0.615)
$B(C_6F_5)_4^-$	0.319	0.061	1.148(0.967)	0.829(0.648)
$F^-@T_8(CH_2CH_2CF_3)_8$	0.321	0.061	1.395	1.074

[a] *vs.* Ag/0.1 M $AgNO_3$ in CH_3CN
[b] *vs.* $E_o^1(BF_4^-)$

The voltammograms of oxidation of phenothiazine with different anions are shown in figure 81, and the corresponding values of E_o and E_p are collected in Table 22. First oxidation peak shows slight anodic shift upon going from BF_4^- anion, taken as a reference, to less coordinating PF_6^- and then to $(C_6F_5)_4B^-$ anion. Though E_p^1 with $F^-@T_8Ph_8$ anion is more positive than that with $(C_6F_5)_4B^-$, the E_o values are similar in these two cases (Table 22). Second oxidation peak shows more dramatic anodic shifts and the ΔE^{2-1} ($E_p^2 - E_o^1$) value is maximal for $F^-@T_8Ph_8$ anion attesting its least ion pairing with the dication of phenothiazine. Similar trends were observed in CH_2Cl_2 (Table 23), the corresponding ΔE^{2-1} value for $F^-@T_8(CH_2CH_2CF_3)_8$ in this case is even greater.
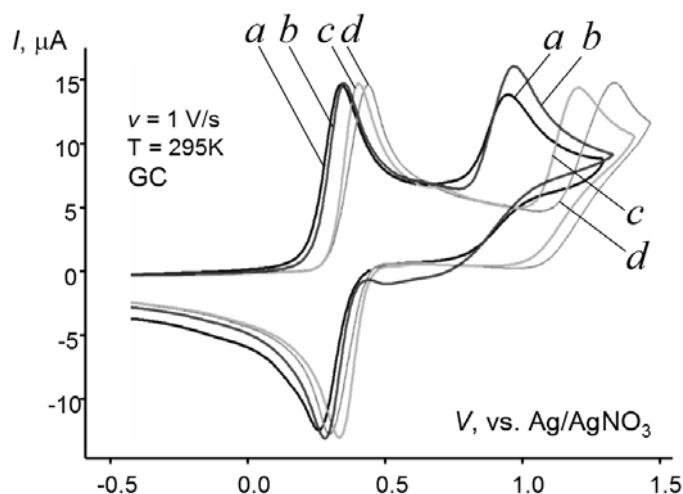
Figure 81: Oxidation of phenothiazine (2×10^{-3} mol/L) at a GC disk electrode in CH_3CN using different supporting TBA salts. (*a*) $TBABF_4$, (*b*) $TBAPF_6$, (*c*) $TBAB(C_6F_5)_4$, (*d*) $TBA(F^-@T_8Ph_8)$.

The THF/0.07 M $Bu_4N(F^-@T_8Ph_8)$ system was used for EPR-spectroelectrochemical study of one-electron reduction (Scheme 17) of 9-halofluorene [107]. Reconstruction of the observed spectrum (Figure 82) using Simphonia program (Bruker) was possible with the parameters (g = 2.0026; $a_{9-H} = 13.89$ G, $a_{1,1'-H} = 3.92$ G, $a_{2,2'-H} = 0.88$ G, $a_{3,3'-H} = 3.81$ G, $a_{4,4'-H} = 0.68$ G) close to those reported for free fluorenyl radical. It is supposed that Ph groups of the silsesquioxane anion serve as a kind of aromatic matrix accommodating and stabilizing fluorenyl radical.
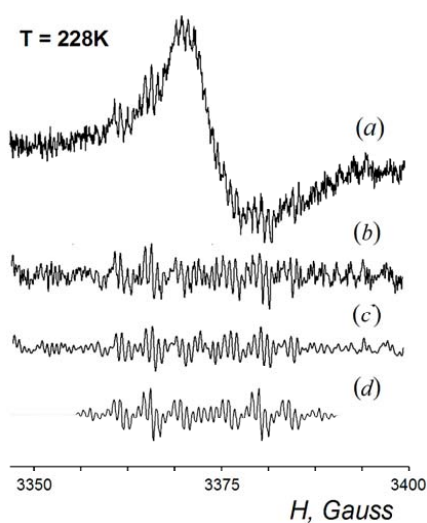
Figure 82: EPR spectra from the reduction of 9-iodo-fluorene (in propylene carbonate-THF (1:2 v/v)/0.07 M $Bu_4N(F^-@T_8Ph_8)$. (*a*) experimental, (*b*) high-frequency component, (*c*) same signal after FFT filtering, (*d*) simulated using the parameters in the text.
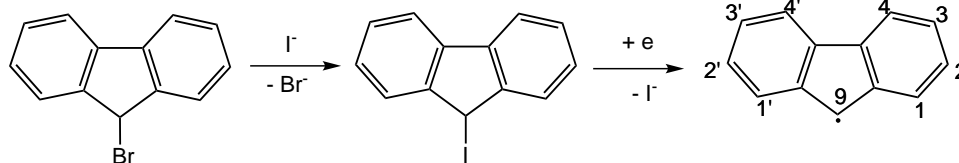
Scheme 17: One-electron reduction of 9-halofluorene.
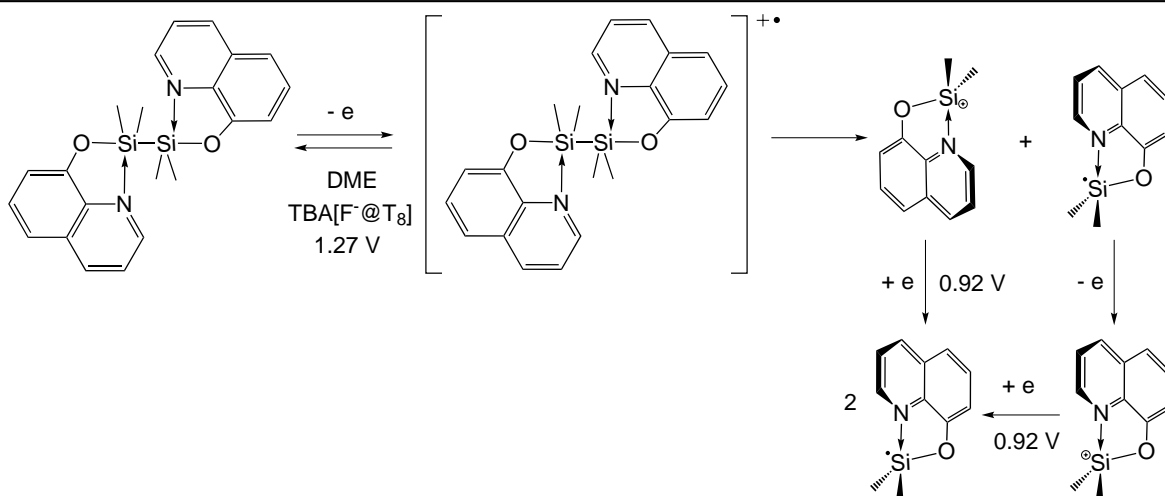
Scheme 18: Oxidation of the model disilane and two short-lived odd-electron species.

Electrooxidation of specially prepared ligand-stabilized 1, 1, 2, 2-tetramethyl-1, 2-bis (quinolin-8-yloxy) disilane (the process is EPR-silent in $CH_3CN/0.05$ M $TBAPF_6$) in EPR spectroelectrochemical cell using (DME-CH_2Cl_2, 3:1 v/v) as solvent and TBA($F^-@T_8Ph_8$) as supporting electrolyte at 253 K allowed to detect two odd-electron species, supposedly short-lived cation radical of this disilane and the radical product of its cleavage (Scheme 18). First species (g = 2.01, a_{Si} = 39.2 G) is obviously a Si-centered radical, the integration of its ^{29}Si satellites ($\approx$9%) indicates the spin localization on two Si atoms. Second species is an organic radical, as follows from its g-factor (2.0033). Spin density in this radical is distinctly delocalized over the quinoline moiety (a_N = 3.78 G, a_{H4} = 6.86 G, a_{H5} = 4.03 G, a_{H7} = 2.08 G, a_{H3} = 1.20 G, a_{H6} = 1.12 G) with an additional *hfc* constant, either from ^{13}C or ^{29}Si (a = 7.1 G), the quality of the spectrum edges not allowing a more precise assignment.

The TBA($F^-@T_8R_8$) supporting salts are chemically stable and can be stored without any decomposition while solid; their solutions in the tested solvents are also stable, at least within the timeframe of typical electrochemical experiments. However, as was first pointed out by Bassindale [104] and as follows from the above DFT consideration (Figure 78), they are sensitive to the presence of small cations in solution, namely of Li^+ and H^+. Figure 83 shows that in CH_3CN, if $LiClO_4$ is added to the solution, the "leakage" of F^- anion from the $F^-@T_8(CH_2CN)_8$ cage to form LiF/TBAF and an empty $T_8(CH_2CN)_8$ is practically accomplished within 9-10 hours. In a similar way, the protons liberated during 30 min experiments

(voltammetry of methylanthracene) in $F^-@T_8(CH_2CH_2CF_3)_8$ in liquid SO_2, caused the appearance of free F^- in the solution, though this process became visible in ^{19}F NMR only upon 4 hours of staying of the used solution. Supposedly, the solvent polarity and the efficiency of free F^- solvation play here an important role, as pointed out above.
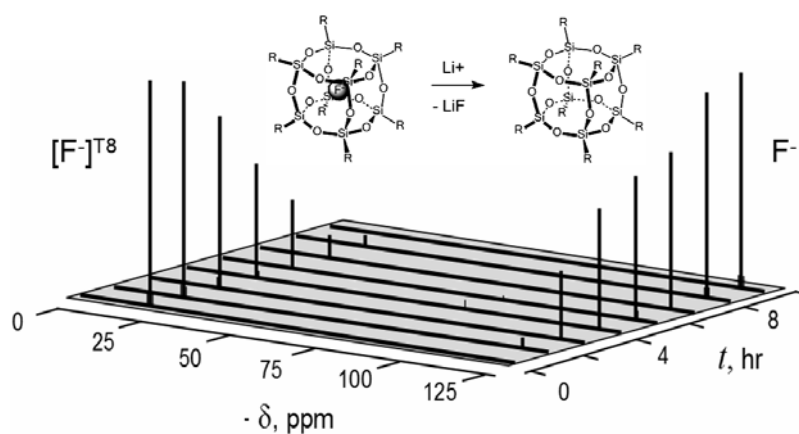

Figure 83: ^{19}F NMR-monitored leakage of F^- anion from the T_8R_8 cage (R = CH_2CN) in the presence of $LiClO_4$. Solvent: CH_3CN, T = 20 °C.

CONCLUSION

6 Conclusion

Seven simple 1-R-silatranes have been synthesized. Four of their structures are characterized by X-ray diffraction (XRD). Electrochemical measurements show that electrooxidation of tolylsilatrane, 2-cyanoethylsilatrane and *t*-butylsilatrane are electrochemically reversible creating cation radicals by one electron transfer; these species can be detected by cyclic voltammetry, UV spectroscopy and real-time EPR spectroelectrochemistry. N and Si atoms from the atrane moiety and substituent atom at α-position to Si compose a 3c-4e conjugated system responsible for the redox properties of these compounds. The π-orbital of Ar substituents, are orthogonal to this system, so the electrooxidation of silatranes with Ar substituent are only affected by inductive effect of the substituent.

Three bis-(silatranyl)alkanes have been synthesized but the structures were not diffractive by XRD because of the difficulty of obtaining the single crystals. However, electrochemical measurements show that anodic oxidation of bis-(silatranyl)octane is electrochemically reversible and results in relatively stable cation radicals. There are two electron transfers during the process. Bis-(silatranyl)methane has 7c-8e bonding system whereas bis-(silatranyl)hexane and bis-(silatranyl)octane have long carbon chains between two atrane structures which are flexible but not long enough to let the two atrane parts face each other in a line to form a 6c-8e bonding system.

Three bi-silatranes have been synthesized. Their structure differs from other silatranes in that the N atom is now included in the plan formed by the 3 adjacent carbon atoms, as XRD spectroscopy has shown. In fact, the whole molecule is perfectly symmetrical in relation to this plane. This has consequences on the electrochemistry of these compounds. Though the electrooxidation is still proceeding via a one-electron step, the electrooxidation of these compounds is reversible (even at low scan rates for di(ethyl)-bi-silatrane and di(phenyl)-bi-silatrane). We have proved that the chemical structure, and most importantly the effect of the substituents, are the main factors explaining the electrochemical behavior of bi-silatranes. In line with the position of the N atom in the middle of the plan formed by its three carbon neighbors, we did record a noticeable anodic shift of the oxidation peak toward higher potentials.

Electrochemical measurements show that anodic oxidation of *p*-aminophenylsilatrane, *p*-(*tert*-butyl)-phenylmethoxystannatrane and tolylsulfylstannatrane occurs via electrochemically reversible electron transfer resulting in corresponding cation radicals detected by cyclic voltammetry and real-time EPR spectroelectrochemistry. The own oxidation potential of the X-Ar substituent in these compounds is lower than that of the silatranyl and stannatranyl moiety, so *p*-aminophenylsilatrane, *p*-(*tert*-butyl)-phenylmethoxystannatrane and tolylsulfylstannatrane follow the oxidation pattern and form the cation radicals of the corresponding aromatic derivatives substituted with a silatranyl or stannatranyl group.

Tetrabutylammonium salts with fluoride-encapsulating octaorganosilsesquioxane anions

TBA($F^-@T_8R_8$) met several electrochemical tests on their suitability as low-coordinating non-nucleophilic supporting electrolytes. They provide good ionic conductivity in the solvents of low polarity (THF, perfluoroisopropanol, liquid SO_2) and fair conductivity in acetonitrile and allow one carrying out voltammetry and EPR experiments on unstable electrogenerated electrophilic and radical species. Since F^- anion can leave the T_8 cage and to appear in the solution in free form, the use of the supporting salts with $F^-@T_8$ anions is subject to the limitations imposed by the kinetics of this process. In the systems where the exohedral fluoride is thermodynamically more favorable than encapsulated *endo*-form, the interference of F^- will occur. Fortunately, this process seems rather slow, leaving, at least in our experiments, more than 30 min working period before it becomes seen by means of voltammetry and NMR. In general, first results on the use of these new salts as supporting electrolytes are very promising, though more extensive studies on their advantages and limitations are necessary.

<u>REFERENCES</u>

References

[1] Frye, C. L.; Vogel, G. E. and Hall, J. A., *Journal of the American Chemical Society*, 1961, **83**, 996–7.

[2] Lukevics, E. and Ignatovich, L. M., *The Chemistry of Organic Germanium, Tin and Lead Compounds*, 1995, pages 857–863.

[3] Lukevics, E.; Pudova, O. and Rappoport, Z., *NY: Wiley*, 2002, **2**, 1653–1683.

[4] Lukevics, E. and Ignatovich, L., The use of metals in medicine, 2005.

[5] Broka, K.; Stradins, J.; Glezer, V.; Zelcans, G. and Lukevics, E., *Journal of Electroanalytical Chemistry*, 1993, **351**(1-2), 199–206.

[6] Sidorkin, V. F.; Pestunovich, V. A. and Voronkov, M. G., *Doklady Akademii Nauk SSSR*, 1977, **6**, 1363–1366.

[7] Voronkov, M. G.; Keiko, V. V.; Sidorkin, V. F.; Pestunovich, V. A. and Zelcans, G., *Khimiya Geterotsiklicheskikh Soedinenii*, 1974, **5**, 613–617.

[8] Voronkov, M. G.; Sidorkin, V. F.; Shagun, V. A.; Pestunovich, V. A. and Zelchan, G. I., *Khimiya Geterotsiklicheskikh Soedinenii*, 1975, **5**, 715–716.

[9] Voronkov, M. G., *Pure Appl Chem*, 1966, **13**, 35.

[10] Voronkov, M. G., *Vestnik Akad Nauk SSSR*, 1968, **38**, 48.

[11] Lukevics, E.; Zelcans, G.; Solomennikova, I. I.; Liepins, E. E.; Jankovska, I. and Mazeika, I., *Zhurnal Obshchei Khimii*, 1977, **47**, 109–112.

[12] Lukevics, E., *Latvijas PSR Zinatnu Akademijas Vestis, Kimijas Serija*, 1974, **3**, 351–354.

[13] Egorov, Y. P.; Voronkov, M. G.; Lutsenko, T. B. and Zelcans, G., *Khimiya Geterotsiklicheskikh Soedinenii*, 1966, **1**, 24–33.

[14] Shestakov, E. E.; Voronkov, M. G.; Reikhsfel'd, V. O. and Zelcans, G., *Zhurnal Obshchei Khimii*, 1973, **43**, 308–313.

[15] Voronkin, M. G.; Frolov, Y. L.; Brodskaya, E. I.; Shevchenko, S. G.; D'yakov, V. M. and Sorokin, M. S., *Doklady Akademii Nauk SSSR*, 1976, **228**, 636–638.

[16] Petukhov, V. A.; Gudovich, L. P.; Zelcans, G. and Voronkov, M. G., *Khimiya Geterotsiklicheskikh Soedinenii*, 1969, **6**, 968–969.

[17] Timms, R. E., *Journal of the Chemical Society [Section] A: Inorganic, Physical, Theoretical*, 1971, **12**, 1969–1974.

[18] Voronkov, M. G.; Frolov, Y. L.; Zasyadko, O. A. and Emel'yanov, I. S., *Doklady Akademii Nauk SSSR*, 1973, **213**, 1315–1318.

[19] Voronkov, M. G.; Zelcans, G.; Lapsina, A. and Pestunovich, V. A., *Zeitschrift fuer Chemie*, 1968, **6**, 214–217.

[20] Voronkov, M. G.; Dyakov, V. M.; Florentsova, O. N.; Baryshok, V. P.; Kuznetsov, I. G. and Chvalovsky, V., *Collection of Czechoslovak Chemical Communications*, 1977, **42**, 480–483.

[21] Popowski, E.; Michalik, M. and Kelling, H., *Journal of Organometallic Chemistry*, 1975, **88**, 157–164.

[22] Lukevics, E.; Solomennikova, I. I.; Zelcans, G.; Judeika, I.; Liepins, E.; Jankovska, I. and Mazeika, I., *Zhurnal Obshchei Khimii*, 1977, **47**, 105–108.

[23] Zeldin, M. and Ochs, J., *Journal of Organometallic Chemistry*, 1975, **86**(3), 369–382.

[24] Mueller, R. and Frey, H. J., *Latvijas PSR Zinatnu Akademijas Vestis, Kimijas Serija*, 1969, **368**, 113–119.

[25] Voronkov, M. G.; Emel'yanov, I. S.; Vitkovskii, V. Y.; Kapranova, L. V.; D'yakov, V. M. and Baryshok, V. P., *Zhurnal Obshchei Khimii*, 1977, **47**, 382–387.

[26] Voronkov, M. G.; Mileshkevich, V. P. and Yuzhelevskii, Y. A., *Uspekhi Khimii*, 1976, **45**, 2253–2273.

[27] D'yakov, V. M.; Sorokin, M. S. and Voronkov, M. G., *U.S.S.R.*, 1977, **SU 550394**.

[28] Puri, J. K.; Singh, R. and Chahal, V. K., *Chem. Soc. Rev.*, 2011, **40**(3), 1791–1840.

[29] Voronkov, M. G.; Dyakov, V. M. and Kirpichenko, S. V., *Journal of Organometallic Chemistry*, 1982, **233**(1), 1–147.

[30] Pestunovich, V.; Kirpichenko, S. and Voronkov, M., *Patai's Chemistry of Functional Groups*, 1998.

[31] Chernyshev, E. A.; Knyazev, S. P.; Kirin, V. N.; Vasilev, I. M. and Alekseev, N. V., *Russian journal of general chemistry*, 2004, **74**(1), 58–65.

[32] Musher, J. I., *Angewandte Chemie International Edition in English*, 1969, **8**(1), 54–68.

[33] Soualmi, S.; Ignatovich, L.; Lukevics, E.; Ourari, A. and Jouikov, V., *Journal of Organometallic Chemistry*, 2008, **693**(7), 1346–1352.

[34] Soualmi, S.; Ignatovich, L. and Jouikov, V., *Applied Organometallic Chemistry*, 2010, **24**(12), 865–871.

[35] Farnham, W. B.; Dixon, D. A. and Calabrese, J. C., *Journal of the American Chemical Society*, 1988, **110**(25), 8453–8461.

[36] Nikonov, G. I.; Kuzmina, L. G.; Lemenovskii, D. A. and Kotov, V. V., *Journal of the American Chemical Society*, 1995, **117**(40), 10133–10134.

[37] Nakanishi, W.; Hayashi, S. and Itoh, N., *The Journal of Organic Chemistry*, 2004, **69**(5), 1676–1684.

[38] Nakanishi, W.; Hayashi, S.; Furuta, T.; Itoh, N.; Nishina, Y.; Yamashita, M. and Yamamoto, Y., *Phosphorus, Sulfur, and Silicon and the Related Elements*, 2005, **180**(5-6), 1351–1355.

[39] Mehrotra, R. C., *Indian J. Chem*, 1965, **3**, 497.

[40] Malachesky, P. A., *Analytical Chemistry*, 1969, **41**(11), 1493–1494.

[41] Bernasconi, C. F. and Weissberger, A., *Investigation of rates and mechanisms of reactions*, Vol. 1, Wiley, 1986.

[42] Cherkasov, A. R.; Galkin, V. I. and Cherkasov, R. A., *Russian chemical reviews*, 1996, **65**, 641.

[43] Karlov, S. S.; Tyurin, D. A.; Zabalov, M. V.; Churakov, A. V. and Zaitseva, G. S., *Journal of Molecular Structure: THEOCHEM*, 2005, **724**(1), 31–37.

[44] Li, J.; Liao, R. and Xie, Q., *Progress in Natural Science*, 1994, **4**(1), 68–72.

[45] Ravenscroft, M. D. and Roberts, R. M. G., *Journal of organometallic chemistry*, 1986, **312**(1), 45–52.

[46] Li, J.; Tang, Y. J.; Liu, H.; Dong, S. P. and Xie, Q. L., *Chemical Journal of Chinese Universities - Chinese Edition*, 1998, **19**, 1074–1077.

[47] Kolosova, N. D. Z.; Shriro, V. S.; Kocheskov, K. A. and Barminova, N. P., 1979.

[48] Belyakov, S.; Ignatovich, L. and Lukevics, E., *Journal of organometallic chemistry*, 1999, **577**(2), 205–210.

[49] Alekseev, N. V.; Knyazev, S. P. and Chernyshev, I. A., *Journal of Structural Chemistry*, 2005, **46**(3), 387–392.

[50] Ignatyev, I. S.; Sundius, T. R.; Vrazhnov, D. V.; Kochina, T. A. and Voronkov, M. G., *Journal of Organometallic Chemistry*, 2007, **692**(26), 5697–5700.

[51] Mann, C. K. and Barnes, K. K., Electrochemical reactions in nonaqueous solvents, 1970.

[52] Hill, M. G.; Lamanna, W. M. and Mann, K. R., *Inorganic Chemistry*, 1991, **30**(25), 4687–4690.

[53] Sawyer, D. T.; Sobkowiak, A.; Roberts, J. L. and coworkers, , *Electrochemistry for chemists*, Vol. 170, Wiley New York, 1995.

[54] Fry, A. J., *Techniques in Electroanalytical Chemistry*, P.T. Kissinger and WR.Heineman, Eds, 2nd ed., Marcel Dekker, NY, 1996.

[55] Stewart, M. P.; Paradee, L. M.; Raabe, I.; Trapp, N.; Slattery, J. S.; Krossing, I. and Geiger, W. E., *Journal of Fluorine Chemistry*, 2010, **131**(11), 1091–1095.

[56] Camire, N.; Mueller-Westerhoff, U. T. and Geiger, W. E., *Journal of Organometallic Chemistry*, 2001, **637**, 823–826.

[57] Fry, A. J., *Tetrahedron*, 2006, **62**(27), 6558–6565.

[58] Adams, C. J.; Da Costa, R. C.; Edge, R.; Evans, D. H. and Hood, M. F., *The Journal of Organic Chemistry*, 2010, **75**(4), 1168–1178.

[59] Reed, C. A., *ChemInform*, 1998, **29**(26), no–no.

[60] Pauling, L., *Journal of the American Chemical Society*, 1932, **54**(9), 3570–3582.

[61] Bruker, 2002.

[62] et al., A. 1999.

[63] Sheldrick, 1997.

[64] Frarrugia, 1997.

[65] Ghilane, J.; Hapiot, P. and Bard, A. J., *Analytical chemistry*, 2006, **78**(19), 6868–6872.

[66] Bard, A. J. and Faulkner, L. R., *Electrochemical methods: fundamentals and applications*, Vol. 2, Wiley New York, 1980.

[67] Zeitouny, J. and Jouikov, V., *Phys. Chem. Chem. Phys.*, 2009, **11**(33), 7161–7170.

[68] Bruker WINEPR System, v. ., Bruker-franzen analytic gmbh, 1990-1996.

[69] WINEPR SimFonia, v. ., Bruker analytische messtechnik gmbh, 1994-1996.

[70] Nasim, M.; Saxena, A. K.; Pal, I. P. and Pande, L. M., *Synthesis and Reactivity in Inorganic and Metal-Organic Chemistry*, 1987, **17**(10), 1003–1009.

[71] Jie, Y. *Tris (1, 3-dihydroxy-2-propyl) amine, a planar trialkylamine: Synthesis, structure, and properties. A potential precursor to hypervalent nitrogen* PhD thesis, Graduate Faculty of Auburn University, 2006.

[72] Murray-Rust, P.; McManus, J.; Lennon, S. P. and Porter, A E Aand Rechka, J. A., *J. Chem. Soc., Perkin Trans. 1*, 1984, (0), 713–716.

[73] Husinec, S.; Juranic, I.; Llobera, A. and Porter, A. E. A., *Synthesis*, 1988, **1988**(9), 721–723.

[74] Broka, K.; Glezer, V. T.; Stradins, J. and Zelcans, G., *Zhurnal Obshchei Khimii*, 1991, **61**, 1374–1378.

[75] Allen, F. H., *Acta Crystallographica Section B: Structural Science*, 2002, **58**(3), 380–388.

[76] Hammett, L. P., *J. Am. Chem. Soc.*, 1937, **59**, 96.

[77] Taft, R. W., *The Chemistry of Organic Germanium, Tin and Lead Compounds*, number Table V, Wile an d Sons: New York,, 1956.

[78] Taft, R. W. and Lewis, I. C., *J. Am. Chem. SOC.*, 1958, **80**, 2643.

[79] Taft, R. W. and Topsom, R. D., *Prog. Phys. Org. Chem.*, 1987, **16**, 1.

[80] Taft, R. W.; Price, E.; Fox, I. R.; Lewis, I. C.; Andersen, K. K. and Davis, G. T., *J. Am. Chem. SOC.*, 1963, **85**, 709.

[81] Wendt, H. and Hoffelner, H., *Electrochimica Acta*, 1983, **28**(10), 1465–1472.

[82] Jouikov, V. and Simonet, J., *Encyclopedia of electrochemistry*, 2004, **8**, 235.

[83] Soualmi, S.; Ignatovich, L.; Lukevics, E.; Ourari, A. and Jouikov, V. V., *ECS Transactions*, 2008, **13**(24), 63–69.

[84] Markusova, K.; Kladekova, D. and Zezula, I., *Chemicke Zvesti*, 1980, **34**(6), 726–39.

[85] Weiner, S., *Journal of the American Chemical Society*, 1972, **94**(2), 581–584.

[86] Pokhodenko, V. and Kalibabchuk, N., *Teoreticheskaya i Eksperimental'naya Khimiya*, 1970, **6**(1), 124–128.

[87] Gerson, F. and Huber, W., *Electron spin resonance spectroscopy of organic radicals*, Wiley-VCH, 2006.

[88] Jouikov, V., *ECS Transactions*, 2010, **28**(12), 5–16.

[89] Iley, J., *NY: Wiley*, 1995, page 267?290.

[90] Devaud, M. and Le Moullec, Y., *Electrochimica Acta*, 1976, **21**(6), 395–400.

[91] Savall, A.; Mahenc, J. and Lacoste, G., *Journal of Applied Electrochemistry*, 1981, **11**(1), 69–75.

[92] Ishiwata, T.; Nonaka, T. and Umezawa, M., *Chemistry Letters*, 1994, **23**(9), 1631–1634.

[93] Dessy, R. E.; Kitching, W. and Chivers, T., *Journal of the American Chemical Society*, 1966, **88**(3), 453–459.

[94] Holm, A.; Brinck, T. and Daasbjerg, K., *Journal of the American Chemical Society*, 2005, **127**(8), 2677–2685.

[95] Sutton, A.; Davis, B.; Bhattacharyya, K.; Ellis, B.; Gordon, J. and Power, P., *Chemical Communications*, 2010, **46**(1), 148–149.

[96] Davies, A.; Sella, A. and Sivasubramaniam, R., *Journal of organometallic chemistry*, 2006, **691**(16), 3556–3561.

[97] Booth, M. and Fleet, B., *Analytical Chemistry*, 1970, **42**(8), 825–831.

[98] Mazzocchin, G.; Seeber, R. and Bontempelli, G., *Journal of Organometallic Chemistry*, 1976, **121**(1), 55–62.

[99] Tanaka, H.; Ogawa, H.; Suga, H.; Torii, S.; Jutand, A.; Aziz, S.; Suarez, A. and Amatore, C., *The Journal of Organic Chemistry*, 1996, **61**(26), 9402–9408.

[100] Mochida, K.; Itani, A.; Yokoyama, M.; Tsuchiya, T.; Worley, S. and Kochi, J., *Bulletin of the Chemical Society of Japan*, 1985, **58**(7), 2149–2150.

[101] Bassindale, A. R.; Pourny, M.; Taylor, P. G.; Hursthouse, M. B. and Light, M. E., *Angewandte Chemie International Edition*, 2003, **42**(30), 3488–3490.

[102] Bassindale, A. R.; Parker, D. J.; Pourny, M.; Taylor, P. G.; Horton, P. N. and Hursthouse, M. B., *Organometallics*, 2004, **23**(19), 4400–4405.

[103] Franco, R.; Kandalam, A. K.; Pandey, R. and Pernisz, U. C., *The Journal of Physical Chemistry B*, 2002, **106**(7), 1709–1713.

[104] Taylor, P. G.; Bassindale, A. R.; El Aziz, Y.; Pourny, M.; Stevenson, R.; Hursthouse, M. B. and Coles, S. J., *Dalton Trans.*, 2012, **41**(7), 2048–2059.

[105] Anderson, S. E.; Bodzin, D. J.; Haddad, T. S.; Boatz, J. A.; Mabry, J. M.; Mitchell, C. and Bowers, M. T., *Chemistry of Materials*, 2008, **20**(13), 4299–4309.

[106] Kuznetsova, E. M. and Kirsanov, R. S., *Russian journal of physical chemistry*, 1999, **73**(10), 1596–1601.

[107] Simonet, J. and Jouikov, V., *Electrochemistry Communications*, 2011.

RESUME

1 Introduction général

Depuis qu'en 1960, un nouvel organosilane, baptisé triptych-siloxazolidine, a été découvert pour la première fois par Frye et al. les métallatranes ont fait l'objet d'études et de recherches intensives pendant plus de 50 ans, non pas seulement en raison de son unique interaction transannulaire entre l'atome métallique (Si, Ge, ou Sn) et un atom d'azote, mais également en raison des nombreuses applications en médecine et en biologie qui utilisent ces composés. Cependant, les propriétés électrochimiques des métallatranes n'ont pas autant attiré l'attention des chercheurs, et ont été peu étudiées pendant une longue période. Les métallatranes ont pourtant un potentiel très élevé en électrochimie en raison de leur structure particulière: l'atome métallique peut être vu comme pentacoordiné, avec une liaison hypervalente. En efet, pour commencer, la liaison hypervalente N-Métal limite la zone de probabilité de présence de la paire d'électron. Ensuite, en raison de la présence des trois branches alkoxysilanes, le doublet électronique est "piégé" dans la cage du métallatrane. Enfin, la structure atrane peut être étendue linéairement par répétition du même motif. Les molécules formées d'une chaine silylée normale sont soit instables chimiquement, ou bien font preuve d'une mauvaise conduction électronique en raison du mauvais recouvrement des orbitales des atomes de silicium. En revanche, une chaine atrane possède une liaison Si-O forte, permettant de garantir la stabilité de la molécule, et la paire d'électrons libres de l'atom d'azote peut être partagée avec 2 atomes de silicium, permettant le transfert d'électrons le long de la chaine (Figure 1). Il s'agit d'un concept nouveau de chaine moléculaire, ou les électrons peuvent être transférés le long de la chaine.

Une autre caractéristique des métallatranes est dûe aux radicaux cations correspondants à leur forme oxydée. La distance entre l'atome d'azote et l'atome de métal dans le radical cation est différente de celle exhibée dans le métallatrane sous forme réduite, ce qui permet de changer la longueur de la molécule selon le potentiel. Cette flexibilité des systèmes atranes peut-être utilisée et modulée en ajoutant différents substituants permettant la réalisation de différentes fonctions électrochimiques.

Pour toutes ces raisons, nous avons décidé de porter notre attention sur les comportements électrochimiques des métallatranes, et nous en avons fait le sujet de recherche traité dans cette thèse. Dans le cadre de cette étude, nous avons étudié les métallatranes depuis leur voie de synthèse jusqu'aux calculs de chimie quantique, en passant par la caractérisation structurale de ces molécules et l'étude de leur comportement électrochimique.
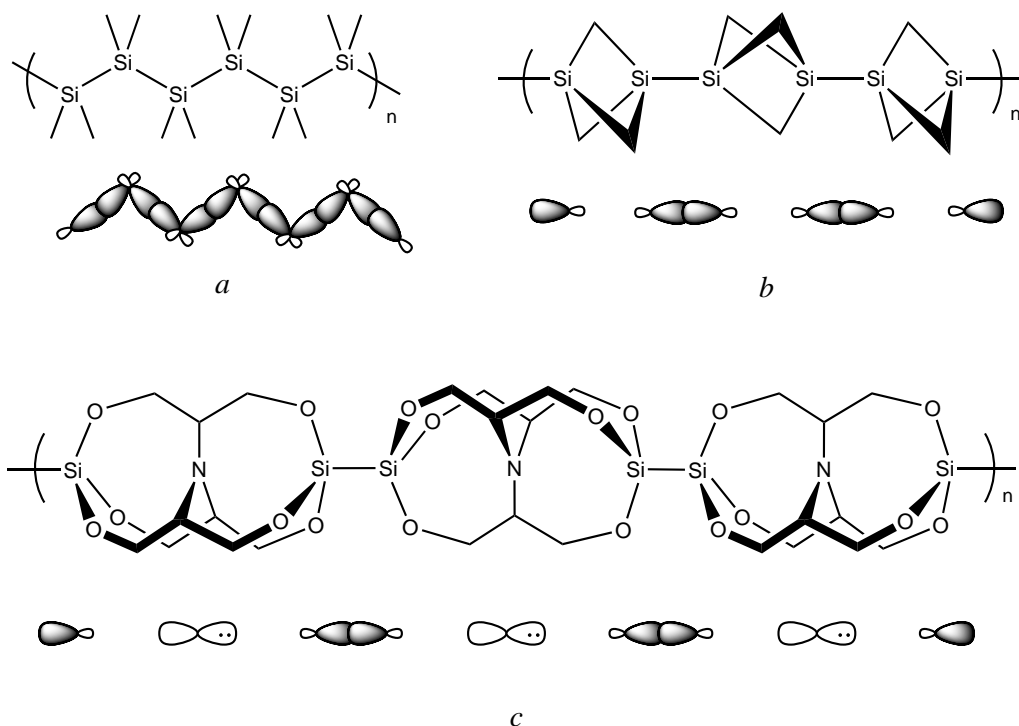
Figure 1: Différents types de chaines silylées. a. Chaine moléculaire possédant une bonne conductivité électrochimique, mais une forte instabilité; b. Chaine silylée stable chimiquement, mais exhibant de faibles recouvrements orbitalaires. c. Nouvelle chaine moléculaire incorporant la structure atrane, permettant une bonne stabilité moléculaire et des transferts électronqiues faciles.

2   1-R-silatranes

Si l'on se concentre sur la famille des 1-R-silatranes (métallatranes dont l'atome métallique est le silicium), bien qu'elle soit extrêmement large, elle a fait comme les autres familles d'atranes l'objet de peu d'études électrochimiques. La comparaison des quelques données disponibles sur l'électro-oxydation de cette classe de molécules avec les travaux effectués sur des germatranes similaires peut permettre de supposer que la structure électronique des radicaux cations des silatranes substitués par un groupement aliphatique ou aromatique, d'une part, et ceux substitués par un groupement benzilique d'autre part, auraient un comportement électrochimique différent. Cette différence est intrisèquement liée à la nature des interactions liantes entre les atomes des molécules de silatrane sous leur forme réduite (neutre).

Afin d'élucider les caractéristiques spécifiques de ces effets, et d'étudier la possibilité d'étendre un système électronique basé sur des liaisons à 3 centres et 4 électrons (3c-4e) à un système plus large, à 5 centres et 6 électrons (5c-6e), voire plus large encore $(5c - 6e)_n$, nous avons commencé par réaliser la synthèse et l'étude de plusieurs "silatranes modèles".

7 structures de 1-R-silatranes, étudiées dans la section suivante, ont été préparées selon des méthodes publiées.
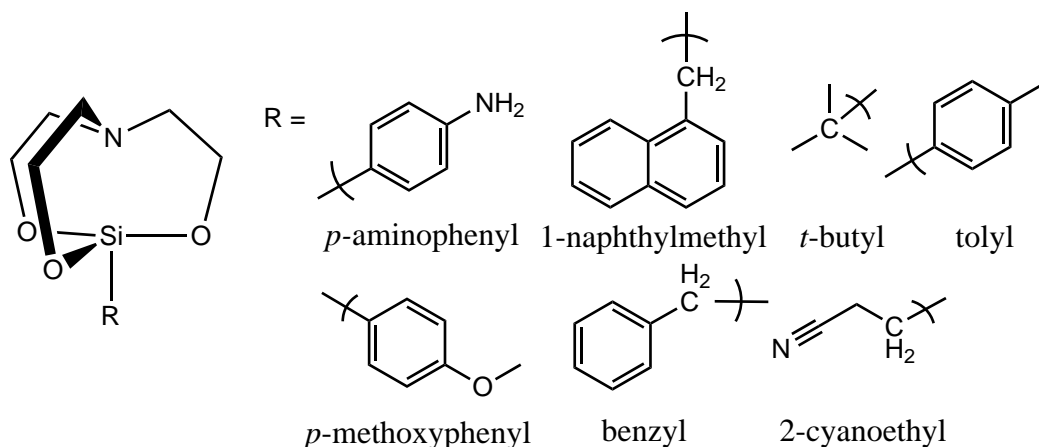
Figure 2: 1-R-silatranes

Bien qu'ils s'agisse de composés déjà connus et que leur structure cristalline ait même déjà fait l'objet de quelques publications, Nous avons noté qu'elles n'avaient fait l'objet d'aucun dépôt dans la CCDB, et que les détails de ces structures, eux, n'avaient pas été publiés. Nous avons donc estimé utile de nous pencher sur ces aspects manquants. Les structures de 4 de ces silatranes ont été étudiées par diffraction des rayons X sur monocristal. La structure des *p*-aminophenylsilatrane, 1-naphthylmethylsilatrane, *p*-methoxyphenylsilatrane et benzylsilatrane ont été les premières que nous avons caractérisées.

L'oxydation de 7 silatranes Si-substitués a été étudiée dans des solutions d'acétonitrile contenant 0.1M de tétrabutylammonium hexafluorophosphate ($\mathrm{TBAPF_6}$), sur une électrode de platine. nous avons utilisé une électrode microdisque de Pt comme électrode de travail dans la mesure où cela nous a permis d'obtenir des voltammogrammes mieux formés que ceux obtenus avec d'autres types d'électrodes (des électrodes de carbone vitreux ont notamment aussi été essayées). Les potentiels des pics d'oxydation de ces composés se trouvent dans une fenêtre de 0.78-1.45V (vs. SCE), selon la nature du substituant R (table 1). Soumis à oxydation, 3 de ces 7 silatranes exhibent un pic réversible distinct. Nous avons observé l'existence d'une loi de proportionnalité entre le courant de pic (i_p) et la concentration de substance électroactive. Une loi de proportionnalité a également été observée entre le courant de pic et la racine carrée de la vitesse de balayage ($i_p/v^{1/2} = $ const.) pour des vitesses de balayage suffisamment élevées *(v > 0.5 V/s)*. Ces 2 résultats suggèrent une cinétique controlée par la diffusion. Le nombre d'électrons transférés durant l'étape d'oxydation a été déterminé par la méthode proposée par Malachesky, basée sur les relations suivantes.

Le courant de pic i_p pour un voltammogramme à balayage linéaire d'un système rédox réversible peut-être exprimé par:

$$i_p = 2.68 \times 10^5 n^{3/2} A C D^{1/2} v^{1/2}$$

3

Parallèlement, en chronoampérométrie potentiostatique [**?**]:

$$it^{1/2} = nFACD^{1/2}\pi^{-1/2}$$

La combinaison de ces 2 équations donne la relation suivante:

$$R = \frac{i_p/v^{1/2}}{it^{1/2}} = 4.92n^{1/2}$$

Le qui permet d'évaluer directement la stoechiométrie électronique du mécanisme. Ce résultat est indépendant des incertitudes dues aux differents coefficients de diffusion D, ainsi que de la valeur de la concentration en silatrane à la surface de l'électrode, contrairement à la méthode basée sur la comparaison des i_p avec un composé standard comme le ferrocène. En appliquant cette relation au cas de l'oxydation des 7 silatranes, nous avons abouti à la conclusion qu'ils suivent tous un mécanisme mono-électronique à E'_p (Table 1).

Table 1: Paramètres de l'oxydation electrochimique des silatranes par une electrode à disque de platine, à v = 1V/s[a]

R	E_p^a(V)	E_p^c(V)	E^o(V)	n	$E_p^a - E_{p/2}^a$ (mV)	$\Delta E_p^a/\Delta lg(V)$ (mV)	α[b]
p-aminophenyl	0.78	–	–	1	93	14	0.50
1-naphthylmethyl	1.10	–	–	1	88	28	0.50
t-butyl	1.22	1.14	1.18	1	91	10	0.50
tolyl	1.35	1.26	1.30	1	72	14	0.65
p-methoxyphenyl	1.37	–	–	1	66	40	0.72
benzyl	1.42	–	–	1	150	40	0.32
2-cyanoethyl	1.45	1.30	1.38	0.9	81	23	0.58

[a] Voltammetrie cyclique réalisée dans un melange CH_3CN / 0.1 M $TBAPF_6$. Tous les voltammogrammes sont corrigès par SCE.

[b] Coefficient de transfert estimé par α avec $E_p - E_{p/2} = 1.85RT/\alpha F$.

Comme mentionné précédemment, les effets électroniques des substituants R affectent significativement les potentiels d'oxydation des silatranes. Parmi les 7 silatranes testés, les t-butyl et tolyl-silatranes exhibent un signal distinct d'électrooxydation réversible même à faible vitesse de balayage (v = 0.5 V/s). Le tolylsilatrane a un pic d'oxydation à E_p =1.35 V (vs. SCE), avec un pic cathodique correspondant à 1.26V (vs. SCE). Quant au dérivé tert-butyl, il s'agit d'un substituant présentant un fort effet inductif donneur, ce qui conduit à une oxydation

aisée de ce silatrane (1.22 V vs. SCE).

Les 4 autres silatranes montrent des comportements électrochimiques différents sous les mêmes conditions. Leurs pics d'oxydation (table 1) sont irréversibles même à des vitesses de balayage plus élevées (v = 10 V/s). Afin de rationnaliser ces données, les structures électroniques et les mécanismes possibles de transmission des effets électroniques de ces systèmes ont été étudiés en détail.

On peut noter que le méthoxyphénylsilatrane a un potentiel de pic d'oxydation E_p =1.37 V vs. SCE (table 1), soit un potentiel plus élevé que celui du pic d'oxydation du naphtylméthyl-silatrane (E_p =1.10 V). En effet, le 1-naphtylméthylsilatrane (contrairement aux dérivés tolyl- et anisyl-) profite d'un effet global π-donneur du groupe naphtyl. De façon remarquable, le système π du groupe naphtyl et la liaison σ(C–Si) de la liaison 3c-4e sont hyperconjugués, ce qui conduit à une délocalisation électronique (figure 3).
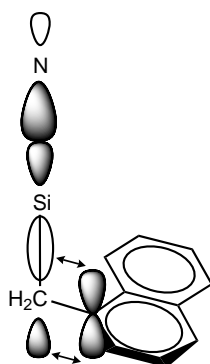

Figure 3: Hyperconjugaison de la liaison 3c-4e avec le système π du 1-naphtylméthylsilatrane.

Le même mécanisme de conjugaison permet la délocalisation électronique du radical cation dans le système π du naphtyl. L'électron libre, localisé sur l'atome d'azote et isolé dans la cage atrane des alkyl ou aryl silatranes, devient dans le cas des naphtylsilatranes, visible de l'extérieur de la cage pour des entités radicalophiles externes en raison de sa présence sur les cycles aromatiques naphtyl, principalement en position 4. De là, la diminution observée du potentiel d'oxydation de ce silatrane est dûe à deux facteurs: la contribution thermody-namique (donneur électronique) du substituant, et la rapidité de la réaction de consommation des radicaux cations électrogénérés qui s'ensuit (contribution cinétique provoquant un shift de la valeur de E_p). Par conséquent, ce composé a sans surprise l'un des potentiels de pic d'oxydation parmi les plus bas de la table 1, à E_p =1.10 V vs. SCE.

Le caractère réversible de l'oxydation du phénylsilatrane (le pic retour de réduction du cation radical est détecté dès v = 0.2 V/s) nous permet d'étudier ce silatrane par spectroélec-trochimie EPR. Quand on oxide le phénylsilatrane sur une microélectrode placée dans une cellule EPR, le signal de l'électron libre de l'espèce générée apparait à E = 0.7 V. Le spectre exhibe un aspect caractéristique, 9 groupes d'un motif qui se répète, la séparation entre ces 9

groupes rejoignant la ligne de base.

Le spectre EPR du radical cation d'un phénylsilatrane (figure 4) a une importante largeur de spectre (~160G), et consiste en plus de 184 bandes parfaitement résolues. Etant donnée la largeur importante du spectre, la partie de ce spectre située aux champs les plus hauts montre une distortion dûe aux effets de 2e ordre, ce qui rend difficile sa reconstruction à l'aide de l'outil simple inclus dans le pack Brüker Symphonia.

Néanmoins, les paramètres suivants ont été extraits de la partie situés aux champs bas, permettant une reconstruction de ce spectre avec 99.8% de qualité: g = 2.0037; aN = 18.41 G; $3 \times a^{\alpha}H_{ax}$ = 37.93 G; $3 \times a^{\alpha}H_{lat}$ = 0.23 G; $6 \times a^{\beta}H$ = 1.8 G. Ce spectre correspond à des espèces dont l'atome d'azote est pratiquement plan. Celui ci porte la majorité de la densité électronique libre, et possède un forte interaction avec les 3 protons α orientés de façon axiale. Les liaisons C-H avec les 3 autres protons α sont presque orthogonales à l'axe de la molécule, de sorte que leur interaction avec le champ magnétique est près de 160 fois plus faible que celle des protons α axiaux.
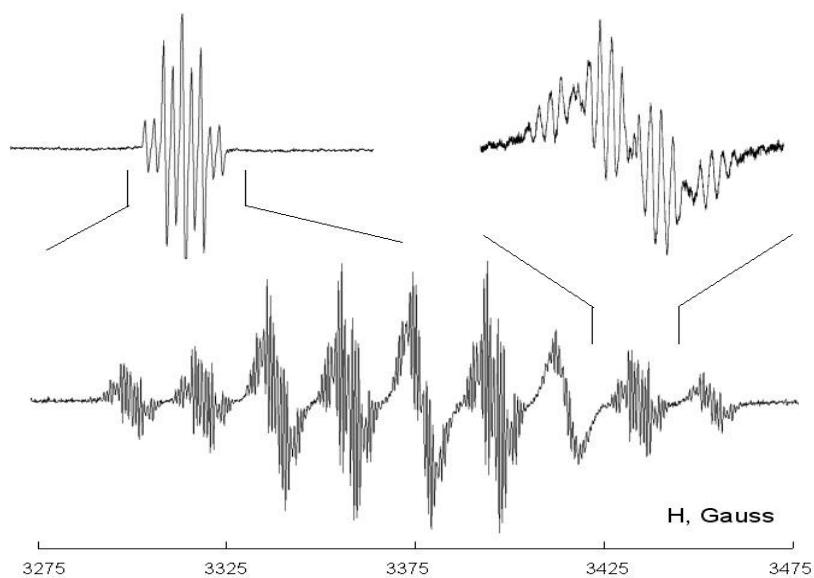

Figure 4: Spectre EPR du cation radical du phénylsilatrane. Electrode: microplaque de Pt. Fréquence des micro-ondes f = 9.46 GHz; Modulation d'amplitude a = 0.25 G. T = 223 K. E = 0.7 V.

3   Bis-(silatranyl)alkanes

Nous allons à présent présenter les résultats de voltammétrie cyclique de 3 bis-(silatranyl)alkanes: le bis-(silatranyl)méthane, le bis-(silatranyl)hexane et le bis-(silatranyl)octane qui ont été étudiés dans des solutions d'acétonitrile (CH_3CN) contenant 0.1 M de tétrabutylammonium hexafluoro-

phosphate (TBAPF$_6$). Quelques gouttes de dichlorométhane ont été ajoutées à ces solutions pour permettre une bonne dissolution de ces produits.

Tous les composés de cette série exhibent un pic d'oxydation, suivi d'une seconde étape d'oxydation. Ce second pic d'oxydation a été observé dans les mesures de voltammétrie cyclique de chacun des 3 composés.

Les courants de pic d'oxydation de ces composés, mesurés à différentes vitesses de balayage, sont proportionnels à la racine carrée de la vitesse de balayage ($i_p/v^{1/2}$ = const.), ce qui implique que l'électrooxydation à ce potentiel suit un contrôle diffusionnel. Le nombre de moles d'électrons transférés durant la réaction d'électrooxydation a été calculé à partir de la valeur du courant de pic i_p et de la racine carrée de la vitesse de balayage correspondante $\sqrt{v}$, en utilisant le coefficient de Cottrell issu des courbes *i=f(t)*. Ces courbes *i=f(t)* ont été obtenues par chronoampérométrie à double saut de potentiel, et toutes les mesures ont été réalisées sur la même électrode et dans la même solution. Les premiers potentiels de pic d'oxydation de ces composés sont compris dans une fenêtre de 0.78-1.05 V (vs. SCE), selon la nature du fragment central.

Dans cette série de 3 composés, le pic d'oxydation du bis-(silatranyl)hexane est le plus bas, à E$_p^c$ = 0.78 V, et ce pic est irréversible à faible vitesse de balayage. Le coefficient apparent de transfert α du bis-(silatranyl)hexane, déterminé à partir de la largeur de pic, est de 0.21, ce qui n'est pas compatible avec le caractère réversible de l'oxydation et indique probablement que des interactions d'absorption déforment le voltammogramme.

Le bis-(silatranyl)octane présente un pic réversible même à faible vitesse de balayage (*v* = 0.5 V/s), et à le pic d'oxydation le plus étroit en largeur ($E_p - E_{p/2}$ = 117.20 mV) des 3 composés. Mais même pour ce composé, la largeur de pic apparente est trop large pour pouvoir correspondre à un processus rédox parfaitement réversible.

Tous ces composés ont un second pic d'oxydation à des potentiels de valeur positive plus élevée, en particulier le bis-(silatranyl)octane, dont le second pic d'oxydation réversible se trouve à E_p = 1.30 V. Ceci suggère que le cation radical instable formé à l'issue de la première réaction a été par la suite réoxidé pour donner N$^+$.

Les bis-(silatranyl)hexane et bis-(silatranyl)octane ont tous deux une longue chaine alkyle faisant la liaison entre les deux groupes atrane. Ceci laisse penser que la flexibilité d'une chaine aussi longue pourrait permettre le rapprochement des deux groupes atrane, donnant lieu à une nouvelle liaison hypervalente: 6c-8e. Cependant, pour ces deux composés, même la longueur importante de la chaine $(CH_2)_8$ n'est pas suffisante pour permettre l'alignement axial requis des 2 groupes terminaux silatranyls, ce qui amène finalement à penser en l'existence de 2 liaisons 3c-4e indépendantes (figure 5). Il est probable qu'une chaine alkyle de plus de 12 atomes de carbone pourrait conduire à un tel arrangement intramoléculaire (figure 6).

Dans une liaison 5c-6e classique, les 2 ligands central et terminal sont très électronégatifs
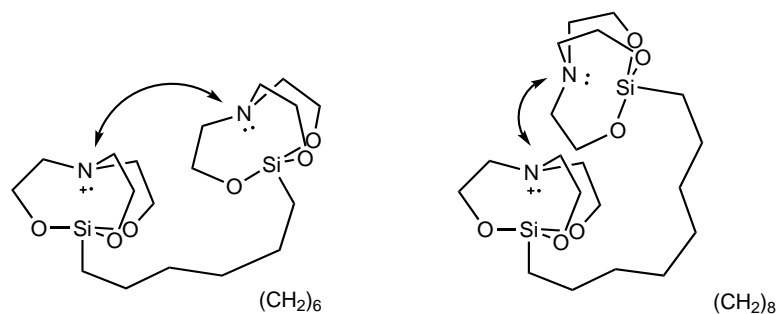
Figure 5: 2 liaisons indépendantes 3c-4e dans les molécules de bis-(silatranyl)hexane et de bis-(silatranyl)octane
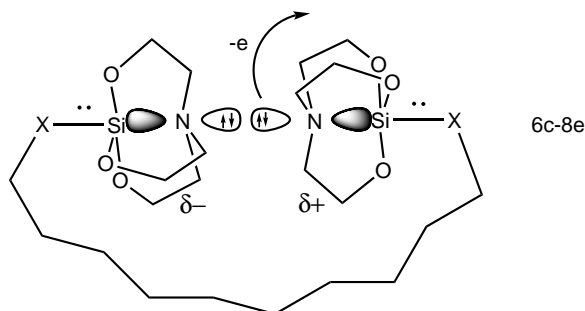

Figure 6: Liaison hypervalnte 6c-8e, pour un nombre d'atomes de carbones de la chaine alkyle supérieur à 12.

par rapport au silicium. Dans le cas du bis-(silatranyl)méthane, par exemple, ces positions (l'atome de carbone central et les deux atomes d'azote terminaux) sont effectivement occupées par des éléments plus électronégatifs. Dans cette section, une série de composés possédant 2 structures silatranes fusionnées, ce qui les différencient du bis-(silatranyl)méthane, ont été synthétisées.

D'un certain point de vue, l'atome d'azote peut maintenant être considéré comme l'atome central de la liaison 5c-6e (parfaitement linéaire dans ces molécules), et les deux atomes de carbone des substituants considérés, commes les atomes terminaux. Le comportement électrochimique de ces composés va être discuté dans la section qui suit.

4   Bi-silatranes

Deux nouvelles structures de bi-silatranes ont été synthétisées et analysées par DRX. La structure de ces bi-silatranes peut être vue de deux façons. Premièrement, les deux parties atranes peuvent être considérées comme deux bipyramides distordues, avec les deux atomes de silicium au centre et les 3 atomes d'oxygène, l'atome de carbone du substituant, et l'atome d'azote partagé formant les sommets (figure 7 *a*).

Deuxièmement, le bi-silatrane peut être considéré comme une bipyramide non distordue

formée de l'atome d'azode au centre, les 3 atomes de carbone adjacents et les 2 atomes de silicium formant les sommets. (figure 7 *b*).
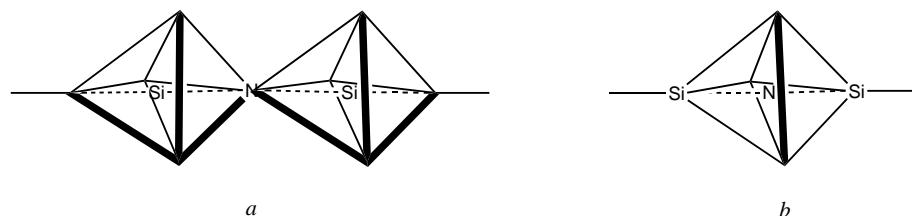

Figure 7: Structure des bi-silatranes. *a.* 2 bipyramides distordues avec les 2 atomes de silicium au centre; *b.* Une bipyramide non distordue, l'atome d'azote occupant le centre.

Pour une meilleure compréhension de l'oxydation chimique des bi-silatranes, nous avons conduit une série d'expériences de voltammétrie cyclique sur ces composés, et avons comparé ces résulats à ceux obtenus avec un précurseur de ces molécules, la tris(1,3-dihydroxy-2-propyl)amine. L'électrooxydation procède par transfert monoélectronique dans les 4 cas que nous avons considéré. Les diéthyl- et diphényl- bi-silatranes montrent distinctement une étape d'électrooxydation réversible même à faible vitesse de balayage (*v* = 0.5 V/s). Pour les di(benzyl)- et di(éthyl)-bi-silatranes, E_p augmente avec la vitesse de balayage légèrement plus qu'anticipé pour que le processus électrochimique suivant cette oxydation en cation-radical soit du premier ordre (un accroissement du premier ordre avec une pente de 30 mV par décade de la vitesse de balayage devrait avoir lieu). La largeur du pic d'oxydation du di(phenyl)-bi-silatrane est la plus faible de la série des trois composés, ce qui indique que l'on se rapproche d'un pur système Nernstien. De plus, la pente $\Delta E_p/\Delta lg(v)$ est proche de 20 mV plutôt que de 30 mV, ce qui semble indiquer un transfert électronique réversible et signifie donc que ce composé subit une rapide réaction du deuxième ordre après oxydation, au contraire des autres composés de la série.

Les di(éthyl)-bi-silatrane et di(phényl)-bi-silatrane ont tous deux un pic d'oxydation réversible même à faible vitesse de balayage (*v* = 0.5 V/s), ce qui atteste de la bonne stabilité de ces 2 radicaux cations. Par conséquent, l'oxydation mono-électronique de bi-silatranes aboutit au radical-cation correspondant.

5 1-R-stannatranes et distannatrane

D'après des études antérieures des métallatranes par diverses méthodes physico-chimiques, il ressort que l'interaction dative N→M est de plus en plus forte au fur et à mesure que l'on descend dans les atomes du groupe 14, dans l'ordre $Si < Ge < Sn$. Il est prévisible que la disponibilité du doublet libre de l'azote décroisse selon le même ordre, et donc que l'attaque électrophile du métallatrane soit de plus en plus difficile. Aucune donnée sur l'électrochimie

Table 2: Resultats de voltammetrie cyclique pour l'oxydation de bi-sialtranes. Tous les echantillons sont pris à $v = 1$V/s et les potentials sont corrigès par SCE.

Compound	E_p^c(V)	E_p^a(V)	E^o(V)	n	$E_p - E_{p/2}$(mV)
Tris(1,3-dihydroxy-2-propyl)amine	0.84	0.69	0.76	1	72
di(benzyl)-bi-silatrane	1.45	–	–	1	81
di(ethyl)-bi-silatrane	1.62	1.49	1.55	1	81
di(phenyl)-bi-silatrane	1.68	1.59	1.63	1	67

$\Delta E_p/\Delta lgV$(mV)	α^a
34	0.7
33	0.6
36	0.6
18	0.7

[a]Coifficient de transfert estimé avec α de $E_p - E_{p/2} = 1.85RT/\alpha nF$.

des stannatranes n'a été rapportée à ce jour, à notre connaissance, et nous avons donc porté notre attention sur l'oxydation de quelques stannatranes que nous avons sélectionné, dans les mêmes conditions que celles décrites précédemment.

Afin d'obtenir un aperçu des interactions électroniques intramoléculaires dans les nouveaux stannatranes avec lesquels nous avons travaillé, leur comportement électrochimique a été observé. Selon leur solubilité, les expériences de voltammétrie cyclique sur les composés **12, 13, 14** et **15** (figure 8) ont été menées dans l'acétonitrile (CH_3CN), le dichlorométhaneCH_2Cl_2 ou dans un mélange binaire (CH_3CN/CH_2Cl_2, 1:1 v/v), contenant dans tous les cas 0.1M de Bu_4NPF_6.
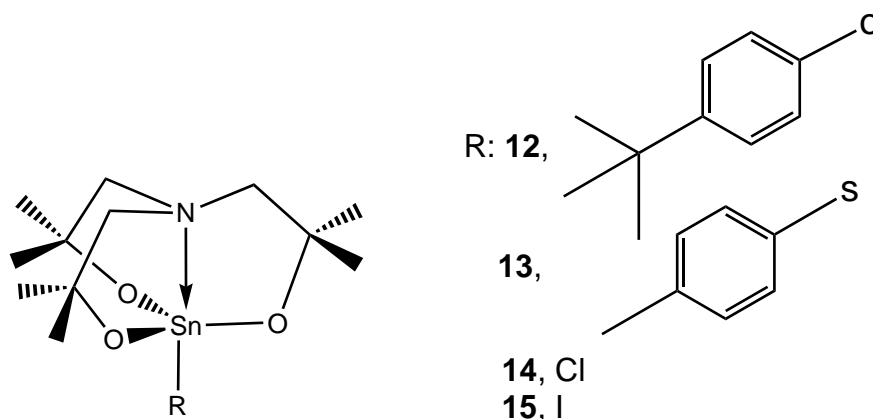

Figure 8: 1-R-stannatranes **12**, **13**, **14** et **15**

A l'opposé des silatranes et des germatranes, les stannatranes **12** et **13** n'exhibent un signal d'oxydation distinct que sur électrode de Pt. Les courants limitants i_p des stannatranes

12 et **13** sont tous deux sous contrôle diffusionnel ($i_p/v^{1/2}$ =const; lg(i_p)/lg(v) = 0.45 et 0.46 pour **12** et **13**, respectivement), et comme on peut le voir en comparant le rapport $i_p/v^{1/2}$ à la pente de Cottrell obtenue à partir d'une expérience de chronoampérométrie sur la même électrode, le nombre d'électrons transférés au cours de cette étape est n = 1. La dépendance à la température de lg(i_p^1) pour **13** nous donne E_a = 2.46 kJ/mol (2.85 kJ/mol pour le deuxième pic), ce qui correspond à l'énergie d'activation du flux de diffusion du solvant. Les largeurs de demi-pics $E_p - E_{p/2}$ de **12** et **13** sont trop larges pour de simples procédés résersibles mono-électroniques, probablement en raison d'interactions d'absorption ou d'une réorganisation structurelle substantielle accompagnant le transfert électronique.

Dans un solvant moins polaire comme CH_2Cl_2, l'oxydation de **13** procède en 2 étapes (figure 9), la seconde étant réversible dès v = 0.5 V/s. Si l'on fixe le potentiel maximum avant le début du second pic d'oxydation (E_v = 1.45 V), le premier pic commence aussi à exhiber un pic cathodique lui correspondant (à v > 50 V/s). Par conséquent, les deux signaux d'oxydation découlent de processus électrochimiques réversibles.
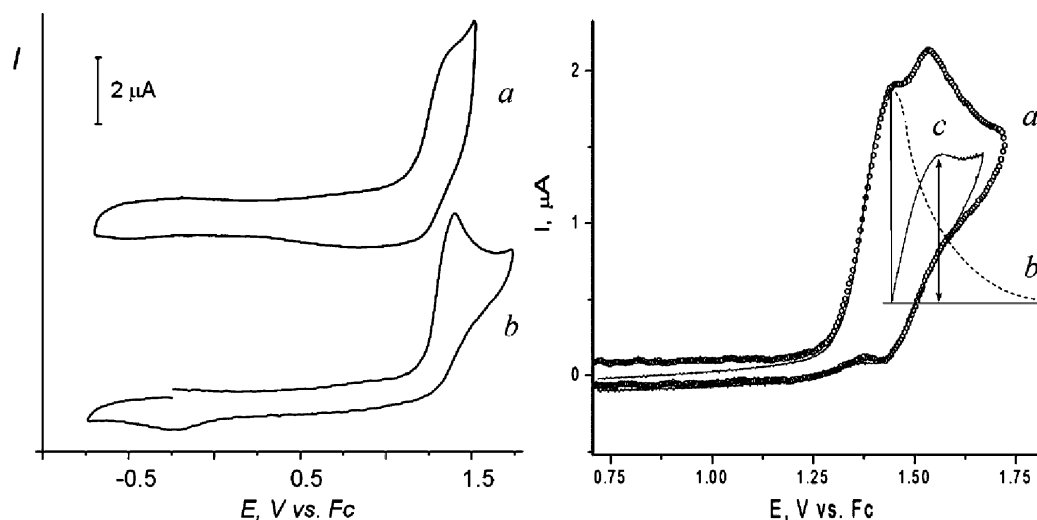

Figure 9: Voltammétrie cyclique sur les composés **12, 13**. Gauche: (a) − **12** et (b) − **13** (10^{-3} mol/L) in CH_3CN/0.1 M Bu_4NPF_6 at a Pt disk electrode; v = 5 V/s. Right: I–E curve of **13** (1.1×10^{-3} mol/L) in CH_2Cl_2/0.1 M Bu_4NPF_6 at a Pt disk electrode. (a) normal scan; (b) I−t curve after the hold at E_p. (c) diffusion limiting current of the second oxidation step. v = 0.5 V s^{-1}; T = 22 °C.

En raison d'une HOMO située à un faible niveau d'énergie, les halostannatranes sont très difficiles à oxyder. Ils ont au contraire une LUMO localisée sur une orbitale anti-liante σ^*(Sn–X), qui peut accepter relativement facilement un électron supplémentaire, et donc permettre leur électroréduction.

Par conséquent, nous avons tenté d'obtenir un dimère de stannatrane par électroréduction. Le résultat est montré figure 10: en *a* est représenté le voltammogramme cyclique du

chlorostannatrane avant électrolyse, et en *b* après 1h d'électrolyse. Il est évident que le pic de réduction du chlorostannatrane a disparu après électrolyse, ce qui indique qui n'y a plus de chlorostannatrane en solution (les distannatranes ne peuvent pas être réduits).

Après séparation et purification, nous avons de fait obtenu le dimère de chlorostannatrane. Nous avons réalisé une électrolyse similaire sur deux composés organostanniques utilisés comme modèles (chlorure de triphénylétain et chlorure de tributylétain), et nous avons également obtenu les dimères correspondants. La table 3 montre les déplacement chimiques observés en RMN du ^{119}Sn. On constate un large déplacement du pic vers les champs élevés quand on passe du monomère au dimère (table 3). Les résultats d'analyses de GC-MS on également démontré la présence de dimère après électrolyse dans le cas du chlorure de triphényl- et de tributyl-étain.
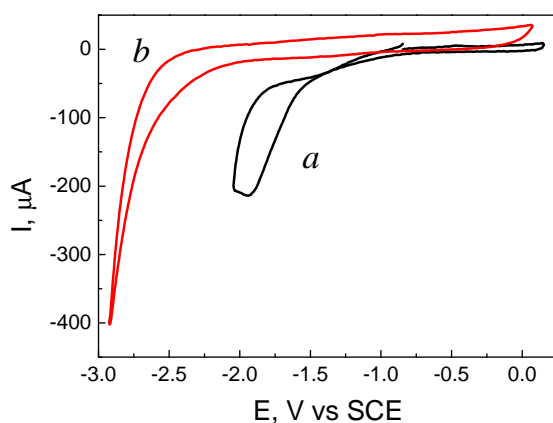

Figure 10: Suivi voltammétrique de l'électrolyse du chlorure de stannatranne. E = -1.94 V sur électrode de carbone vitreux dans CH_3CN/0.1 M $LiClO_4$ *a*. Electroréduction avant électrolyse; *b*. Après 1 h d'électrolyse.

Table 3: Dimère SnSn (d'après analyse GC-MS)

Compound	δ^{119}Sn (ppm)	E (V)	Product	Q (F/mol)	δ^{119}Sn (ppm)
Chlorure de triphénylétain	-44.90	-0.54	Tris(*n*-phenyl)distannane	29.03	-143.27
Chlorure de tributylétain	156.88(144)	-0.93	Tris(*n*-butyl)distannane	35.57	-82.66
Chlorure de stannatrane	-243	-1.94	Bis-stannatrane	11.06	-639.72

6 Nouvel electrolyte supportant

Les anions faiblement coordinants utilisés dans les électrolytes de support peuvent arbitrairement être sépares en 4 groupes (figure 11) : ceux dont l'atome central, acide de Lewis lui-même, porte en plus des substituants électro-accepteurs (a : BF_4^-, PF_6^-, AsF_6^-, SbF_6^-), ceux

qui portent de gros groupements organiques permettant la délocalisation des charges électroniques (b : Ph_4B^-), ceux combinant ces 2 caractéristiques en même temps (c : larges groupes aromatiques portant des substituants électroattracteurs $(C_6F_5)_4B^-$, $[(CF_3)_2C_6H_3]_4B^-$ et $[(CF_3)_3CO]_4Al^-$), et les carboranes icosaédriques CB_{11} ne contenant aucune orbitale π, d'utilisation relativement récente (d: $CB_{11}H_6X_6^-$ avec X=Cl ou Br).

D'autre part, plusieurs systèmes basés sur des « pièges quantiques » (e) sont connus, dans lesquels un atome ou un ion est piégé dans une cavité sans qu'il n'y ait de liaison covalente entre la paroi de la cavité et l'espèce piégée. On peut penser à titre d'exemple aux métaux piégés dans des fullerènes ($M@C_{60}$), ou aux atomes d'hydrogène piégés dans des silsesquioxanes octaédraux ($H^\bullet@T_8$), ainsi qu'à des anions fluorures dans des zéolites. Récemment, Bassindale *et al* ont découvert une nouvelle classe de structures silsesquioxane, dont l'anion F^- est encapsulé dans une cage T_8Ph_8. La charge négative de ce type de système est cachée au centre d'une boite siloxane inerte, interdisant toute coordination directe avec des électrophiles extérieurs et ne permettant que des interactions purement électrostatiques.
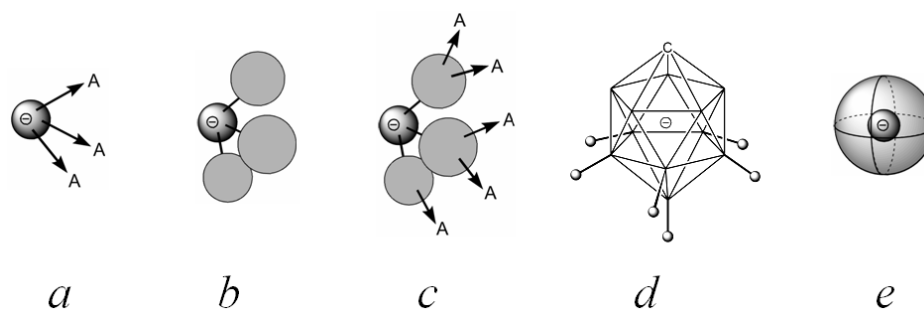

Figure 11: Différents types d'anions faiblement coordinants pour utilisation dans des électrolytes support

Ainsi, comme des calculs de DFT B3LYP/6-311G(d,p) l'ont démontré, il n'y a pas de transfert de charge substantiel entre l'anion F^- central et les atomes environnants de la cage silsesquioxane. La charge NBO de F^- varie de -1 à -0.89 quand on passe de l'état libre à l'état piégé dans un T_8. Etant donné que l'ion F^- peut entrer dans la cage du T_8 et en sortir, l'utilisation de solvants polaires est à bannir, dans la mesure où ils vont déstabiliser le système $F^-@T_8$ par solvatation de l'ion F^- libre.

La charge négative, cartographiée sur la surface de solvant disponible et visible par les électrophiles extérieurs est montrée figure 12 pour $F^-@T_8R_8$ (avec R= CH_2CN et Ph), et est comparée à celle de plusieurs anions communs. Alors que l'anion F^- libre est disponible à 100% depuis n'importe quelle direction, seuls les électrophiles de taille très réduite (H^+, Li^+, Na^+) peuvent approcher des zones présentant un caractère nucléophile significatif dans $F^-@T_8(CH_2CN)_8$ et $F^-@T_8Ph_8$.

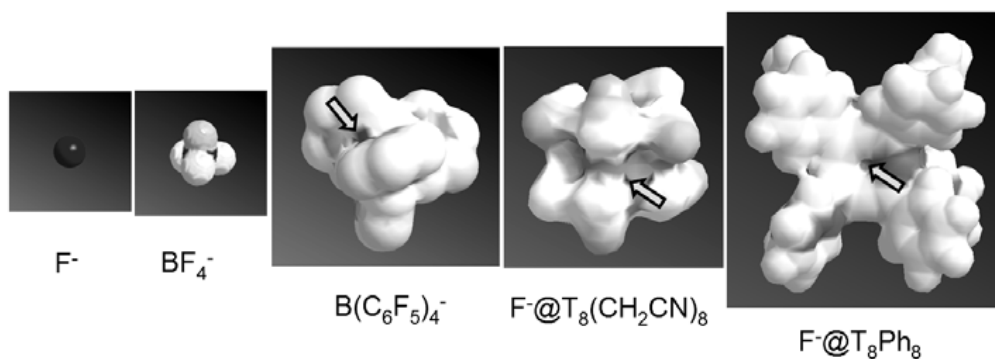Le système THF/0.07M $Bu_4N(F^-@T_8Ph_8)$ a été utilisé pour l'étude par spectroélec-

Figure 12: Charges négatives (zones sombres pour F^- and BF_4^-, et marquées par des flèches pour les autres anions), cartographiées sur la surface de solvant disponible pour des anions faiblement coordinants (selon calculs DFT B3LYP/6-311G(d,p)); F^- et BF_4^- sont donnés pour comparaison.

trochimie EPR de la réduction mono-électronique (Schéma 17) des 9-halofluorènes. La reconstruction du spectre observé (figure 13) grâce au programme Simphonia (Bruker) a été réalisé, conduisant à des paramètres (g = 2.0026; $a_{9-H} = 13.89$ G, $a_{1,1'-H} = 3.92$ G, $a_{2,2'-H} = 0.88$ G, $a_{3,3'-H} = 3.81$ G, $a_{4,4'-H} = 0.68$ G) proche de ceux rapportés pour le radical fluorenyl libre. On peut supposer que les groupes phényl de l'anion silsesquioxane agissent comme une sorte de matrice aromatique stabilisant le radical fluorenyl.
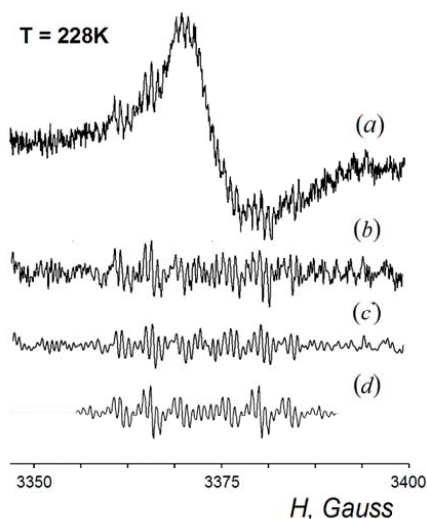

Figure 13: Spectres EPR de la réduction du 9-iodofluorene (dans un système propylene carbonate : THF - 1:2 - v:v / 0.07M $Bu_4N(F^-@T_8Ph_8)$. (a) : Expérimental. (b) : Section des hautes fréquences. (c) : Le même signal après traitement FFT. (d) : Simulé en utilisant les paramètres du texte.

Les sels supports de $TBA(F^-@T_8R_8)$ sont chimiquement stables, et peuvent être stockés sous forme solide sans crainte de décomposition. Leurs solutions dans les solvants testés

sont stables également, du moins pendant la durée typique d'une expérience d'électrochimie. Cependant, comme cela a été remarque pour la première fois par Bassindale et comme on peut le déduire des calculs DFT ci-dessus (figure 12), ils sont sensibles à la présence de petits cations en solution, spécifiquement Li^+ et H^+.

La figure 14 montre que dans l'acétonitrile, si on ajoute $LiClO_4$ à la solution, l'anion F^- fuit hors de la cage du système $F^- @ T_8(CH_2CN)_8$ pour former LiF/TBAF, et on obtient des cages $T_8(CH_2CN)_8$ entièrement vides en 9-10 heures en pratique. De façon similaire, les protons libérés au cours des 30 minutes d'expérience (voltammètrie du méthylanthracène) dans le cas de $F^- @ T_8(CH_2CH_2CF_3)_8$ dans le SO_2 liquide ont provoqué l'apparition de F^- libre en solution, bien que ce processus ne soit devenu visible en RMN du ^{19}F qu'après 4 heures de repos de la solution utilisée. Il est probable que la polarité du solvant et l'efficacité de la solvatation des F^- libres aient joué un rôle essentiel, comme mentionné précédemment.
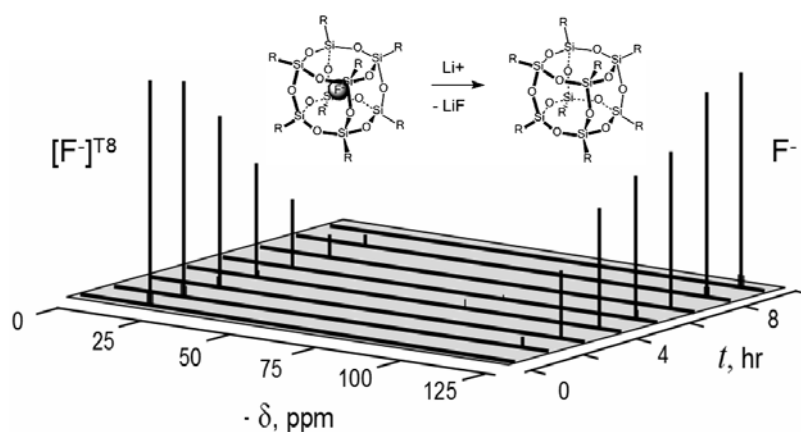

Figure 14: Fuite des anions F^- suivie par RMN du ^{19}F hors d'une cage de T_8R_8 ($R = CH_2CN$), en présence de $LiClO_4$. Solvant: CH_3CN, $T = 20°C$.